Self-Controlled Regulation of Mu Opioid Receptor Trafficking

by

Amanda L. Soohoo

A thesis submitted in partial fulfillment of the requirements for the degree of

Doctor of Philosophy in the field of Biological Sciences

Department of Biological Sciences
Carnegie Mellon University
Pittsburgh, Pennsylvania

May 4, 2015

Thesis Advisor: Dr. Manojkumar A. Puthenveedu, M.B., Ph.D.

For my first advisor, So Ying Soohoo

Acknowledgments

First, I'd like to thank my advisor, Dr. Manoj Puthenveedu who took in a young, audacious 21-year old wannabe-biochemist, and taught her how to be a cell biologist. As my project quickly became much more difficult than I thought it ever could be, he always believed and always encouraged me to get right back on the horse (or sometimes a slightly different horse) and keep trekking on. He constantly reminded me to embrace the fact that yes, experiments are fun, and that staring at the images coming in through our scope were just as beautiful and fascinating as any star system. He also taught me that the answer is yes you do want another gin & tonic. Or Sazerac.

My committee members: Dr. Tina Lee, Dr. Jon Minden, and Dr. Alexander Sorkin were like an extended family of support and encouragement. I looked forward to my meetings, where we would just sit around a table and discuss my data with openness and curiosity. Although, I know they are all very busy people, they were always 100% engaged at these meetings and I am truly grateful for all of the time, care and attention they gave me.

It's no secret that the Puthenveedu Lab is the coolest lab in Mellon Institute. We constantly collaborate, help, talk-through problems and support each other. We also hang out and party together all the time, like some kind of work-place sitcom. In truth, we were much more than labmates, and more like a lab-family. Dr. Rachel Vistein, Shanna Bowman, Dan Shiwarski, and Zach Weinberg: I will miss you terribly.

I also want to thank the groups in our two joint lab meetings. The Lee and Linstedt Labs, and the Friedman, Villdaga, Romero, Bisello Labs all whose feedback inside and outside of lab meetings were so instrumental in shaping the many avenues of my thesis work.

Finally, I'd like to thank my family and friends. My parents whose unwavering support will no doubt lead them to reading most of this thesis, despite having no background in biology. My first labmate Andy, and his awesome wife Jackie who have supported me through so much. Megan, the Kirk to my Spock. My unofficial sister, Amelia. My oldest bro, Alexis. Pablo, Jennifer and their impossibly awesome dog Annabelle. My cell bio girls: Ritika, Idil, and Sim. K$ and the Puthen-Ford crew. The Mellon Fit team for helping me shake it off. Will, Chelsea, Jon, Neil, Erik, and the rest of Butterjoint bar staff for giving me a third home. And my fiancé, Adam Zajac for his endless belief and support.

Abstract

Our cells rely extensively on external signals for key cellular and systematic functions. Many of these signals take the form of small molecules that are recognized by receptors on the cell surface. G-protein coupled receptors (GPCRs) are the largest group of surface signaling receptors. GPCRs respond to a diverse array of signals including: light, pain, adrenaline and serotonin. The capability of a certain type of GPCR to receive its signals is dependent on the number of receptors on the cell surface available to receive that extracellular signal. Intracellular trafficking determines the surface receptor number. Since GPCRs relay such vital signals it has become increasingly clear that their intracellular trafficking is tightly regulated and intertwined with the received and transmitted signals by the GPCRs.

This thesis focuses on the clinically, relevant mu-opioid receptor (MOR) which is the primary target of exogenous opiate drugs such as morphine and endogenous opiates such as endorphins and endomorphins. Once activated the MOR internalizes through clathrin-mediated endocytosis. Chapter 1 shows that the MOR is not passive in clathrin-mediated endocytosis, but has the ability to alter the duration of its own endocytosis events. Chapter 2 suggests that this change in endocytosis duration has a functional effect via changes in downstream signaling. Chapter 3 details how protein kinase C (PKC) serves as the control point for two regulatory mechanisms for the post-endocytic recycling of the MOR; one stemming from the pain receptor neurokinin-1 and the second downstream of the G-protein signaling of the MOR itself. Chapter 4 explores a proteomic approach using stable isotope labeling of amino acids in cell culture (SILAC) to further elucidate the mechanisms governing MOR endocytosis and recycling.

Table of Contents

List of Figures

Introduction

> *"Here was the secret of happiness, about which philosophers had disputed for so many ages, at once discovered; happiness might now be bought for a penny, and carried in the waistcoat-pocket; portable ecstasies might be had corked up in a pint-bottle; and peace of mind could be sent down by the mail."*

Excerpt From: "Confessions of an English Opium-Eater" by Thomas De Quincey.

Thomas De Quincey's autobiographical tale about his use, abuse and addiction to opium was an instant best-seller in 1820s England. Similar to today, people were both intrigued and horrified by the strange behaviors and motivations of opiate addicts. Opium, the extract from the opium poppy, was a godsend for its ability to cause analgesia or relieve pain. Although, opium use was prevalent in Regency England, its use predates De Quincey by thousands of years to Ancient Greek and Egyptian times (Brownstein, 1993). Even today, nearly 200 years after De Quincey, the opiate derivatives are still nonpareil in the analgesic world. However, as De Quincey depicted, opiates have the propensity to be devastatingly addictive. This is still evident today, in the United States in 2010 more people died from opiates (World Health Organization) than from car accidents (37,485 vs. 30,296) (National Highway Traffic Safety Administration). What is perhaps more horrifying than any statistic is to examine the individual lives of addicts, such as this account from the mother of an addict:

"My son discovered narcotics at the age of 13. He experienced a severe orthopedic sports injury. There seems to be nothing that can induce him to stop for any appreciable length of time. I had

him arrested May of 2006 for heroin possession and identity fraud, he stole 900 dollars from our checking account while I was in Connecticut burying my dad and his sister" (Volkow, Baler, & Goldstein, 2011).

Just like the teenager described above and De Quincey, many addicts start taking opiates to mediate their pain (Hansen, 2005), and later fall to addiction. De Quincey's opiate of choice was laudanum, a mixture of opium and alcohol that was the most commonly distributed form of the drug. During his lifetime both morphine and codeine were isolated from opium in the hope that these purified compounds would contain the pure analgesic power and the other compounds in opium contained the addictive chemicals. Unfortunately, codeine was less effective at treating pain and morphine proved to be just as addictive. Many more opiate derived compounds have been synthesized over the years with the same goal in mind- to create an opiate with high analgesic effect and low addictive potential, but it has been to little avail. The broad effects of the opiates and their receptors have been well characterized but the cellular mechanisms that define and control the receptors for the opiates is still poorly understood.

Both the positive analgesic effects and negative addiction effects of morphine are attributed to the mu-opioid receptor (MOR) (Matthes et al., 1996). The mu-opioid receptor is a G-protein coupled receptor (GPCR). The ligands that bind to and activate the receptor are known as agonists. The ligands that the bind to and inhibit the receptor are known as antagonists. Agonist binding typically results in the activation of canonical signaling including inhibition of adenylyl cyclase and activation of inwardly rectifying

potassium channels, as well as internalization of the receptor (Jordan & Devi, 1998). Antagonist binding does not result in these pathways, and can occasionally induce the opposite effect (Jordan & Devi, 1998). Most exogenous opiate drugs preferentially bind the mu-opioid receptor over the delta or kappa opioid receptors. Additionally, many endogenous opiates also target the mu-opioid receptor. Surprisingly the binding affinities of both endogenous and exogenous opiates to the receptor are surprisingly similar (Gillan, Kosterlitz, & Paterson, 1980). However, the downstream cellular consequences have been shown to be different between different opiate treatments. Phosphorylation of the receptor at T370 has been shown to only occur with an enkephalin activated receptor and not with a morphine activated receptor (Grecksch et al., 2011). Furthermore, differences in downstream signaling levels and pathways used have been shown between the different agonists (Chu, Zheng, Zhang, Loh, & Law, 2010) (Rivero et al., 2012). Recently, in the GPCR field there has been a focus towards understanding not only what the downstream signals of a receptor are, but where these signals are coming from. The localization of the receptor is determined by its membrane trafficking.

Membrane trafficking has a great ability to control the signaling of a GPCR. This control acts on how the GPCR can detect its incoming signals. The agonists that activate most GPCRs, including the MOR, are not cell permeable and so the receptor must be present on the cell surface to sense the agonists. When agonist binding occurs, it typically leads to endocytosis of the receptor. This internalization of the GPCRs de-sensitizes the cell to further signaling. Conversely, the MOR can be recycled back to the

cell surface from endosomal compartments. This re-sensitizes the cell to agonist stimulation once again. In a less general sense, different trafficking and signaling scaffolds are found throughout the cell. Thus, control of signaling through trafficking leads to precise spacial-temporal control of signaling (Sorkin & Zastrow, 2009).

Endocytosis

The process of clathrin-mediated endocytosis (CME) is the most well characterized form of endocytosis. It consists of over 30 proteins working together to successfully internalize cargo (McMahon & Boucrot, 2011). In the case of certain GPCRs, like MOR, the receptors must be activated before they can be internalized through CME. (Zastrow & Kobilka, 1992) The CME endocytosis of GPCRs can be broken up into 5 stages: (1) Activation, (2) Initiation, (3) Coat Formation, (4) Scission and (5) Uncoating. Each step is characterized by the arrival of certain proteins and an overall change in shape of the newly forming vesicle (Kaksonen, Toret, & Drubin, 2005) (McMahon & Boucrot, 2011) (Taylor, Perrais, & Merrifield, 2011).

Activation

Activation occurs when an agonist activates a GPCR. This process is schematized in Figure 0-1. The receptor undergoes a conformational change to allow it to act as a guanine exchange factor (GEF) to the coupled G-Protein (Cassel & Selinger, 1978) (Neer & Clapham, 1988) (Bourne, Sanders, & McCormick, 1990). The G-protein becomes GTP bound and the G-protein alpha subunit (often abbreviated G_{α})

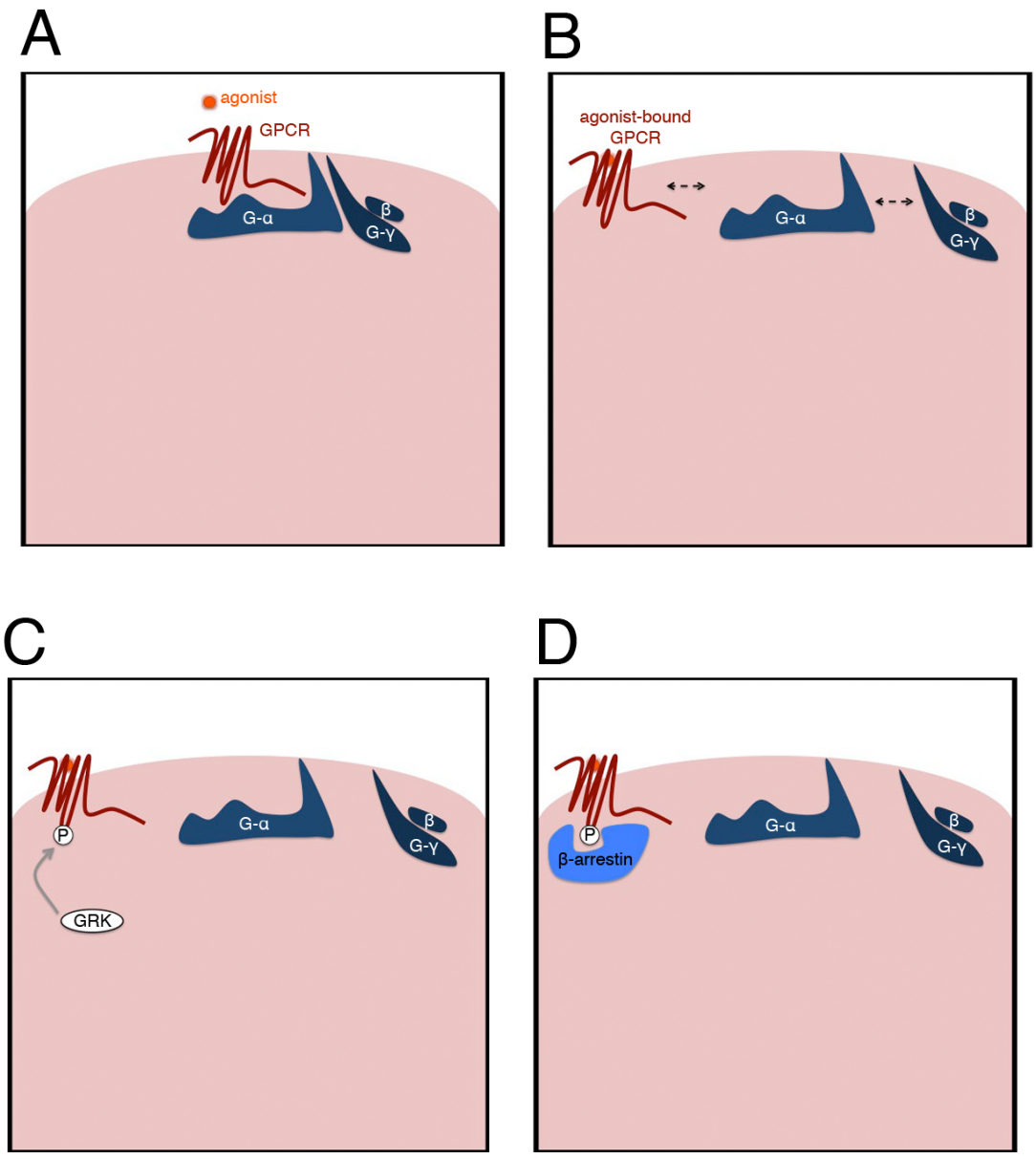

Figure 0-1: Activation
Activation is the series of steps that lead to activation of the GPCR and end with its binding to β-arrestin. A) The GPCR (dark red) and the trimeric G-protein (dark blue) are bound together at the plasma membrane before agonist (orange) binding. B) Upon agonist binding, the GPCR, G-α and G-βγ are no longer bound together. C) GRK (white) phosphorylates the cytoplasmic side of the GPCR D) β-arrestin (bright blue) binds to the activated GPCR at the GRK phospho-site

dissociates from the receptor and G-protein beta & gamma subunits (abbreviated $G_{\beta\gamma}$), as shown in Figure 0-1A-B (Wall, Posner, & Sprang, 1998). Both G_{α} and $G_{\beta\gamma}$ amplify separate downstream signaling events, amplifying the signal of the activated GPCR (Bourne et al., 1990) (McCudden, Hains, Kimple, Siderovski, & Willard, 2005). There are several different subtypes of G_{α}: $G_{\alpha/s}$, $G_{\alpha/i}$, $G_{\alpha/q}$, $G_{12/13}$, transducin and gustducin. The different downstream signaling proteins that are inhibited or activated characterize these G_{α} subtypes. Transducin and gustductin are a special case as they mediate the GPCR signals for sight and taste, respectively (B K Fung, 1981) (McLaughlin & Margolskee, 1992). The MOR couples to $G_{\alpha/i}$, which is named for its ability to inhibit adenylyl cyclase. A GPCR will typically couple to only one type of G_{α} however there is growing literature in the field to where a switch to other G_{α} subtypes have been observed (Quoyer et al., 2013) (Magocsi, Vizi, Selmeczy, Brózik, & Szelenyi, 2007).

The activated GPCR in its GEF state is able to activate its G-protein. This discontinues once the G-protein coupled Receptor Kinase (GRK, also known as beta-2 adrenergic receptor kinase or βARK) phosphorylates the cytoplasmic domain of the GPCR (Premont, Inglese, & Lefkowitz, 1995), as shown in Figure 0-1C. GRK is sterically hindered by the G-protein and cannot phosphorylate the receptor until the G-protein is disassociated (Wilden, Hall, & Kühn, 1986) (Benovic et al., 1987). This phosphorylation by GRK serves a dual purpose: to prevent re-association by the G-protein and allow for binding of β-arrestin (Benovic et al., 1987) to the receptor (depicted in Figure 0-1D).

β-arrestin was named for its ability to arrest the G-protein signal (Benovic et al., 1987) (Wilden et al., 1986). β-arrestin acts as both an adaptor to clathrin-mediated endocytosis machinery (Goodman et al., 1996) and as a signaling scaffold (DeWire, Ahn, Lefkowitz, & Shenoy, 2007). β-arrestin binds to both clathrin and AP-2, directly connecting the activated receptor to the clathrin-endocytosis machinery (Laporte et al., 1999). β-arrestin has been shown to scaffold to the ERK pathway, resulting in a second wave of signaling (DeWire et al., 2007). My work explores how changes in endocytosis could affect this β-arestin based signaling. Since β-arrestin can only bind to the activated receptor due to the GRK phosphor-site specificity (Burtey et al., 2007) it serves as a regulation point to only connect the activated GPCRs to be endocytosed. However, there are a few GPCRs that by-pass this mechanism of control and endocytose in an arrestin-independent manner, for example the serotonin 5HT2C receptor is consitutively endocytosed (Bhatnagar et al., 2001), as well as the thrombin protease activated receptor, PAR1 (Paing, Stutts, Kohout, Lefkowitz, & Trejo, 2002).

Initiation

Initiation has two main goals: nucleation and cargo loading. Nucleation, is defined as the step where the plasma membrane is primed for CME events. This involves changes in the membrane composition and shape to facilitate CME (McMahon & Boucrot, 2011). Phosphatidylinositol 4,5-bis phosphate ($PIP_{(4,5)}$) has been implicated at this step (Posor et al., 2013). Many initiation stage localizing endocytosis accessory proteins preferentially bind for $PIP_{(4,5)}$ (Posor et al., 2013). Proteins shown with this

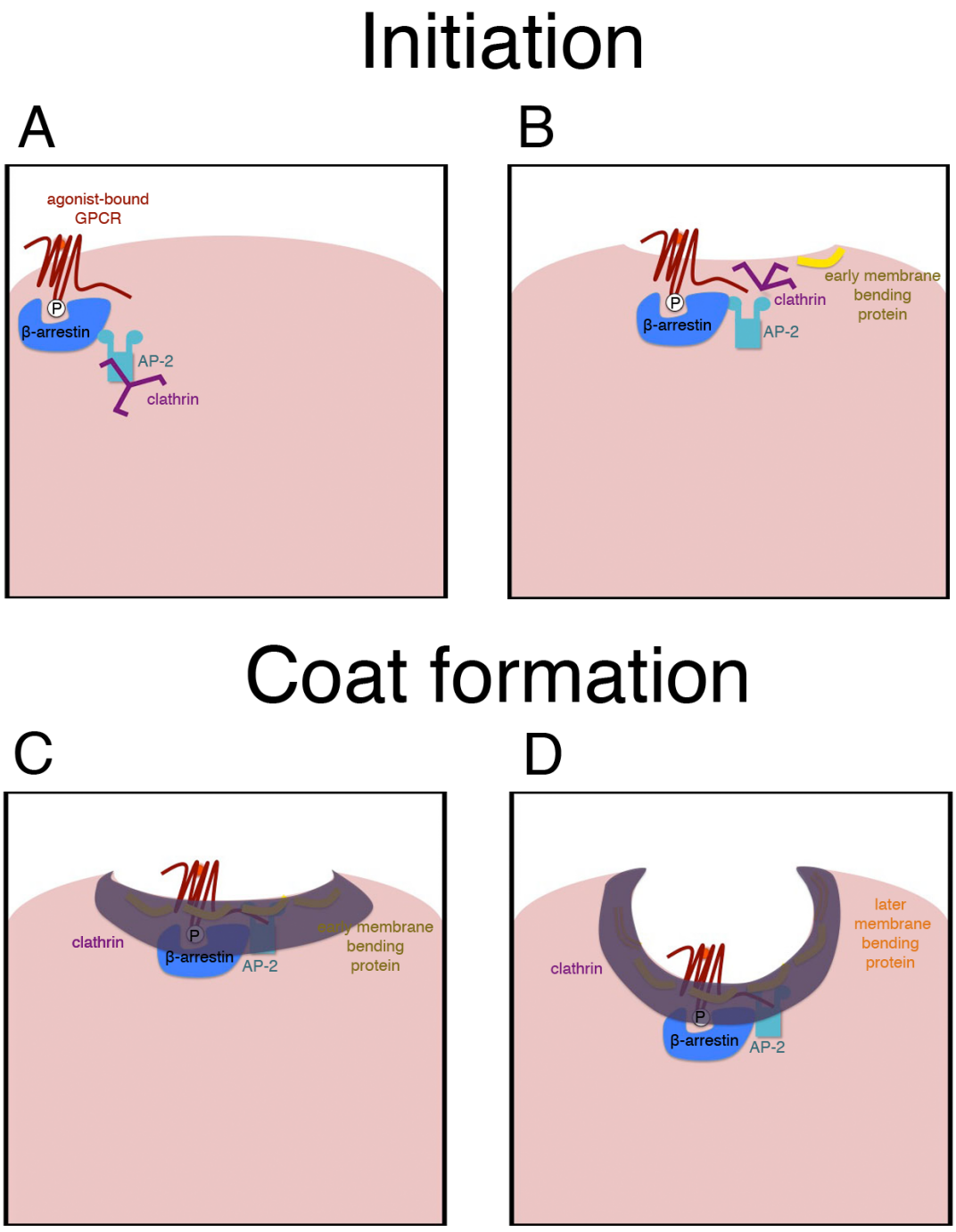

Figure 0-2: Endocytosis, Part I
Initiation A) β-arrestin (blue) binds to both AP-2 (teal) and clathrin (purple). Connecting the active GPCR to the endocytosis machinery. B) clathrin and early membrane bending proteins (yellow) start to reshape the plasma membrane into a vesicle. *Coat Formation* C) Clathrin (purple) assembles into a large coat-structure. D) Clathrin and its accessory proteins work to make the vesicle larger. Later stage membrane bending proteins (orange) arrive.

preference for $PIP_{(4,5)}$ include FCH (Fer and CIP4 homology) domain only proteins (usually abbreviated, FCHo1/2), epsin, and intersectin. FCHo1/2 has an F-BAR domain that preferentially binds $PIP_{(4,5)}$ and gently bends the plasma membrane. This initial bending was proposed for requirement to help start the endocytosis process. The role of FCHo1/2 as a nucleator for endocytosis has been both suggested (Henne et al., 2010) and contested (Umasankar et al., 2012). The Henne et. al 2010 paper demonstrates that clathrin-mediated endocytosis does not occur in a FCHo1/2 knockdown. Clathrin and AP2 fail to localize into clathrin-coated pits as determined by TIRF microscopy. However, the Umasankar et. al 2012 paper shows that FCHo1/2 morphant zebrafish are not completely deficient in clathrin-mediated endocytosis.

Epsin is unqiue in its roles to both reshape the membrane and sequester cargo. Epsin has an ENTH domain that wedges itself in-between the phospholipid bilayer in order to cause membrane re-shaping. Epsin also contains ubiquitin binding domains that have been shown to sequester ubiquinated cargo proteins (Kazazic et al., 2009).

β-arrestin binds directly to clathrin and AP-2 and the receptor is sequestered in a clathrin-coated pit (CCP), loading the GPCR cargo into the CCP. It has also been suggested that cargo loading can serve as a CME checkpoint (Loerke et al., 2009) (Mettlen, Loerke, Yarar, Danuser, & Schmid, 2010) (Liu, Aguet, Danuser, & Schmid, 2010), where CCPs that are not loaded with cargo are become abortive pits and are quickly disassembled.

Coat formation

Coat formation builds up to the apex of the CME process, a full-sized and fully shaped clathrin coated vesicle. The goals of coat formation are two-fold: to shape a full sized clathrin vesicle and to prepare the system for scission and uncoating.
The module of recruited proteins during coat-formation reflects these two goals. A large influx of clathrin is needed, as they are the building blocks for the growing clathrin coat. There is also a continued accumulation of accessory proteins from the initiation stage such as epsin, CALM, that help in shaping the clathrin coated vesicle. Additionally several BAR domain proteins are also recruited at the later end of the coat-formation stage. The banana-shaped BAR domain proteins amphiphysin, endophilin, and SNX9 have all been shown to have abilities to bend and even tubulate membranes. These proteins can also work in concert with dynamin to complete vesicle scission. Additionally, amphiphysin preferentially binds $PIP_{(3)}$ and endophilin binds $PIP_{(3,4)}$ (Daumke, Roux, & Haucke, 2014) indicating their sensitivity to the gradual conversion of lipids throughout endocytosis.

This is the stage of endocytosis that is typically modified by pathogens when they have hijacked endocytosis as a mode of cell entry. The conventional 100nm CCV is too small to fit a bacteria. *E. coli* can modify clathrin via phosphorylation to recruit actin at this earlier to stage to help with its invasion of the host cell (Bonazzi et al., 2011).

Scission

Once the vesicle reaches a critical mass, the scission step occurs. At this point the clathrin-coated vesicle has reached its full size, but is still attached to the plasma

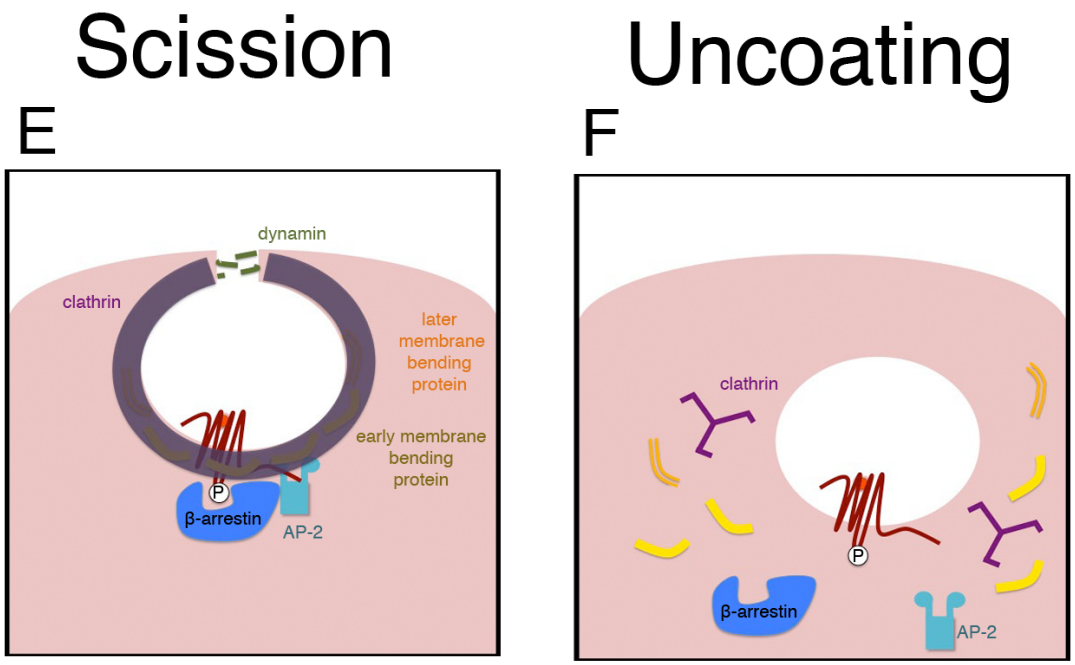

Figure 0-2: Endocytosis, Part II
Scission. E) Dynamin assembly (green) at the membrane neck separates the vesicle from the plasma membrane *Uncoating* F) Once the vesicle is free, the clathrin coat falls off and the all adaptor proteins are removed, including β-arrestin.

membrane by a small membrane neck. The goal of the scission step is to cut off this remaining connection. The GTPase dynamin is the protein primarily responsible for this step, it assembles in a GTP dependent at the membrane neck. Mutation of the GTPase active site renders dynamin inactive and endocytosis does not occur (Hinshaw & Schmid, 1995). There has been debate as to whether dynamin acts as a “pop-ase” or “constrict-ase.” In other words, does dynamin assembly free the CCV from the membrane by stretching the neck until it pops or by making it smaller and smaller with every turn (S. M. Ferguson & De Camilli, 2012)? Current views have come to favor the later model. In fact, it seems that dynamin only needs to make one-and-a-half turns to cleave the membrane neck (Cocucci, Gaudin, & Kirchhausen, 2014). Perhaps this is attributed to the growing evidence that dynamin does not work alone (Ramachandran et al., 2009). The BAR domain proteins work in concert with dynamin to aid is scission (Daumke et al., 2014) (Meinecke et al., 2013) . Additionally, there is growing debate in the role that actin may play in mammalian cell endocytosis (Grassart et al., 2014).

Scission serves as a very good control point for the clathrin endocytosis process, as it appears that this is where receptor mediated control seems to take place. The GPCR, the beta-2 adrenergic receptor delays the scission step by delaying dynamin recruitment (Puthenveedu & Zastrow, 2006). Our studies on the MOR show that MOR also works to delay vesicle scission, but by a different mechanism.

Uncoating

The clathrin coat becomes unstable soon after scission and the clathrin-complex falls off. It is thought that scission and uncoating are very much interlinked. As the CCP transitions to a fully-fledged vesicle, its shape change can be sensed and this is what triggers uncoating. Hsc70 and auxilin (and its non-neuronal isoform GAK) are the critical uncoating proteins (McMahon & Boucrot, 2011). Auxilin is localized to the vertexes of the clathrin coat (Fotin et al., 2004). When uncoating occurs, auxilin recruits Hsc70 to open up and pry the clathrin legs part from each other (Xing et al., 2009). This results in the uncoating of the newly internalized vesicle. It is possible that external factors, such as cargo could impact and uncouple the processes of uncoating and scission, which would alter the course of endocytosis. Such an example has not been shown.

Recycling

Once internalized, the vesicles containing the activated receptors traffick to small organelles known as endosomes. This first endosome compartment, the early endosome, functions as a rotary or sorting center for cellular trafficking. Here the receptors face two possible fates: to stay the course in the endosomal pathway en route to degradation in the lysosome, or to exit the endosome and return to the cell surface via the recycling pathway.

For cargo receptors, the road to degradation in the lysosome requires staying in the endosome until it fuses with the lysosome. Over time endosomes grow larger, more acidic, and more perinuclear (Huotari & Helenius, 2011). Microdomains containing specific phosphoinositide lipids that recruit specific RabGTPases and their regulatory

specific phosphoinositide lipids that recruit specific RabGTPases and their regulatory proteins are critical in process of endosomal maturation (Huotari & Helenius, 2011). The endosome trades its early RabGTPases such as a Rab4 for later ones such as Rab7 (Rink, Ghigo, Kalaidzidis, & Zerial, 2005). This process is known as endosomal maturation. During the process of endosomal maturation, certain membrane cargos are sequestered and brought inside the lumen of the endosome to multivesicular bodies (MVB) via the ESCRT machinery (Wollert & Hurley, 2010). Ubiquitinated proteins are commonly recognized as being destined for degradation. Ubiquitinated proteins are recognized by ESCRT-0 proteins and are sequestered together, creating a concentrated micro-domain of cargo (Raiborg & Stenmark, 2009). Then the subsequent members of the ESCRT complex (ESCRT I, II, III) load these cargos into MVBs for degradation (Hurley, 2008). The contents of the MVBs are digested by liposomal hydrolases upon fusion with lysosome (Huotari & Helenius, 2011).

Leaving the endosomal pathway to recycle back to the cell surface can occur all along the course of endosomal maturation. Different time scales for different cargos for recycling have been reported (Seachrist & Ferguson, 2003) (Wang, Chen, Zhang, & Ma, 2008) and are thought to serve as a point of regulation in higher order signaling through the receptor. Recycling of cargo receptors has been shown to occur through tubules (Puthenveedu et al., 2010). Tubules are elongated membrane projections that stem off of endosomes. Recent advances in microscopy have enabled a closer look at tubules, which showcase them as a micro-domain of the endosome in their own right made of more specialized protein and lipid populations (Puthenveedu et al., 2010) (Vistein &

Puthenveedu, 2013). Understanding these micro-domains is critical in understanding the regulation and mechanisms that control the clear temporally regulated recycling of signaling receptors. Tubules have been characterized as actin-independent tubules and actin-associated tubules. The actin-associated tubules have also been shown to co-localize with the retromer complex (Temkin et al., 2011) (Lauffer et al., 2008). Trans-Golgi network proteins also use these retromer-associated tubules to sort back to the Golgi (Bonifacino & Hurley, 2008). Cargo receptors have been shown to both use, and not use these two groups of tubules. In fact, the β2-adrenergic receptor, a GPCR, can switch between the actin associated and non-actin associated tubules depending on the presence of phosphorylation by PKA (Vistein & Puthenveedu, 2013). The MOR can also recycle back to the cell surface. The tubule population through which the MOR recycles through still needs to be further explored. However, one point of regulation occurs through a sequence in the C-terminal tail of the MOR required for its ability to recycle (Tanowitz & Zastrow, 2003). Beyond this required sequence, the mechanisms and signals controlling MOR recycling have not been well defined nor well characterized in living cells. However, understanding this regulation is critical because it determines when a cell can receive a signal through the MOR again.

The goal of this project was to determine how the MOR could control its own trafficking. This control in trafficking is very important for its ability to convey downstream signals and receive new signals. We approached our work by using live-cell microscopy techniques. We showed that the MOR could extend its own clathrin-

coated pits. This has significant implications in the amount of β-arrestin based signaling the receptor can employ. We also showed that the MOR can increase its own recycling via activation of PKC though activation of the G-protein beta-gamma subunits. This effect is dependent on two PKC phosphorylation sites on the receptor itself. Furthermore, a pain receptor Neurokinin-1 also activates PKC and results in increased recycling of MOR. Finally, to further elucidate the cellular mechanisms controlling MOR trafficking we preformed a Stable Isotope Labeling of Amino Acids in Cell Culture (SILAC) labeled co-immunoprecipitation to determine MOR binding partners. We have preformed an *in silico* analysis to narrow down a list of candidates and have developed medium through put screens to assay for functional effects.

References

Benovic, J. L., Kühn, H., Weyand, I., Codina, J., Caron, M. G., & Lefkowitz, R. J. (1987). Functional desensitization of the isolated beta-adrenergic receptor by the beta-adrenergic receptor kinase: potential role of an analog of the retinal protein arrestin (48-kDa protein). *Proceedings of the National Academy of Sciences of the United States of America*, *84*(24), 8879–8882.

Bhatnagar, A., Willins, D. L., Gray, J. A., Woods, J., Benovic, J. L., & Roth, B. L. (2001). The Dynamin-dependent, Arrestin-independent Internalization of 5-Hydroxytryptamine 2A (5-HT2A) Serotonin Receptors Reveals Differential Sorting of Arrestins and 5-HT2A Receptors during Endocytosis. *Journal of Biological Chemistry*, *276*(11), 8269–8277. doi:10.1074/jbc.M006968200

Bonazzi, M., Vasudevan, L., Mallet, A., Sachse, M., Sartori, A., Prevost, M. C., et al. (2011). Clathrin phosphorylation is required for actin recruitment at sites of bacterial adhesion and internalization. *The Journal of Cell Biology*, *195*(3), 525–536. doi:10.1083/jcb.201105152

Bonifacino, J. S., & Hurley, J. H. (2008). Retromer. *Current Opinion in Cell Biology*, *20*(4), 427–436. doi:10.1016/j.ceb.2008.03.009

Bourne, H. R., Sanders, D. A., & McCormick, F. (1990). The GTPase superfamily: a conserved switch for diverse cell functions. *Nature*, *348*(6297), 125–132. doi:10.1038/348125a0

Brownstein, M. J. (1993). A brief history of opiates, opioid peptides, and opioid receptors. *Proceedings of the National Academy of Sciences of the United States of America*, *90*(12), 5391.

Burtey, A., Schmid, E. M., Ford, M. G. J., Rappoport, J. Z., Scott, M. G. H., Marullo, S., et al. (2007). The Conserved Isoleucine-Valine-Phenylalanine Motif Couples Activation State and Endocytic Functions of β-Arrestins. *Traffic*, *8*(7), 914–931. doi:10.1111/j.1600-0854.2007.00578.x

Cassel, D., & Selinger, Z. (1978). Mechanism of adenylate cyclase activation through the beta-adrenergic receptor: catecholamine-induced displacement of bound GDP by GTP. *Proceedings of the National Academy of Sciences of the United States of America*, *75*(9), 4155–4159.

Chu, J., Zheng, H., Zhang, Y., Loh, H. H., & Law, P.-Y. (2010). Agonist-dependent μ-opioid receptor signaling can lead to heterologous desensitization. *Cellular*

Signalling, *22*(4), 684–696. doi:10.1016/j.cellsig.2009.12.003

Cocucci, E., Gaudin, R., & Kirchhausen, T. (2014). Dynamin recruitment and membrane scission at the neck of a clathrin-coated pit. *Molecular Biology of the Cell*, *25*(22), 3595–3609. doi:10.1091/mbc.E14-07-1240

Daumke, O., Roux, A., & Haucke, V. (2014). BAR Domain Scaffoldsin Dynamin-Mediated Membrane Fission. *Cell*, *156*(5), 882–892. doi:10.1016/j.cell.2014.02.017

DeWire, S. M., Ahn, S., Lefkowitz, R. J., & Shenoy, S. K. (2007). Beta-arrestins and cell signaling. *Annual Review of Physiology*, *69*, 483–510. doi:10.1146/annurev.ph.69.013107.100021

Ferguson, S. M., & De Camilli, P. (2012). Dynamin, a membrane-remodelling GTPase. *Nature Reviews Molecular Cell Biology*, *13*(2), 75–88. doi:10.1038/nrm3266

Fotin, A., Cheng, Y., Grigorieff, N., Walz, T., Harrison, S. C., & Kirchhausen, T. (2004). Structure of an auxilin-bound clathrin coat and its implications for the mechanism of uncoating. *Nature*, *432*(7017), 649–653. doi:10.1038/nature03078

Fung, B.K, Hurley, J. B., & Stryer L. (1981). Flow of information in the light-triggered cyclic nucleotide cascade of vision. *Proceedings of the National Academy of Sciences of the United States of America*, *78*(1), 152.

Gillan, M. G., Kosterlitz, H. W., & Paterson, S. J. (1980). Comparison of the binding characteristics of tritiated opiates and opioid peptides. *British Journal of Pharmacology*, *70*(3), 481–490.

Goodman, O. B., Jr, Krupnick, J. G., Santini, F., Gurevich, V. V., Penn, R. B., Gagnon, A. W., et al. (1996). β-Arrestin acts as a clathrin adaptor in endocytosis of the β2-adrenergic receptor. *Nature*, *383*(6599), 447–450. doi:10.1038/383447a0

Grassart, A., Cheng, A. T., Hong, S. H., Zhang, F., Zenzer, N., Feng, Y., et al. (2014). Actin and dynamin2 dynamics and interplay during clathrin-mediated endocytosis. *The Journal of Cell Biology*, *205*(5), 721–735. doi:10.1083/jcb.201403041

Grecksch, G., Just, S., Pierstorff, C., Imhof, A. K., Gluck, L., Doll, C., et al. (2011). Analgesic Tolerance to High-Efficacy Agonists But Not to Morphine Is Diminished in Phosphorylation-Deficient S375A μ-Opioid Receptor Knock-In Mice. *Journal of Neuroscience*, *31*(39), 13890–13896. doi:10.1523/JNEUROSCI.2304-11.2011

Hansen, G. R. (2005). The Drug-Seeking Patient in the Emergency Room. *Emergency Medicine Clinics of North America*, *23*(2), 349–365. doi:10.1016/j.emc.2004.12.006

Henne, W. M., Boucrot, E., Meinecke, M., Evergren, E., Vallis, Y., Mittal, R., & McMahon, H. T. (2010). FCHo Proteins Are Nucleators of Clathrin-Mediated Endocytosis. *Science*, *328*(5983), 1281–1284. doi:10.1126/science.1188462

Hinshaw, J. E., & Schmid, S. L. (1995). Dynamin self-assembles into rings suggesting a mechanism for coated vesicle budding. *Nature*, *374*(6518), 190–192. doi:10.1038/374190a0

Huotari, J., & Helenius, A. (2011). Endosome maturation. *The EMBO Journal*, *30*(17), 3481–3500. doi:10.1038/emboj.2011.286

Hurley, J. H. (2008). ESCRT complexes and the biogenesis of multivesicular bodies. *Current Opinion in Cell Biology*, *20*(1), 4–11. doi:10.1016/j.ceb.2007.12.002

Jordan, B., & Devi, L. A. (1998). Molecular mechanisms of opioid receptor signal transduction. *British Journal of Anaesthesia*, *81*(1), 12–19.

Kaksonen, M., Toret, C. P., & Drubin, D. G. (2005). A Modular Design for the Clathrin- and Actin-Mediated Endocytosis Machinery. *Cell*, *123*(2), 305–320. doi:10.1016/j.cell.2005.09.024

Kazazic, M., Bertelsen, V., Pedersen, K. W., Vuong, T. T., Grandal, M. V., Rødland, M. S., et al. (2009). Epsin 1 is Involved in Recruitment of Ubiquitinated EGF Receptors into Clathrin-Coated Pits. *Traffic*, *10*(2), 235–245. doi:10.1111/j.1600-0854.2008.00858.x

Laporte, S. A., Oakley, R. H., Zhang, J., Holt, J. A., Ferguson, S. S. G., Caron, M. G., & Barak, L. S. (1999). The 2-adrenergic receptor/ arrestin complex recruits the clathrin adaptor AP-2 during endocytosis. *Proceedings of the National Academy of Sciences*, *96*(7), 3712–3717. doi:10.1073/pnas.96.7.3712

Lauffer, B. E. L., Chen, S., Melero, C., Kortemme, T., Zastrow, von, M., & Vargas, G. A. (2008). Engineered Protein Connectivity to Actin Mimics PDZ-dependent Recycling of G Protein-coupled Receptors but Not Its Regulation by Hrs. *Journal of Biological Chemistry*, *284*(4), 2448–2458. doi:10.1074/jbc.M806370200

Liu, A. P., Aguet, F., Danuser, G., & Schmid, S. L. (2010). Local clustering of transferrin receptors promotes clathrin-coated pit initiation. *The Journal of Cell Biology*, *191*(7), 1381–1393. doi:10.1083/jcb.201008117

Loerke, D., Mettlen, M., Yarar, D., Jaqaman, K., Jaqaman, H., Danuser, G., & Schmid, S. L. (2009). Cargo and dynamin regulate clathrin-coated pit maturation. *PLoS Biology*, *7*(3), e1000057.

Magocsi, M., Vizi, E. S., Selmeczy, Z., Brózik, A., & Szelenyi, J. (2007). Multiple G-protein-coupling specificity of β-adrenoceptor in macrophages. *Immunology*, *122*(4), 503–513. doi:10.1111/j.1365-2567.2007.02658.x

Matthes, H. W., Maldonado, R., Simonin, F., Valverde, O., Slowe, S., Kitchen, I., et al. (1996). Loss of morphine-induced analgesia, reward effect and withdrawal symptoms in mice lacking the *μ*-opioid-receptor gene.

McCudden, C. R., Hains, M. D., Kimple, R. J., Siderovski, D. P., & Willard, F. S. (2005). G-protein signaling: back to the future. *Cellular and Molecular Life Sciences*, *62*(5), 551–577. doi:10.1007/s00018-004-4462-3

McLaughlin, S. K., & Margolskee, R. F. (1992). Gustducin is a taste-cell-specific G protein closely related to the transducins. *Nature*, *357*(6379), 563–569. doi:10.1038/357563a0

McMahon, H. T., & Boucrot, E. (2011). Molecular mechanism and physiological functions of clathrin-mediated endocytosis. *Nature Reviews Molecular Cell Biology*, *12*(8), 517–533. doi:10.1038/nrm3151

Meinecke, M., Boucrot, E., Çamdere, G., Hon, W.-C., Mittal, R., & McMahon, H. T. (2013). Cooperative recruitment of dynamin and BIN/amphiphysin/Rvs (BAR) domain-containing proteins leads to GTP-dependent membrane scission. *Journal of Biological Chemistry*, *288*(9), 6651–6661. doi:10.1074/jbc.M112.444869

Mettlen, M., Loerke, D., Yarar, D., Danuser, G., & Schmid, S. L. (2010). Cargo- and adaptor-specific mechanisms regulate clathrin-mediated endocytosis. *The Journal of Cell Biology*, *188*(6), 919–933. doi:10.1083/jcb.200908078

Neer, E. J., & Clapham, D. E. (1988). Roles of G protein subunits in transmembrane signalling. *Nature*, *333*(6169), 129–134. doi:10.1038/333129a0

Paing, M. M., Stutts, A. B., Kohout, T. A., Lefkowitz, R. J., & Trejo, J. (2002). Beta-Arrestins Regulate Protease-activated Receptor-1 Desensitization but Not Internalization or Down-regulation. *The Journal of Biological Chemistry*, *277*(2), 1292–1300. doi:10.1074/jbc.M109160200

Posor, Y., Eichhorn-Gruenig, M., Puchkov, D., Schöneberg, J., Ullrich, A., Lampe, A., et al. (2013). Spatiotemporal control of endocytosis by phosphatidylinositol-3,4-bisphosphate. *Nature*. doi:10.1038/nature12360

Premont, R. T., Inglese, J., & Lefkowitz, R. J. (1995). Protein kinases that phosphorylate activated G protein-coupled receptors. *FASEB Journal : Official Publication of the Federation of American Societies for Experimental Biology*, *9*(2), 175–182.

Puthenveedu, M. A., & Zastrow, von, M. (2006). Cargo Regulates Clathrin-Coated Pit Dynamics. *Cell*, *127*(1), 113–124. doi:10.1016/j.cell.2006.08.035

Puthenveedu, M. A., Lauffer, B., Temkin, P., Vistein, R., Carlton, P., Thorn, K., et al. (2010). Sequence-Dependent Sorting of Recycling Proteins by Actin-Stabilized Endosomal Microdomains. *Cell*, *143*(5), 761–773. doi:10.1016/j.cell.2010.10.003

Quoyer, J., Janz, J. M., Luo, J., Ren, Y., Armando, S., Lukashova, V., et al. (2013). Pepducin targeting the C-X-C chemokine receptor type 4 acts as a biased agonist favoring activation of the inhibitory G protein. *Proceedings of the National Academy of Sciences*, *110*(52), E5088–E5097. doi:10.1073/pnas.1312515110

Raiborg, C., & Stenmark, H. (2009). The ESCRT machinery in endosomal sorting of ubiquitylated membrane proteins. *Nature*, *458*(7237), 445–452. doi:doi:10.1038/nature07961

Ramachandran, R., Pucadyil, T. J., Liu, Y.-W., Acharya, S., Leonard, M., Lukiyanchuk, V., & Schmid, S. L. (2009). Membrane insertion of the pleckstrin homology domain variable loop 1 is critical for dynamin-catalyzed vesicle scission. *Molecular Biology of the Cell*, *20*(22), 4630–4639. doi:10.1091/mbc.E09-08-0683

Rink, J., Ghigo, E., Kalaidzidis, Y., & Zerial, M. (2005). Rab Conversion as a Mechanism of Progression from Early to Late Endosomes. *Cell*, *122*(5), 735–749. doi:10.1016/j.cell.2005.06.043

Rivero, G., Llorente, J., McPherson, J., Cooke, A., Mundell, S. J., McArdle, C. A., et al. (2012). Endomorphin-2: a biased agonist at the μ-opioid receptor. *Molecular Pharmacology*, *82*(2), 178–188. doi:10.1124/mol.112.078659

Seachrist, J. L., & Ferguson, S. S. G. (2003). Regulation of G protein-coupled receptor endocytosis and trafficking by Rab GTPases. *Life Sciences*, *74*(2-3), 225–235. doi:10.1016/j.lfs.2003.09.009

Sorkin, A., & Zastrow, von, M. (2009). Endocytosis and signalling: intertwining molecular networks, 1–14. doi:10.1038/nrm2748

Tanowitz, M., & Zastrow, von, M. (2003). A Novel Endocytic Recycling Signal That Distinguishes the Membrane Trafficking of Naturally Occurring Opioid Receptors. *Journal of Biological Chemistry*, *278*(46), 45978–45986. doi:10.1074/jbc.M304504200

Taylor, M. J., Perrais, D., & Merrifield, C. J. (2011). A High Precision Survey of the Molecular Dynamics of Mammalian Clathrin-Mediated Endocytosis. *PLoS Biology*, *9*(3), e1000604. doi:10.1371/journal.pbio.1000604.g008

Temkin, P., Lauffer, B., Jäger, S., Cimermancic, P., Krogan, N. J., & Zastrow, von, M. (2011). SNX27 mediates retromer tubule entry and endosome-to-plasma membrane trafficking of signalling receptors. *Nature Cell Biology*, *13*(6), 717–723. doi:10.1038/ncb2252

Umasankar, P. K., Sanker, S., Thieman, J. R., Chakraborty, S., Wendland, B., Tsang, M., & Traub, L. M. (2012). Distinct and separable activities of the endocytic clathrin-coat components Fcho1/2 and AP-2 in developmental patterning. *Nature Cell Biology*, *14*(5), 488–501. doi:10.1038/ncb2473

Vistein, R., & Puthenveedu, M. A. (2013). Reprogramming of G protein-coupled receptor recycling and signaling by a kinase switch. *Proceedings of the National Academy of Sciences*, *110*(38), 15289–15294. doi:10.1073/pnas.1306340110

Volkow, N. D., Baler, R. D., & Goldstein, R. Z. (2011). Addiction: Pulling at the Neural Threads of Social Behaviors. *Neuron*, *69*(4), 599–602. doi:10.1016/j.neuron.2011.01.027

Wall, M. A., Posner, B. A., & Sprang, S. R. (1998). Structural basis of activity and subunit recognition in G protein heterotrimers. *Structure*, *6*(9), 1169–S3. doi:10.1016/S0969-2126(98)00117-8

Wang, F., Chen, X., Zhang, X., & Ma, L. (2008). Phosphorylation state of mu-opioid receptor determines the alternative recycling of receptor via Rab4 or Rab11 pathway. *Molecular Endocrinology*, *22*(8), 1881–1892. doi:10.1210/me.2007-0496

Wilden, U., Hall, S. W., & Kühn, H. (1986). Phosphodiesterase activation by photoexcited rhodopsin is quenched when rhodopsin is phosphorylated and binds the intrinsic 48-kDa protein of rod outer segments. *Proceedings of the National Academy of Sciences of the United States of America*, *83*(5), 1174–1178.

Wollert, T., & Hurley, J. H. (2010). Molecular mechanism of multivesicular body biogenesis by ESCRT complexes. *Nature*, *464*(7290), 864–869. doi:doi:10.1038/nature08849

Xing, Y., Böcking, T., Wolf, M., Grigorieff, N., Kirchhausen, T., & Harrison, S. C. (2009). Structure of clathrin coat with bound Hsc70 and auxilin: mechanism of Hsc70-facilitated disassembly. *The EMBO Journal*, *29*(3), 655–665. doi:10.1038/emboj.2009.383

Zastrow, von, M., & Kobilka, B. K. (1992). Ligand-regulated internalization and recycling of human beta 2-adrenergic receptors between the plasma membrane and endosomes containing transferrin receptors. *The Journal of Biological Chemistry*, *267*(5), 3530–3538.

Chapter 1:
Divergent modes for cargo-mediated control of clathrin-coated pit dynamics

This manuscript appeared as an article in *Molecular Biology of the Cell* and is reprinted here.

Soohoo, A. L. & Puthenveedu, M. A. *Molecular Biology of the Cell* **24** (11), 1725–1734, doi:10.1091/mbc.E12-07-0550 (2013).

Abstract

Clathrin-mediated endocytosis has long been viewed as a process driven by core endocytic proteins, with internalized cargo proteins being passive. Contrary to this, an emerging view suggests that signaling receptor cargo may actively control their own fate by regulating the dynamics of clathrin-coated pits (CCPs) that mediate their internalization. Despite its physiological implications, very little is known about such "cargo-mediated regulation" of CCPs by signaling receptors. Here, using multi-color TIR-FM imaging and quantitative analysis in live cells, we show that the mu-opioid receptor, a physiologically relevant G protein-coupled signaling receptor, delays the dynamics of CCPs in which it is localized. This delay is mediated by the interactions of two critical leucines on the receptor cytoplasmic tail. Unlike the previously known mechanism of cargo-mediated regulation, these residues regulate the lifetimes of dynamin, a key component of CCP scission. These results identify a novel means for selectively controlling the endocytosis of distinct cargo that share common trafficking

components, and indicate that CCP regulation by signaling receptors can operate via divergent modes.

Introduction

Clathrin-mediated endocytosis (CME), the main mode by which cells internalize surface cargo proteins including physiologically relevant signaling receptors, is a highly ordered process mediated by sets of core endocytic proteins (Taylor et al., 2011; McMahon and Boucrot, 2011; Kaksonen et al., 2000; Rao et al., 2012; Boettner et al., 2012). CME is initiated by endocytic cargo and membrane remodeling proteins that recruit adapter proteins, like AP2 and beta-arrestin, and clathrin to the plasma membrane (Wolfe and Trejo, 2007; McMahon and Boucrot, 2011; Kelly and Owen, 2011; Santini et al., 1998). The growing clathrin-coated pit (CCP) is then stabilized by the interactions of adapter proteins with cargo (Ehrlich et al., 2004; Santini et al., 1998). Recent studies, which followed fluorescently tagged components of the clathrin endocytic machinery, have described a modular arrangement for the recruitment of proteins during CME, with relatively distinct sets of proteins acting during the initiation, maturation, completion, and scission phases of vesicle formation during endocytosis (Kaksonen et al., 2000; Taylor et al., 2011).

The traditional view of CME was that it was controlled entirely by a

cascade of interactions of core endocytic proteins, with regulation being mainly at the level of cargo-adapter interactions. This view has recently been challenged by evidence that signaling receptor cargo can regulate the dynamics of the CCPs to which they localize (Puthenveedu and von Zastrow, 2006). This is particularly interesting because the internalization of signaling receptors has several direct physiological consequences to their signaling (Magalhaes et al., 2012; Marchese et al., 2008; Sorkin and von Zastrow, 2009). Currently, the only known examples for signaling cargo that regulate CCPs are the beta-adrenergic receptors - prototypical members of the G protein-coupled receptor (GPCR) family, the largest family of signaling receptors (Pierce et al., 2002). Adrenergic receptors localize to a distinct subset of CCPs and selectively delay the dynamics of those CCPs (Puthenveedu and von Zastrow, 2006). This delay is mediated by interactions of the receptor C-terminal tail with the actin cytoskeleton, which delay the recruitment, but not the activity, of the GTPase dynamin - a key member of the scission module (Ferguson and De Camilli, 2012; Schmid and Frolov, 2011). The fact that B2AR can control CCPs opens up the possibility that cells can exert virtually unlimited selective control over the endocytosis of diverse cargo using shared trafficking components.

The mu-opioid receptor (MOR) is a related and clinically relevant signaling GPCR that is internalized via CCPs (Keith et al., 1996; Segredo et al., 1997). MOR mediates the physiological effects of endogenous opioid neurotransmitters and many abused drugs (Matthes et al., 1996). After activation, MOR is localized

to CCPs via its interaction with the adapter protein beta-arrestin, after which it undergoes internalization (Moore et al., 2007). This has significant effects on opioid signaling, as cellular sensitivity is directly proportional to the number of receptors available on the cell surface (Martini and Whistler, 2007; Sorkin and von Zastrow, 2009). Further, recent data suggest a definite but complex relationship between the development of opioid addiction and MOR endocytosis, underlining its physiological significance (Kim et al., 2008; Koch and Höllt, 2008). Despite this, the mechanisms that regulate MOR endocytosis, especially in the context of the novel cargo-mediated facet of endocytic control, are still largely unknown.

Here, we use multi-color Total Internal Reflection Fluorescence Microscopy (TIR- FM) to visualize individual events that mediate the endocytosis of MOR in living cells. Using time-resolved imaging and quantitative analysis of these events, we show that MOR localizes to a subset of CCPs and specifically delays their dynamics. Analysis of key components of the four main modules in CME revealed that, unlike PDZ-dependent mechanisms, MOR delayed CCPs by controlling the time taken by dynamin to induce scission, but not its recruitment. These results reveal a novel facet of how the internalization and desensitization of a key physiologically relevant signaling receptor is regulated, and suggest divergent modes for direct control of clathrin-mediated endocytosis by signaling receptor cargo.

Results

Mu-Opioid Receptors localize to a subset of clathrin-coated pits

To analyze the internalization of the mu-opioid receptor (MOR) at high spatial and temporal resolution, we first optimized an assay to visualize the endocytosis of MOR at the level of individual endocytic events. We tagged MOR with either a FLAG epitope or a pH-sensitive GFP (SpH) at the extracellular N-terminus. SpH (pKa ~7.1) is fluorescent at the neutral/alkaline pH of the cell surface, but gets rapidly protonated and quenched in the acidic environments (Miesenbock et al., 1998; Yudowski et al., 2009). FLAG- tagged MOR was detected using anti-FLAG antibodies tagged to the pH-insensitive dye Alexa647. The activation and endocytic trafficking of both these tagged receptors appeared grossly unchanged compared to untagged receptors, consistent with published reports (Yu et al., 2010). Both SpH-MOR and FLAG-MOR were predominantly distributed on the plasma membrane in HEK293 cells stably expressing the receptors. When observed by live cell TIR-FM microscopy, the receptor was relatively diffuse on the plasma membrane prior to activation, and clustered in small diffraction limited spots and a few larger structures within 10 sec after addition of the MOR-specific agonist DAMGO (SpH-MOR shown in Fig 1-1A, similar results obtained with FLAG-MOR). The diffraction-limited clusters rapidly disappeared with time, consistent with their endocytosis. Quantitation of total surface receptor fluorescence over time from multiple cells using wide field microscopy showed an exponential decrease ($t_{1/2}$ = 3 min, R^2 = 0.9966) after DAMGO (Fig 1-1B, full curve in Fig S1B). These rates were consistent with

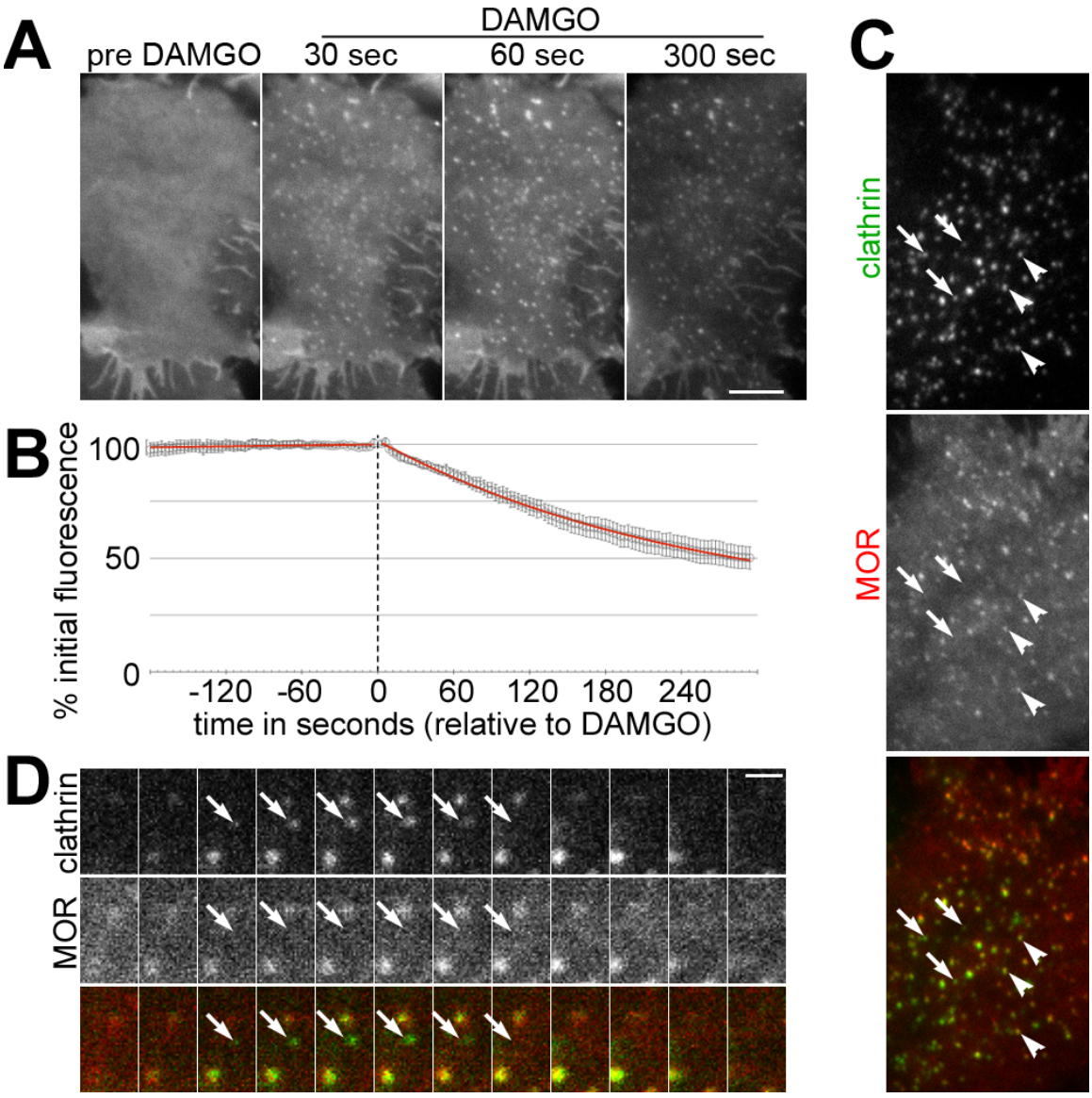

Figure 1-1: MOR internalizes via a subset of clathrin-coated pits. A) Representative images from an example cell expressing SpH-tagged MOR imaged by TIR-FM before, and 30, 60, and 300 sec after activation by the MOR agonist DAMGO, showing rapid MOR clustering. Scale bar is 5µm. B) Average surface fluorescence values over time, ± s.e.m, from multiple cells, from 3 min before to 5 min after DAMGO, showing an exponential decrease after DAMGO. Red line shows curve fit to linear (before) or single-phase decay (after). C) Dual color TIR-FM of MOR (red) and clathrin (green) showing clustering of MOR in a subset of coated pits (arrowheads). Arrows indicate example CCPs without detectable MOR. Scale bar is 5µm. D) Frames from a dual-color TIR-FM time-series, 3 sec apart, showing the complete cycle of an example CCP (arrows), from formation to internalization, without detectable MOR fluorescence. MOR is in red and clathrin in green. Two example CCPs that show MOR clustering are also shown. Scale bar is 1µm.

previously reported rates for MOR endocytosis, and were confirmed by flow cytometry and TIR-FM to detect agonist-induced loss of SpH-MOR from the surface (Fig S1-1A and C). As expected, SpH- and FLAG-MOR showed comparable kinetics of DAMGO-induced endocytosis (Fig S1-1C and D).

The majority of MOR was endocytosed via the clathrin-mediated pathway. Inhibition of clathrin-mediated endocytosis by Pitstop2 (von Kleist et al., 2011), a selective clathrin inhibitor, effectively inhibited MOR internalization (Fig S1-2A and C). Similarly, expression of a version of arrestin lacking its clathrin-binding domain (Kang et al., 2009), which still binds the receptor and acts as a dominant negative, also inhibited MOR internalization (Fig S1-2 B and D). To test whether MOR clusters localized to all clathrin-coated pits (CCPs), we used dual-color TIR-FM to visualize clathrin along with MOR. In cells co- expressing SpH-MOR and dsRed-clathrin, or FLAG-MOR and GFP-clathrin, clathrin fluorescence was seen as distinct puncta on the cell surface before addition of DAMGO, while MOR fluorescence was diffuse similar to Fig 1-1A without obvious concentration in these puncta. Upon DAMGO addition, MOR puncta colocalized with CCPs, but only a subset of them, as indicated by CCPs that did not contain a detectable MOR cluster (Fig 1-1C). Quantitative analysis across multiple cells revealed that 46.5% of the CCPs showed detectable MOR concentration (n=290), defined as a 25% increase in fluorescence over the surrounding membrane (see Fig S1-3). By time- lapse imaging, we followed individual CCPs from their formation to their endocytosis, denoted by abrupt disappearance in the large majority of cases (Fig

S1-4), as described previously by us and others (Taylor et al., 2011; Loerke et al., 2009; Ehrlich et al., 2004). Strikingly, approximately 50% of the CCPs never acquired detectable MOR clusters in their entire lifetime (example in Fig 1-1D). This suggests that MOR endocytosis is mediated by a distinct set of CCPs.

MOR extends the lifetimes of CCPs in which it clusters

To determine whether MOR exerts cargo-mediated control over CCPs, we compared the dynamics of individual CCPs with MOR and CCPs without detectable MOR. Individual CCPs without detectable MOR were internalized relatively fast after their appearance (example in Fig 1-2A). In contrast, CCPs with MOR stayed noticeably longer on the surface before they disappeared (Fig 1-2A). To quantify this delay, we manually tracked CCPs and calculated their lifetimes. The lifetimes of CCPs were calculated from their initial appearance to the detection of an endocytic event, as evidenced by disappearance, a positional shift, and/or splitting off of clathrin spots (Fig S1-4A). These criteria have been used by our lab and others previously to detect CCP endocytosis (e.g., Puthenveedu and von Zastrow, 2006; Ehrlich et al., 2004; Merrifield et al., 2002; Loerke et al., 2009; Doyon et al., 2011). Quantitation of over 500 CCPs indicated that the distribution of CCP lifetimes before MOR activation was between 20 and 60 sec, with the median value being ~35 sec. As further verification of this lifetime distribution, we imaged the recruitment of dynamin-GFP into CCPs and its disappearance as an independent index of vesicle scission and endocytosis. Consistent with previous studies (e.g., Merrifield et al., 2002; Puthenveedu and

von Zastrow, 2006; Doyon et al., 2011), dynamin fluorescence showed a transient spike just before an endocytic event (Fig S1-4B). Importantly, the lifetime distribution we observed using dynamin fluorescence matched the lifetimes we observed using our criteria for defining endocytosis (Fig S1-4C). Consistent with this, in our experimental system, the majority of CCPs identified showed dynamin recruitment and scission, suggesting that most CCPs were productive. This is consistent with our population distribution centered around the mean lifetime of ~35 sec (Fig S1-4D), and with observations that the absolute CCP lifetimes vary extensively depending on experimental conditions (e.g., Loerke et al., 2009; Taylor et al., 2011; Batchelder and Yarar, 2010; Saffarian and Kirchhausen, 2009; Mattheyses et al., 2011; Doyon et al., 2011; Nakatsu et al., 2010).

To test the effect of MOR clustering without the cell-to-cell variability of absolute lifetime distributions, we quantitated MOR clustering in the same cells before vs. after DAMGO. After DAMGO, while there were still short-lasting coated pits, many CCPs with lifetimes over 90 sec were observed, with the median lifetime across the whole population increasing to ~70 sec (example cell in Figure S1-5, multiple cells in Fig 1-2B). A similar increase in the lifetimes of the CCP population was observed also when Imaris (Bitplane) was used to detect and track clathrin spots, although the absolute lifetimes differed from our manually verified population (Fig 1-2C). Cumulative distribution graphs of the manually verified lifetimes showed a distinct shift to the right (k=37 sec, R^2=0.9932 before

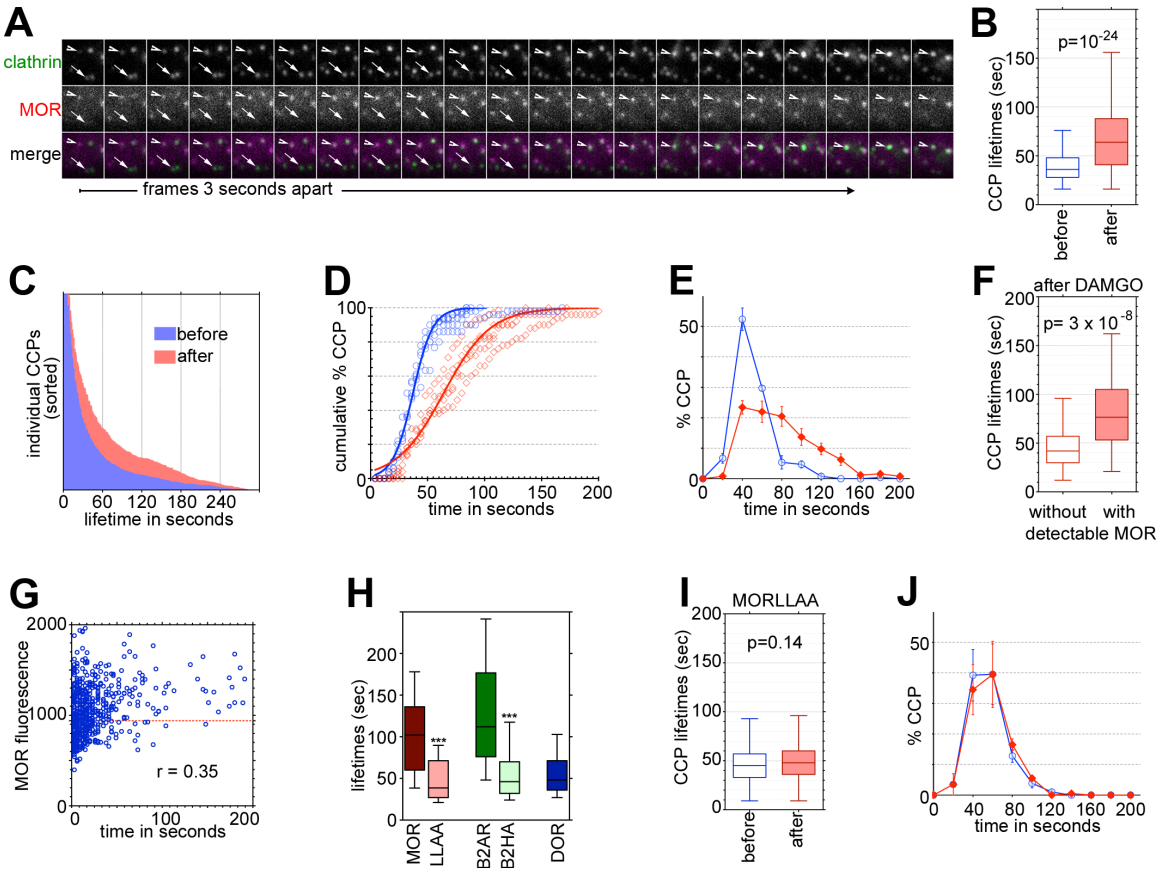

Figure 1-2: MOR extends the lifetimes of a subset of CCPs, using a C-terminal "bileucine" sequence. A) Frames from dual color TIR-FM time series of CCPs, 3 sec apart. CCPs containing a detectable MOR cluster (one example shown by arrowhead) lasts a noticeably longer time than a CCP without (arrows). B) Box plots showing the range and median of CCP lifetimes in the same cells before vs. after MOR clustering. C) Sorted lifetimes from >2500 CCPs detected using automated spot detection and tracking, before vs. after MOR clustering by DAMGO. Consistent with our conclusions, CCP lifetimes are increased after DAMGO-induced MOR clustering. D) Example cumulative distribution graphs of CCP lifetimes from 5 cells before (blue) vs. after (red) MOR clustering. Lines show curve fits across all cells. E) Lifetimes of clathrin spots on the cell surface, obtained from the same cells before (open blue circles) vs. after (closed red diamonds) MOR clustering, were separated into 20s bins. F) Box plots of lifetimes of CCPs with detectable MOR clustering vs. those that do not, defined as in Fig S1-3. CCPs with MOR show significantly longer lifetimes. G) Plot of raw MOR fluorescence vs. CCP lifetimes, showing a positive correlation. The red line shows the estimated cutoff as per Fig S1-3. H) Surface residence times of individual clusters of MOR, MOR-LLAA, B2AR, B2AR-HA, and DOR after agonist exposure were quantitated from multiple cells. Box plots show the median and range. *** denotes p value of less than 0.0001 for the mutants compared to wild type. I) Box plots showing the range and median of CCP lifetimes in the same cells before vs. after MOR-LLAA clustering. J) Clathrin spot lifetimes, obtained from the same cells before (open blue circles) vs. after (closed red diamonds) MOR-LLAA clustering, were fit as in D. There was no observable difference in the CCP lifetime distributions after MOR-LLAA clustering. Box plots are Tukey, and error bars on column graphs are s.e.m.

DAMGO, vs. k=64 sec, R^2=0.9894 after DAMGO) (Fig 1-2D). To better analyze this at the level of CCP populations, we binned the clathrin lifetimes per cell into 20 sec bins. Before MOR clustering, the lifetimes of the majority of CCPs (~50%) fell between 20 and 40 seconds. In contrast, in the same cells after MOR clustering, a much more diffuse distribution of lifetimes was observed, with each of the bins of longer lifetimes (>60 sec) containing betweemn 10 and 20% of CCPs (Fig 1-2E). As controls, cells imaged for the same period without DAMGO did not show any difference in lifetimes, and DAMGO did not have any effect in cells not expressing MOR (not shown). This suggests that the delay was not an intrinsic property of CCPs, but that it was induced by MOR clustering.We next compared the lifetimes of CCPs that showed a detectable MOR cluster, defined as a local increase in fluorescence at least 25% above the surrounding membrane (see Fig S1-3), to those that did not. The mean lifetimes of CCPs with MOR clusters (82.2 ± 5.3 sec) were noticeably longer than those without clusters (45.3 ± 2.6 sec) (Fig 1-2F). To further confirm this objectively, without classifying whether a CCP had a detectable cluster or not, we correlated the raw fluorescence of MOR in CCPs to the corresponding CCP lifetimes. Correlation analysis showed a positive correlation (Spearman r= 0.35) between the two parameters, indicating that CCPs with a higher MOR fluorescence showed longer lifetimes (Fig 1-2G). Together, this indicates that MOR actively delays the surface residence times of the CCPs in which it clusters. CCP delay by MOR requires two specific leucines on its cytoplasmic tail. To identify the signal on MOR that

mediates CCP delay, we first focused on a "bileucine" sequence (LENLEAE) on the C-terminal cytoplasmic tail of MOR that has been previously implicated in its trafficking (Tanowitz and von Zastrow, 2003). To disrupt this sequence, we generated a version of MOR, termed MOR-LLAA, where the two leucines were mutagenized to alanines. When cells expressing either wild type MOR, MOR-LLAA, or the delta opioid receptor (DOR, as a negative control for CCP delay) (Puthenveedu and von Zastrow, 2006) were activated by the agonists DAMGO (for MOR) or DADLE (for DOR), robust receptor clustering was seen in all cases. When the lifetimes of individual receptor clusters were quantitated and compiled, MOR clusters resided approximately twice as long on the surface as DOR clusters (Fig 1-2H), comparable to the beta-2 adrenergic receptor (B2AR) which has been previously shown to delay CCPs (Puthenveedu and von Zastrow, 2006). Strikingly, the lifetimes of MOR- LLAA clusters were comparable to DOR clusters and a version of B2AR where the PDZ ligand domain was mutated (B2HA, one way ANOVA not significantly different), indicating that the prolonged surface residence of receptor clusters required the MOR bileucine sequence (Fig 1-2H). Further, the increased lifetimes of CCPs induced by MOR after DAMGO addition was completely abolished in the MOR-LLAA mutant as seen by quantitating average lifetimes (Fig 1-2I) and by binning the lifetimes of CCP populations to 20 second bins (Fig 1-2J) as above. Consistent with the change observed in CCP lifetimes, when loss of surface receptor fluorescence was measured over the whole cell, MOR showed both a delay in the initiation of

fluorescence loss after DAMGO addition and a slower rate of internalization, compare to MOR-LLAA (Fig S1-6). Together, this indicates that MOR, upon activation with DAMGO, selectively delays the CCPs in which it localizes using a specific bileucine sequence on its C-terminal tail.

MOR delays the vesicle scission phase of CCP endocytosis

We considered four modes by which the bileucine sequence on MOR could delay CCPs: 1) by slowing clathrin assembly; 2) by making larger CCPs which require more time to assemble; 3) by delaying the recruitment of the scission machinery; or 4) by regulating the activity of the scission machinery. To test the first possibility, we first measured the fluorescence traces of clathrin over time in CCPs containing MOR clusters and compared them to CCPs devoid of MOR. Before MOR clustering, and in CCPs devoid of MOR, clathrin fluorescence in most CCPs showed a linear increase denoting clathrin coat assembly, followed by a sharp decrease corresponding to scission and movement of vesicles away from the cell surface (example in Fig 1-3A). This fluorescence signature was largely consistent with previous observations by us and other groups (Mettlen et al., 2010; Merrifield et al., 2002; Ehrlich et al., 2004). In contrast, in the longer-lasting CCPs containing detectable MOR clusters that were observed after exposure to agonist in the same cells, clathrin showed a similar linear increase, followed by a plateau phase where there was no further increase, before the rapid loss of fluorescence (example in Fig 1-3B). This suggested that the assembly of the clathrin cage was not affected, and MOR "paused" further

progression of CCP endocytosis after clathrin assembly was complete. Further, to quantitatively estimate the rate assembly of clathrin, we classified CCPs into short (no detectable MOR cluster) and long (with MOR clusters) CCPs. We defined a 'short' CCP as having a lifetime of between 30 and 40 seconds, which approximated the median lifetime of CCPs before MOR activation (Fig 1-2, Fig S1-5). We defined a 'long' CCP as having a lifetime of over 75 seconds. By manual verification of CCP lifetimes, this was over the 90th percentile of CCP lifetimes observed before MOR clustering (e.g., Fig 1-2D). When aligned to the time frame where we first detected clathrin, taken as the initiation of clathrin assembly, the fluorescence traces roughly fit to a linear regression (R^2=0.73 and 0.68 respectively for short and long CCPs). Importantly, the slopes in the assembly phase showed no significant difference ($p = 0.12$, pooled slope = 2.2, pooled $y_{int} = 98$) between l (Fig 1-3C), indicating that the assembly of clathrin was not changed.

To test the second possibility, we compared the peak clathrin fluorescence values in CCPs containing MOR with CCPs without detectable MOR, as an index of the total clathrin present, and, therefore, the size of vesicles formed. We first measured the clathrin fluorescence in CCPs of maximum intensity projections of time series. As shown in Fig 1-3D, there was no statistically significant difference ($p = 0.55$) in the clathrin fluorescence between these CCPs with and without detectable MOR. Consistent with this, we observe no correlation between between peak clathrin fluorescence and CCP lifetimes (Fig 1-3E, Spearman R =

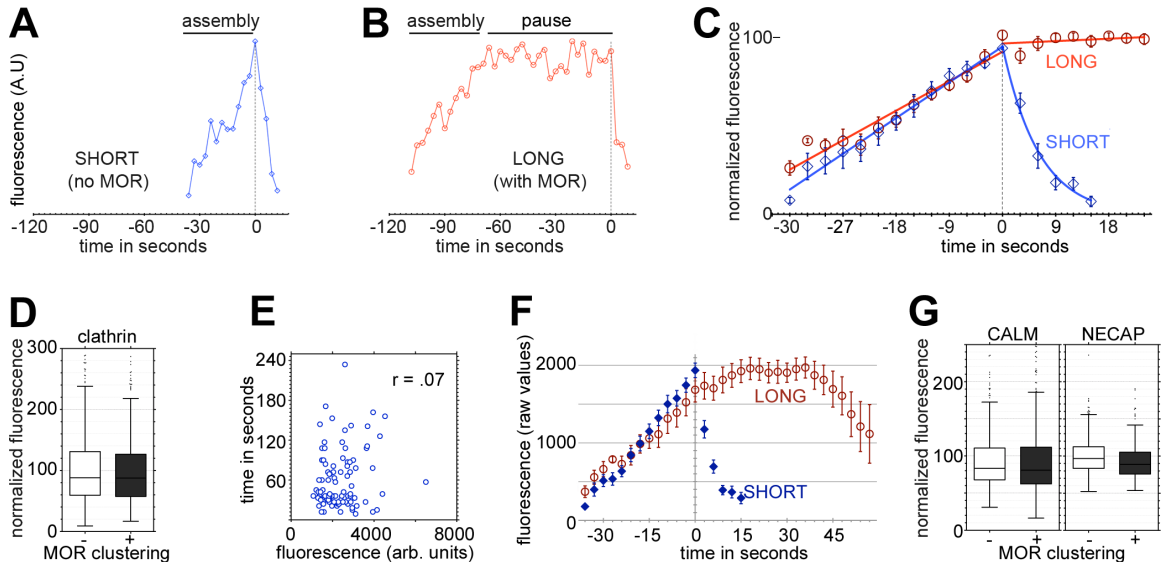

Figure 1-3: MOR pauses CCP progression after clathrin assembly. A) Example traces of clathrin fluorescence over time from short CCPs (lifetimes between 30 and 40 sec) without MOR and long CCPs (>75 sec, see text) with MOR clusters. The short CCPs showed a linear increase in fluorescence followed by a rapid decrease characteristic of scission and endocytosis. The long CCPs showed a distinct "pause" after near- maximum clathrin fluorescence, before endocytosis. C) Averaged normalized fluorescence from 20 short and long CCPs aligned to their initial appearance. The slopes of assembly are not significantly different. D) Tukey box plots of maximum clathrin fluorescence calculated from CCPs without MOR vs. CCPs with MOR, across the same set of cells after DAMGO-induced MOR clustering. Values normalized to the average value without MOR, show no significant difference between the two populations (n>350 in each case). E) Correlation between peak clathrin fluorescence and lifetimes (n=100) showing no correlation between these criteria. F) Average fluorescence values from traces across 20 short and long CCPs show roughly the same peak fluorescence before endocytosis across both populations. G) Tukey box plots of maximum fluorescence values of CALM and NECAP before vs. after DAMGO-induced MOR clustering show no difference.

0.07, p value= 0.45). Additionally, we monitored the clathrin fluorescence over time from multiple example CCPs with and without MOR clusters (defined as in Fig S1-3), and examined the peak values of fluorescence of clathrin in these traces. The average fluorescence traces showed no significant difference in the maximum clathrin fluorescence before endocytosis (Fig 1-3F), indicating that MOR-containing CCPs are not larger. We also observed no difference in the peak fluorescence of NECAP and CALM (Fig 1-3G, p = 0.25 for NECAP and 0.31 for CALM), the two main proteins shown so far to affect the size of clathrin-coated vesicles (Zhang et al., 1998; Ritter et al., 2007; Meyerholz et al., 2005; Maritzen et al., 2012). Further, the lifetimes of NECAP and CALM were not changed by MOR clustering (Fig S1-7A and C). Interestingly, the absolute lifetimes of CALM were increased upon co-expression of clathrin, and, while there was a slight increase in the lifetimes after DAMGO, this did not match the increase in clathrin lifetimes (Fig S1-7B). Interestingly, while CALM has been reported to follow clathrin dynamics, we observed that, in longer lasting CCPs, CALM fluorescence was dissociated from clathrin fluorescence before endocytosis (Fig S1-7D). Together, however, our results suggest that the clathrin assembly and vesicle size were not affected by MOR clustering.

To test the third and fourth possibilities, we directly imaged the behavior of dynamin, a key protein in scission. Cells expressing FLAG-MOR, dynamin-GFP, and clathrin- dsRed were imaged for 5 min before and 5 min after addition of DAMGO, to detect whether DAMGO-induced MOR clustering altered the

behavior of dynamin. Before DAMGO addition, dynamin was recruited just before scission in CCPs, as previously observed. After DAMGO addition, consistent with MOR clustering in a subset of CCPs, we observed that ~30% of dynamin puncta did not colocalize with MOR (e.g., arrows in Fig 1-4A). Strikingly, in CCPs paused by MOR, dynamin was observed for a significantly longer time than in CCPs devoid of MOR (example in Fig 1-4B). This was apparent when the behavior of dynamin puncta was compared in the same cells before vs. after MOR clustering by DAMGO. As shown in the example kymograph following the same cells before vs. after DAMGO-induced MOR clustering (Fig 1-4C), dynamin stays in CCPs much longer after DAMGO. Quantitation of multiple CCPs indicated that the average dynamin lifetimes doubled, from 7 sec to 14 sec, after DAMGO-induced MOR clustering (Fig 1-4D). This increase required the interactions of the C-terminal leucines on MOR, as clustering of MOR-LLAA did not change dynamin lifetimes (Fig 1-4D). This increase in dynamin lifetimes was further confirmed by triple-color live cell TIR-FM of clathrin, dynamin, and MOR. Fluorescence traces from individual CCPs showed that in CCPs showing a detectable increase in MOR fluorescence over background, dynamin was recruited and persisted for a longer period before scission (example trace in Fig 1-4-E, left). In contrast, in CCPs without MOR clusters (where MOR fluorescence stayed at the baseline), dynamin showed the characteristic spike just before scission (Fig 1-4E, right). When dynamin lifetimes from MOR-expressing cells, before vs. after DAMGO, were binned into 9 second bins, the frequency histogram showed a noticeable

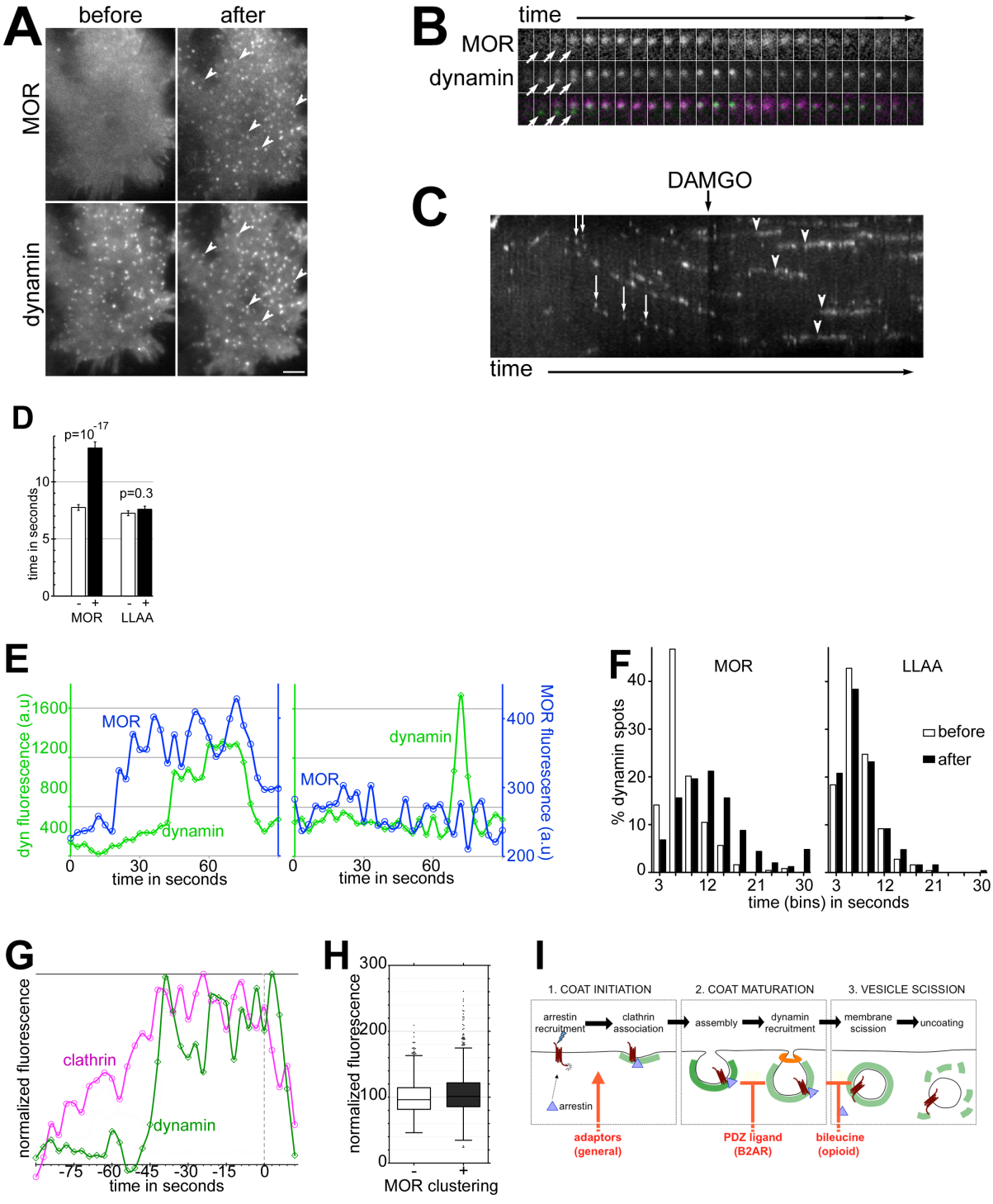
A
before
after
MOR
dynamin
B
time
MOR
dynamin
C
DAMGO
time
D
p=10-17
p=0.3
time in seconds
MOR
LLAA
E
dyn fluorescence (a.u)
MOR fluorescence (a.u)
MOR
dynamin
time in seconds
F
MOR
LLAA
% dynamin spots
before
after
time (bins) in seconds
G
normalized fluorescence
clathrin
dynamin
time in seconds
H
normalized fluorescence
MOR clustering
I
1. COAT INITIATION
2. COAT MATURATION
3. VESICLE SCISSION
arrestin recruitment
clathrin association
assembly
dynamin recruitment
membrane scission
uncoating
arrestin
adaptors (general)
PDZ ligand (B2AR)
bileucine (opioid)

Figure 1-4. MOR pauses CCPs by delaying the endocytic scission module. A) Maximum intensity projection of 30 sec of a time-lapse movie from an example cell expressing MOR and dynamin-GFP, before and after DAMGO. Arrowheads show example dynamin spots without MOR. Scale bar is 5μm. B) Example frames from a time series, 3 sec apart, showing two CCPs with dynamin, one with MOR and one without (arrows). The dynamin in the CCP with MOR lasts significantly longer than in the CCP without MOR. C) Kymograph from a region of a cell imaged 5 min before and 5 min after DAMGO. Dynamin lasts just one or two frames before DAMGO ("spots" denoted by arrows) and much longer ("lines" denoted by arrowheads) after DAMGO. The region of the cell from which the kymograph is shown is noted in Fig S8. D) Average dynamin lifetimes in cells expressing MOR or MOR-LLAA, before vs. after DAMGO ($n > 250$ in each case). The increase in dynamin lifetimes seen after DAMGO with MOR is lost with MOR-LLAA. Error bars are s.e.m. E) Traces of raw fluorescence of FLAG-MOR and dynamin from example CCPs. Dynamin fluorescence stays noticeably longer in the cell showing a MOR cluster. F) Lifetimes of dynamin spots, obtained from the cells expressing MOR (left) or MOR-LLAA) (right) before (open bars) and after (filled bars) MOR clustering, were separated into 9 sec bins. In MOR expressing cells, but not MOR-LLAA cells, dynamin distributions shifted to longer lifetimes after DAMGO. G) Fluorescence trace of clathrin and dynamin, normalized to the maximum, from an example CCP containing MOR. Dynamin localizes near the end of the assembly phase, and lasts through the pause phase. H) Tukey box plots of dynamin fluorescence in CCPs with vs. without MOR, normalized to CCPs without MOR ($n > 1100$ in each case). I) Model for divergent modes of cargo-mediated control of endocytosis by signaling receptors.

shift to longer lifetimes after DAMGO exposure (Fig 1-4F, left). This shift was absent in MOR-LLAA expressing cells. Consistent with this, dynamin was typically recruited at or after the end of the assembly phase of clathrin in CCPs with MOR, and persisted through the "pause" phase till scission (example in Fig 1-4G).

To test whether the delay correlated with an increased amount of dynamin required to cause CCP scission, we quantified the peak fluorescence of dynamin in each CCP as an index of the amount of dynamin, by maximum intensity projections of time-series. When compared to CCPs before DAMGO-mediated MOR clustering, CCPs after MOR clustering showed no significant change (4 ± 4.2%, p=0.36) in dynamin fluorescence (Fig 4H). Together with the normal recruitment and increased lifetimes of dynamin, these results suggest that MOR delays CCPs lifetimes by acting primarily on the vesicle scission module of clathrin-mediated endocytosis (Fig 4I).

Discussion

Cargo-mediated control of individual CCPs is an emerging concept that can potentially explain how cells can selectively control the endocytosis of multiple cargo proteins using shared core trafficking proteins (Puthenveedu and von Zastrow, 2006). In this study, we identify MOR, the main target of opioid neurotransmitters and many clinically abused drugs, as a physiologically relevant signaling cargo that can control dynamics of individual CCPs through interactions

of its C-terminal tail.

The dynamic behavior of CCPs have been recorded extensively in the recent past using live cell TIR-FM imaging (e.g., Taylor et al., 2011; Loerke et al., 2009; Doyon et al., 2011). The range of CCP lifetimes we observe in HEK293 cells broadly match these careful and exhaustive studies. One notable difference is that, unlike with recent published data using automated detection of CCPs, we do not see a significant fraction of short-lasting "abortive" CCPs (Fig 1-2E). Consistent with this, most of the CCPs we observe recruit dynamin and undergo scission (Fig S1-4). It is possible that this reflects differences in detection methods, cell types, or experimental conditions. It has become increasingly clear that the dynamics of individual components and CCP modules in mammalian cells vary highly based on their expression levels, the cell types used, temperature, and imaging conditions (Merrifield et al., 2002; Ehrlich et al., 2004; Puthenveedu and von Zastrow, 2006; Loerke et al., 2009; Taylor et al., 2011; Batchelder and Yarar, 2010; Saffarian and Kirchhausen, 2009; Mattheyses et al., 2011; Doyon et al., 2011; Nakatsu et al., 2010). Variations in culture conditions, such as membrane tension, might also alter the biochemical requirements for endocytosis (Boulant et al., 2011). An additional consideration is that TIR-FM visualizes primarily the bottom surface of the cell, which is attached to a secreted extracellular matrix (ECM) on the coverslip. Clathrin forms both defined CCPs as well as larger and pleiomorphic “plaques” on this surface, and that the morphology and dynamics of these plaques are distinct from that of CCPs

(Saffarian and Kirchhausen, 2009). However, the dynamics of CCPs on the bottom and the top surfaces seem broadly similar (Saffarian and Kirchhausen, 2009). While it is arguable as to which surface best represents the membranes of cells in a three-dimensional ECM, such as neurons in the brain, extensive data suggest that GPCRs robustly cluster in response to agonists on both the attached and the free surface (Goodman et al., 1996; Shenoy et al., 2007; N'Diaye et al., 2008).

While these methodological constraints are certainly to be noted, we believe that the differences in CCP lifetimes we observe after MOR activation are unlikely to be a result of such changes. First, the changes we see are acute, and are observed seconds after agonist addition (Fig 1-2B-E). Second, the changes are largely restricted to CCPs that show detectable MOR concentration over background (Fig 1-2F,G). Third, these changes are not seen with related GPCRs like DOR, and are abolished by mutating two residues on MOR (MOR-LLAA, Fig 1-2H-J). Fourth, there is a detectable difference in endocytic kinetics between MOR and MOR-LLAA, even in assays not restricted to the bottom surface of the cell (Fig S1-6). Fifth, we have restricted our analyses to diffraction limited spots that we can resolve as appearing and disappearing within the time frame of the movie, thereby excluding the majority of plaques. Together, therefore, while the absolute lifetimes that we propose might vary depending on experimental conditions, our results support the conclusion that clustering of MOR in CCPs acutely pauses CCPs, indicating cargo-mediated regulation of CCP behavior by

MOR. How does MOR pause CCPs? Our results suggest that this requires clustering of MOR into CCPs, and that this is not a general downstream effect of MOR signaling. First, the increase in lifetimes was restricted to a subset of CCPs (Fig 1-2B and E). Second, only the subset of CCPs containing detectable MOR clusters showed a noticeable increase in lifetimes (Fig 1-2F). Third, the increase in CCP lifetimes correlated to the intensity of MOR clusters (Fig 1-2G). Fourth, the delay was dependent on a specific sequence motif on the C-terminal tail of MOR (Fig 1-2 H-J). The latter two observations suggest a stoichiometric effect of interactions of the MOR tail in pausing CCPs. Locally clustered MOR possibly regulates the activity of the scission module of endocytosis (Fig 1-4), without affecting the clathrin assembly rate, the total amount of clathrin, or the recruitment of dynamin (Fig 1-3). In MOR-containing CCPs, we observed dynamin recruitment after the end of the clathrin assembly phase at various points in the pause phase (example in Fig 1-4E, G). However, once dynamin was recruited, its lifetimes were significantly increased in MOR-containing CCPs (Fig 1-4D, F). At present, we cannot rule out an additional effect of MOR on the recruitment of the dynamin scission machinery, as the delay in dynamin lifetimes does not precisely match the increased CCP lifetimes. However, our results suggest an active role for interactions of the C-terminal "bileucine" domain of MOR in pausing the progress of CCPs to vesicle scission even after recruitment of the scission machinery. This provides a novel example for regulation of CCP lifetimes by a G protein-coupled signaling receptor (GPCR), and suggests that

cargo-mediated regulation is a general mode of endocytic control by signaling receptors. GPCRs likely work in both initiating CCPs via clustering of the cargo adapters arrestin and AP2 (Santini et al., 1998) and in controlling the dynamics of later steps in CCP assembly and scission. The only other known example of cargo-mediated control by a signaling receptor, the beta 2-adrenergic receptor (B2AR), delayed CCPs using local interactions of its C-terminal PDZ- interacting domain to the cytoskeleton (Puthenveedu and von Zastrow, 2006). Several observations suggest that MOR uses a mechanism distinct from B2AR for pausing CCPs. The B2AR significantly delayed the recruitment of dynamin, while MOR did not. Once dynamin was recruited, B2AR did not affect the time it took to cause vesicle scission, while MOR significantly delayed its lifetimes (Fig 1-4D-G). Further, MOR does not have an identified PDZ ligand, nor is there any evidence that the cytoplasmic tail of MOR can interact with actin. Together, these results suggest that GPCRs can control endocytosis at least at two separate points, with B2AR delaying recruitment of dynamin, and MOR pausing CCPs after dynamin recruitment (Fig 1-4I).

Recent evidence also suggests that different modules in the CCP cycle are cooperative, and that there is complex feedback between dynamin, actin, and other CCP components that act during fission (Taylor et al., 2012; Shin et al., 2008; Ferguson et al., 2009; Meinecke et al., 2013). At present, it is not clear how any of these observed mechanisms modify dynamin lifetimes. One possibility is that MOR modifies dynamin's GTPase activity, as has been proposed for the

adapter protein TTP (Tosoni et al., 2005). However, since dynamin is an assembly-regulated GTPase, its regulation is likely to involve multiple input mechanisms (Ferguson and De Camilli, 2012; Schmid and Frolov, 2011). This leads to the alternate possibility that MOR coordinates the cooperative feedback between different CCP modules, as opposed to the activity of a single component. This might include the scission, uncoating, and actin machineries. In any case, along with PDZ ligands, this suggests multiple divergent cargo-mediated "checkpoints" in the CCP cycle that control vesicle scission.

Such cargo-mediated regulation likely has significant physiological consequences on cellular signaling by GPCRs. The outcomes of receptor endocytosis on cellular sensitization to signals are well established (e.g., reviewed in Sorkin and von Zastrow, 2009; Martini and Whistler, 2007). In addition to the initial G-protein mediated signaling, many GPCRs can induce a distinct signaling pathway after they bind arrestin (Lefkowitz and Shenoy, 2005; Calebiro et al., 2009). Arrestin association with the plasma membrane is sufficient to induce this mode of signaling, and, in the case of GPCR- mediated recruitment of arrestin, the relative strengths of these different phases of signaling often depend on the activating ligand (Terrillon et al., 2004; Reiter et al., 2012). In the case of MOR, arrestin is released immediately upon vesicle scission, suggesting that cargo-mediated signaling might control the second phase of GPCR signaling. Considering that practically all known GPCRs share common trafficking components, including arrestin (Hanyaloglu and von Zastrow,

2008; Pierce et al., 2002), and that multiple receptors are activated concomitantly in many cells, the dynamics of individual CCPs may therefore determine the extent of each phase of signaling by controlling the time that each receptor spends bound to each signaling complex (e.g., arrestin). The divergent modes of CCP regulation identified here therefore likely is a critical aspect of normal signal integration, as it can maintain selective control over different phases of signaling pathways evoked by GPCRs.

While our studies were performed in heterologous systems expressing exogenous receptors, such systems have been established in the field as excellent models to study the molecular mechanisms underlying GPCR behavior, and the principles identified have largely been validated in more complex systems (Hanyaloglu and von Zastrow, 2008; Pierce et al., 2002; Magalhaes et al., 2012; Marchese et al., 2008). In our opinion, the fact that we observe CCP regulation by exogenous GPCRs in HEK293 cells suggests that these cells have the required machinery for cargo-mediated control of CCPs, and, importantly, that CCP delay is likely a general mechanism across cell types. However, while it is clear that GPCRs cluster and internalize in the brain in vivo, the extent of CCP regulation by MOR and related GPCRs in the brain, especially in the context of endogenous levels of receptors, and whether there are distinct physiological consequences in these cells, remain to be tested.

At the broad cell biological level, our results suggest that cargo molecules in general are far more active players in endocytosis than was previously

appreciated. Some cargo can nucleate and stabilize CCPs early (Loerke et al., 2009; Ehrlich et al., 2004), arguably without affecting further dynamics of stabilized CCPs, while others can control CCP dynamics by regulating key core components (Puthenveedu and von Zastrow, 2006; Mettlen et al., 2010; Tosoni et al., 2005). Sequestration of cargo in subsets of CCPs, followed by regulation of those CCPs by cis-sequence determinants on the cargo molecules themselves, allows for nearly unlimited biochemical and functional specialization of CCPs that otherwise share the same trafficking proteins. Emerging data suggest that, in addition to CCPs, GPCR cargo can also influence trafficking at the endosome by regulating the kinetics of the Rab4-dependent recycling pathway (Yudowski et al., 2009). Such functional specialization of trafficking microdomains, generated on demand and regulated by cargo proteins themselves, might provide a general theme to explain the long-standing question as to how cells can constantly transport hundreds of different cargo using shared trafficking components, without significant competition and inhibition between different proteins.

Materials and Methods

Constructs, Cell, and Reagents

Tagged dynamin, clathrin, cortactin, and MOR constructs have been described earlier (Yu et al., 2010; Puthenveedu and von Zastrow, 2006; Puthenveedu et al., 2010). CALM- and NECAP-mCherry constructs were purchased from Addgene (Taylor et al., 2011). HEK 293 cells (ATCC) stably expressing either SSF-MOR or

SpH-MOR and mutants were generated by selection using Geneticin or Zeocin (Invitrogen) as per manufacturer's instructions. Components of the endocytic machinery were transiently transfected using Effectene (Qiagen), and imaged 3-5 days after transfection. Cells were maintained in DMEM with 10% FBS. DAMGO, DADLE, and isoproterenol were purchased (Sigma) and used at 10μM from a 10mM frozen stock. Pitstop 2 was purchased from Abcam.

Microscopy and Image analysis

Cells were imaged using a Nikon Eclipse Ti automated inverted microscope equipped for through-the-objective TIR-FM, and outfitted with a temperature, humidity, and CO_2 controlled chamber. Images were acquired with an iXon+ 897 EM-CCD camera with solid-state lasers of 488, 561, and 647 nm as light sources. The cells were imaged live in Opti-MEM (Invitrogen) with 30mM HEPES and 10% FBS, using a 100x or 60x 1.45 NA TIRF objective (Nikon). Time-lapse movies were collected as tiff stacks and analyzed in ImageJ. For estimating surface receptor fluorescence, Sph-MOR or labeled SSF-MOR cells were imaged for 5 min before DAMGO and 5 min after DAMGO, capturing every three seconds. A 50x50 pixel box in the center of the cell was used to measure fluorescence changes over time, to avoid errors due to changes in cell shape. CCP lifetimes were estimated as described (Puthenveedu and von Zastrow, 2006). Peak fluorescence values of clathrin or dynamin were measured by either of two methods. To analyze a larger number of CCPs, maximum intensity projections of time- lapse movies corresponding to 15 sec each taken before vs.

after exposure to DAMGO, from multiple cells, were analyzed to detect CCPs containing MOR clusters. The corresponding clathrin or dynamin fluorescence were compared to CCPs in the same cells that did not colocalize with MOR clusters. The box plots shown represent cumulated data from >500 CCPs from multiple cells in each case. For obtaining p values, average values were calculated from individual cells, and a T-test was performed across the averages obtained from multiple cells in the two different conditions. These measurements were further confirmed by tracking the fluorescence values of multiple individual CCPs over time, and detecting the peak fluorescence values in these CCPs over their entire lifetimes. Kymographs were obtained by reslicing a region of the cell and maximum intensity projections. Automated tracking of CCPs was performed on the same datasets using the Spots function in Imaris (Bitplane) to detect clathrin fluorescence, and MOR fluorescence was measured on each of these tracks. Raw data sets are shown. These tracks were manually verified in a few cases to explain the difference between the lifetimes observed. All fluorescence quantitations were done on images directly acquired from the camera with no manipulation or adjustments. Simple image math and statistical analyses were done using Microsoft Excel, and curve fits and ANOVA were done using Graphpad Prism.

ACKNOWLEDGEMENTS

We thank S. Bowersox and C. Almaguer for technical help and comments on the manuscript, Dr. M. von Zastrow for essential advice, help, and reagents, Drs. A.D. Linstedt, T.H. Lee, S. Mukhopadhyay, G. Romero, P. Friedman, and P McPherson for advice and critique, C. Szalinski for help with Imaris, and D. Shiwarski, R. Vistein, and Dr. A.G. Henry for valuable comments and discussion. This work was supported by NIH grant DA024698 to M.A.P.

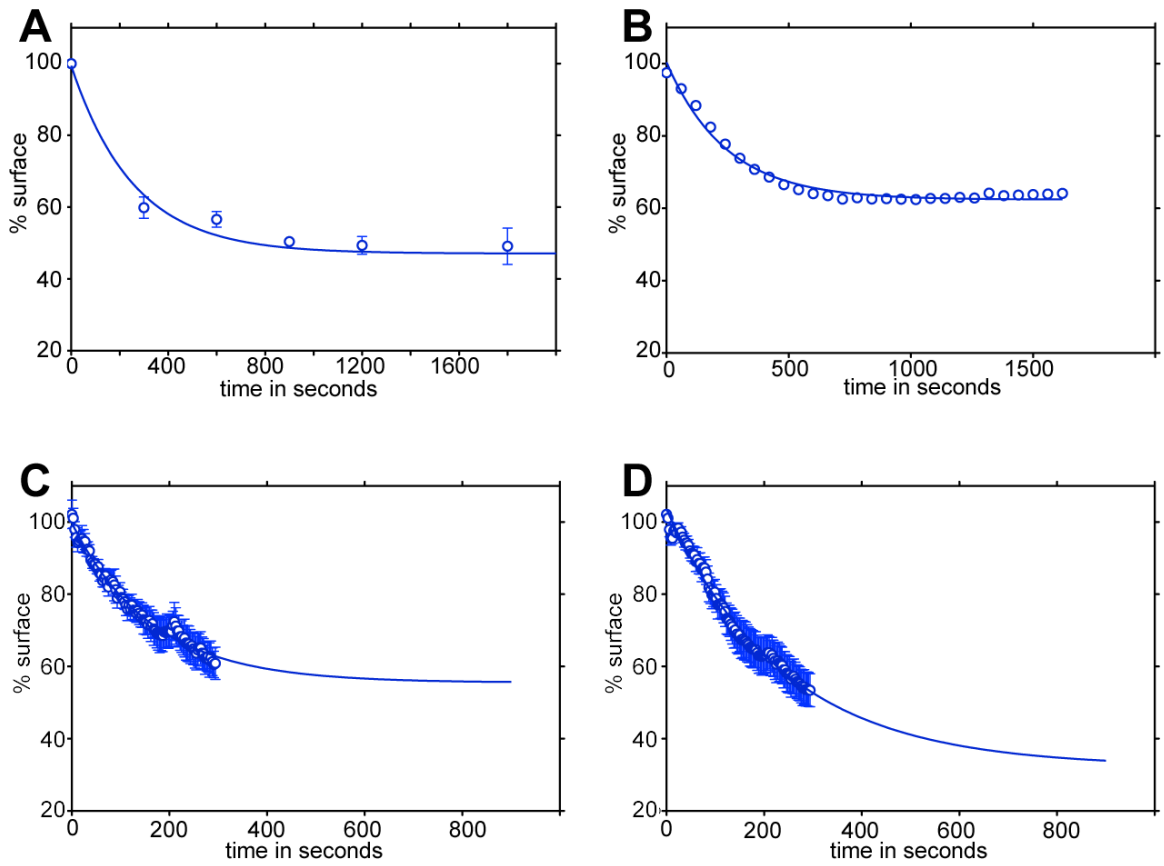

Figure S1-1. Surface MOR fluorescence is rapidly lost in response to DAMGO. A) Flow cytometric analysis of ~50,000 cells at each time point with 5 min time resolution. The curve fits to a single phase decay, with a t1/2 of 178 seconds (R2 =0.96, d.f.=4, Sy,x=4.8). B) Analysis of the change in surface fluorescence of SpH-MOR by live cell imaging, similar to Fig S1-6, over approximately 600 cells over time. The curve fits to a single phase decay with a t1/2 of 221 seconds (R2 = 0.98, d.f.= 25, Sy,x = 1.4). C) Loss of SpH-MOR fluorescence from the surface measured by TIR-FM (n=10) fit to a single-phase decay with a t1/2 = 115 seconds (R2 = 0.98, d.f. = 96, Sy,x = 1.32) D) TIR-FM based quantitation of loss of fluorescence of FLAG-tagged MOR from the cell surface (n=15) with a time resolution of 3 seconds. Loss of fluorescence fit well to a single-phase decay with comparable kinetics as seen with SpH-MOR (t1/2 = 166 seconds, R2 = 0.98, d.f. = 96, Sy,x = 1.68). Error bars are s.e.m.

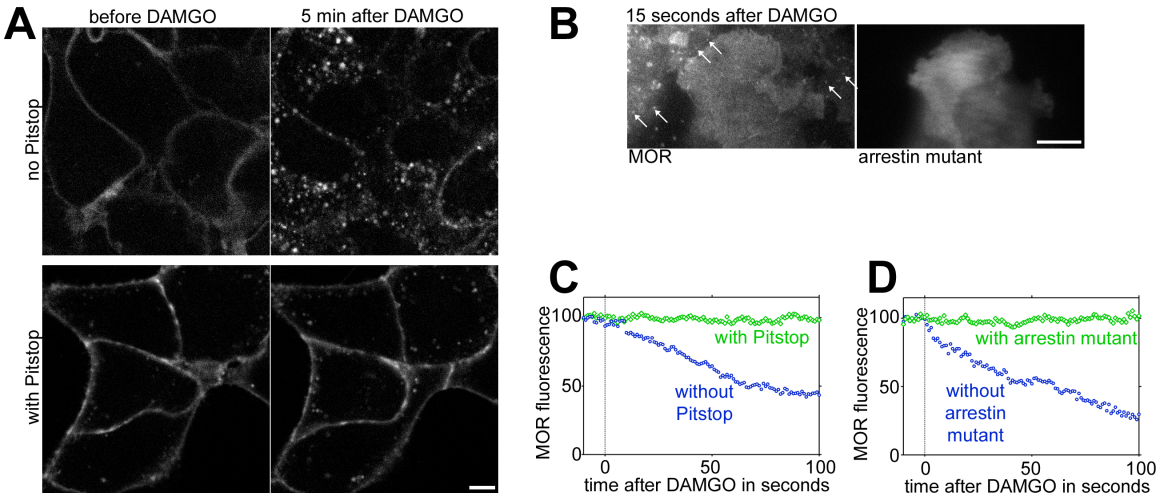

Figure S1-2. MOR endocytosis is predominantly clathrin-dependent. A) Confocal images of FLAG-MOR expressing cells before vs. 5 min after DAMGO, in the presence or absence of Pitstop2, a selective clathrin inhibitor. Pitstop2 prevented DAMGO induced MOR internalization and redistibution into endosomes. B) TIRFM image of a cell expressing a dominant negative arrestin-2 that lacks the clathrin-binding domains, 15 seconds after DAMGO. This arrestin binds MOR, but fails to recruit them to CCPs. In contrast to adjacent cells showing clusters (arrows), the arrestin-expressing cell failed to cluster MOR. C and D) SpH-MOR fluorescence plotted across time from cells exposed to Pitstop (green diamonds in C) or expressing the dominant negative arrestin (green diamonds in D), compared to control cells (blue circles), showing lack of endocytosis when clathrin-mediated endocytosis or receptor localization to CCPs is inhibited. Scale bars are 10μM.

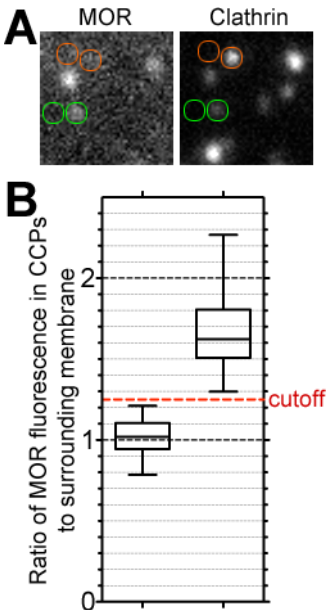

Figure S1-3. Criteria for detection of MOR concentration in CCPs. A) Example TIR-FM image of MOR and clathrin. To quantitate MOR concentration, a circular ROI of the same size (6 px diameter) was drawn around the clathrin spot and a adjacent region without clathrin. The ratio of the MOR fluorescence in the region of the CCP to the adjacent region was then calculated. In this example, the magenta circles show a CCP without detectable MOR concentration, while the green circles denote a CCP with detectable MOR concentration. B) Tukey box plots of the distribution of ratios of MOR fluorescence from an example cell, with the dotted line denoting the cutoff (25%) for classifying whether a CCP had detectable MOR concentration.

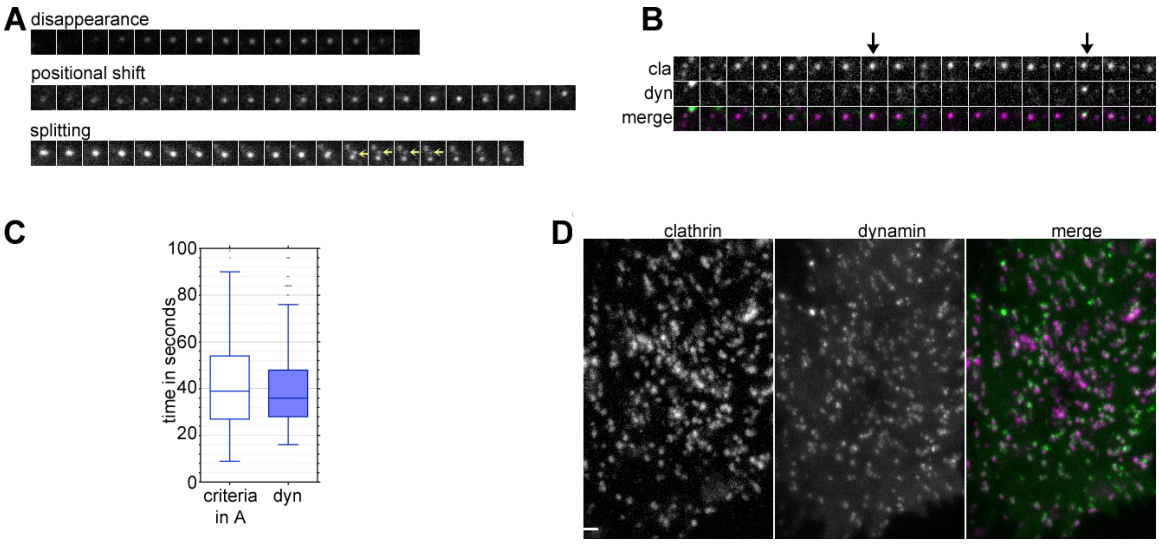

Figure S1-4. Criteria for detection of endocytic CCPs and quantitation of lifetimes. A) Time lapse images from example CCPs showing the three modes of endocytosis as detected by the behavior of clathrin fluorescence. Arrows show a CCP splitting off from a clathrin spot. Frames are every 3 sec. B) Time lapse images from a dual color movie with clathrin (magenta) and dynamin (green), showing a typical spike in dynamin fluorescence immediately before scission. In this example, two scission events are shown (noted by arrows), with a second CCP generated at the same spot after the first scission event. C) Tukey box plots comparing the CCP lifetimes classified based on the criteria in A or on the appearance of dynamin to define scission show no significant difference ($n > 200$ in each case). D) Maximum intensity projections from a 3 minute period of a dual color TIR-FM movie, showing that most of the CCPs show a detectable dynamin spot, indicating that they are productive. Scale bar is 10 μM.

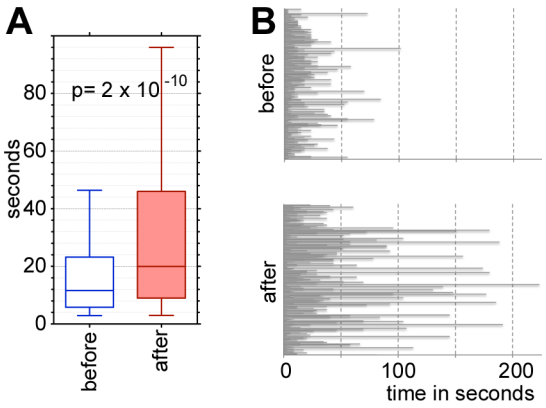

Figure S1-5. CCP lifetimes quantitated using automated spot tracking show an increase after DAMGO. A) Tukey box plots of CCP lifetimes, detected using automated spot tracking, before vs. after DAMGO show a significant increase in the lifetimes. B) Raw plot of the lifetimes (X axis) detected before vs. after DAMGO in an example cell, without binning, show an increased number of CCPs with longer lifetimes.

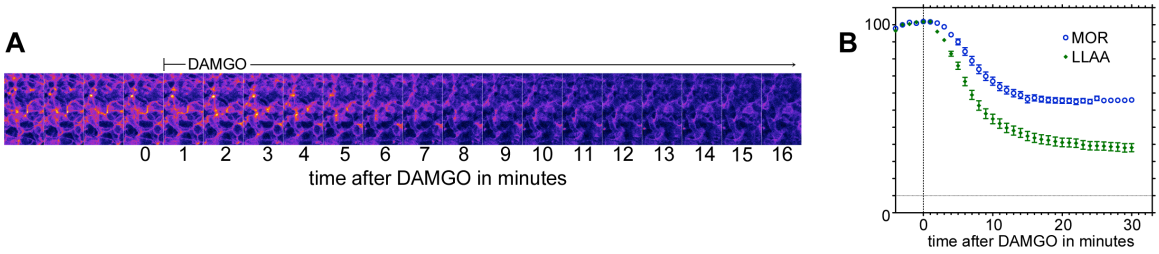

Figure S1-6. MOR-LLAA internalizes faster compared to MOR. A) Heatmap representation of time lapse confocal images of cells expressing SpH-MOR, showing loss of surface fluorescence after addition of DAMGO. B) Quantitation of change in fluorescence for SpH-MOR or SpH-MOR-LLAA after DAMGO addition, showing faster internalization of MOR-LLAA. Error bars are s.e.m.

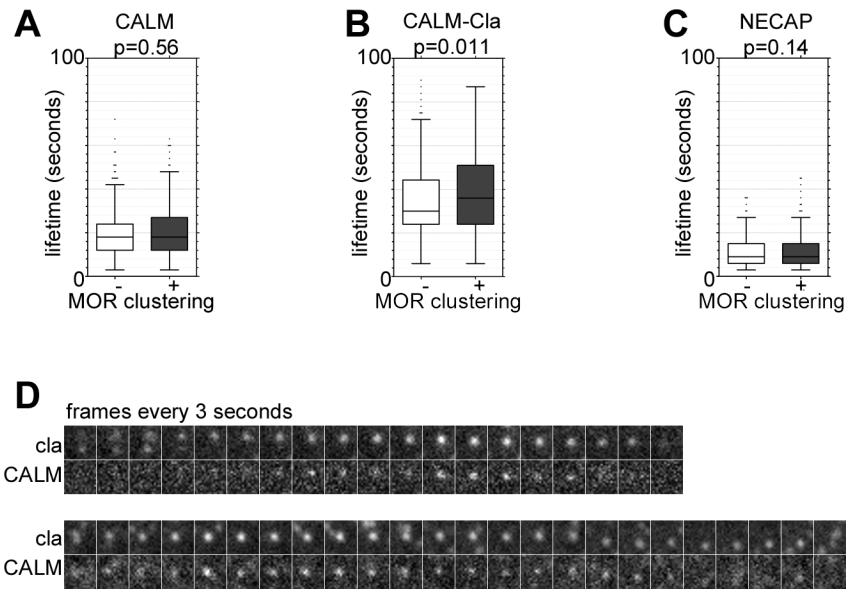

Figure S1-7. CALM and NECAP lifetimes do not show a comparable increase with clathrin after DAMGO. A-C) Tukey box plots of CALM-mCherrry lifetimes in MOR-expressing cells (A), CALM-mCherry lifetimes in cells expressing MOR and clathrin (B), and NECAP-mCherry lifetimes in MOR-expressing cells (C), before vs. after DAMGO. D) Time lapse images from dual color TIR-FM in cells expressing clathrin-GFP and CALM-mCherry, showing shorter CALM lifetimes than clathrin.

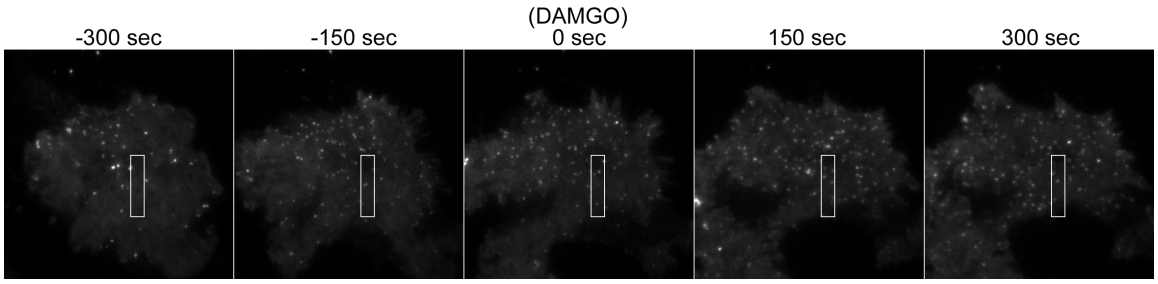

Figure S1-8. Dynamin GFP expression in cells over time. Time lapse images from a representative cell before and after DAMGO, showing no noticeable changes in cell shape. The box shows the region from which the kymograph in Fig 1-4C was derived.

References

Batchelder, E.M., and Yarar, D. (2010). Differential requirements for clathrin-dependent endocytosis at sites of cell-substrate adhesion. Mol Biol Cell 21, 3070-79.

Boettner, D.R., Chi, R.J., and Lemmon, S.K. (2012). Lessons from yeast for clathrin- mediated endocytosis. Nat Cell Biol *14*, 2-10.

Boulant, S., Kural, C., Zeeh, J.C., Ubelmann, F., and Kirchhausen, T. (2011). Actin dynamics counteract membrane tension during clathrin-mediated endocytosis. Nat Cell Biol 13, 1124-131.

Calebiro, D., Nikolaev, V.O., Gagliani, M.C., de Filippis, T., Dees, C., Tacchetti, C., Persani, L., and Lohse, M.J. (2009). Persistent cAMP-signals triggered by internalized G-protein-coupled receptors. PLoS Biol *7*, e1000172.

Doyon, J.B., Zeitler, B., Cheng, J., Cheng, A.T., Cherone, J.M., Santiago, Y., Lee, A.H., Vo, T.D., Doyon, Y., et al. (2011). Rapid and efficient clathrin-mediated endocytosis revealed in genome-edited mammalian cells. Nat Cell Biol 13, 331-37.

Ehrlich, M., Boll, W., Van Oijen, A., Hariharan, R., Chandran, K., Nibert, M.L., and Kirchhausen, T. (2004). Endocytosis by random initiation and stabilization of clathrin- coated pits. Cell *118*, 591-605.

Ferguson, S.M., and De Camilli, P. (2012). Dynamin, a membrane-remodelling GTPase. Nat Rev Mol Cell Biol *13*, 75-88.

Ferguson, S.M., Ferguson, S., Raimondi, A., Paradise, S., Shen, H., Mesaki, K., Ferguson, A., Destaing, O., Ko, G., et al. (2009). Coordinated actions of actin and BAR proteins upstream of dynamin at endocytic clathrin-coated pits. Dev Cell *17*, 811-822.

Goodman, O.B.J., Krupnick, J.G., Santini, F., Gurevich, V.V., Penn, R.B., Gagnon, A.W., Keen, J.H., and Benovic, J.L. (1996). Beta-arrestin acts as a clathrin adaptor in endocytosis of the beta2-adrenergic receptor. Nature 383, 447-450.

Hanyaloglu, A.C., and von Zastrow, M. (2008). Regulation of GPCRs by endocytic membrane trafficking and its potential implications. Annu Rev Pharmacol Toxicol *48*, 537-568.

Kaksonen, M., Peng, H.B., and Rauvala, H. (2000). Association of cortactin with dynamic actin in lamellipodia and on endosomal vesicles. J Cell Sci *113 Pt 24*,

4421-6.

Kang, D.S., Kern, R.C., Puthenveedu, M.A., von Zastrow, M., Williams, J.C., and Benovic, J.L. (2009). Structure of an arrestin2-clathrin complex reveals a novel clathrin binding domain that modulates receptor trafficking. J Biol Chem 284, 29860-872.

Keith, D.E., Murray, S.R., Zaki, P.A., Chu, P.C., Lissin, D.V., Kang, L., Evans, C.J., and von Zastrow, M. (1996). Morphine activates opioid receptors without causing their rapid internalization. J Biol Chem *271*, 19021-4-.

Kelly, B.T., and Owen, D.J. (2011). Endocytic sorting of transmembrane protein cargo. Curr Opin Cell Biol *23*, 404-412.

Kim, J.A., Bartlett, S., He, L., Nielsen, C.K., Chang, A.M., Kharazia, V., Waldhoer, M., Ou, C.J., Taylor, S., et al. (2008). Morphine-induced receptor endocytosis in a novel knock-in mouse reduces tolerance and dependence. Curr Biol *18*, 129-135.Koch, T., and Höllt, V. (2008). Role of receptor internalization in opioid tolerance and

dependence. Pharmacol Ther *117*, 199-206.Lefkowitz, R.J., and Shenoy, S.K. (2005). Transduction of receptor signals by beta-arrestins. Science *308*, 512-7-.

Loerke, D., Mettlen, M., Yarar, D., Jaqaman, K., Jaqaman, H., Danuser, G., and Schmid, S.L. (2009). Cargo and dynamin regulate clathrin-coated pit maturation. PLoS Biol *7*, e57.

Magalhaes, A.C., Dunn, H., and Ferguson, S.S. (2012). Regulation of GPCR activity, trafficking and localization by GPCR-interacting proteins. Br J Pharmacol *165*, 1717- 736.

Marchese, A., Paing, M.M., Temple, B.R., and Trejo, J. (2008). G protein-coupled receptor sorting to endosomes and lysosomes. Annu Rev Pharmacol Toxicol *48*, 601- 629.

Maritzen, T., Koo, S.J., and Haucke, V. (2012). Turning CALM into excitement: AP180 and CALM in endocytosis and disease. Biol Cell

Martini, L., and Whistler, J.L. (2007). The role of mu opioid receptor desensitization and endocytosis in morphine tolerance and dependence. Curr Opin Neurobiol *17*, 556-64-.

Matthes, H.W., Maldonado, R., Simonin, F., Valverde, O., Slowe, S., Kitchen, I., Befort, K., Dierich, A., Le Meur, M., et al. (1996). Loss of morphine-induced analgesia, reward effect and withdrawal symptoms in mice lacking the mu-opioid-receptor gene. Nature *383*, 819-823.

Mattheyses, A.L., Atkinson, C.E., and Simon, S.M. (2011). Imaging single endocytic events reveals diversity in clathrin, dynamin and vesicle dynamics. Traffic 12, 1394- 1406.

McMahon, H.T., and Boucrot, E. (2011). Molecular mechanism and physiological functions of clathrin-mediated endocytosis. Nat Rev Mol Cell Biol *12*, 517-533.

Meinecke, M., Boucrot, E., Camdere, G., Hon, W.C., Mittal, R., and McMahon, H.T. (2013). Cooperative Recruitment of Dynamin and BIN/Amphiphysin/Rvs (BAR) Domain- containing Proteins Leads to GTP-dependent Membrane Scission. J Biol Chem 288, 6651-661.

Merrifield, C.J., Feldman, M.E., Wan, L., and Almers, W. (2002). Imaging actin and dynamin recruitment during invagination of single clathrin-coated pits. Nat Cell Biol *4*, 691-98.

Mettlen, M., Loerke, D., Yarar, D., Danuser, G., and Schmid, S.L. (2010). Cargo- and adaptor-specific mechanisms regulate clathrin-mediated endocytosis. J Cell Biol *188*, 919-933.

Meyerholz, A., Hinrichsen, L., Groos, S., Esk, P.C., Brandes, G., and Ungewickell, E.J. (2005). Effect of clathrin assembly lymphoid myeloid leukemia protein depletion on clathrin coat formation. Traffic *6*, 1225-234.

Miesenbock, G., De Angelis, D.A., and Rothman, J.E. (1998). Visualizing secretion and synaptic transmission with pH-sensitive green fluorescent proteins. Nature *394*, 192-5-.

Moore, C.A., Milano, S.K., and Benovic, J.L. (2007). Regulation of receptor trafficking by GRKs and arrestins. Annu Rev Physiol *69*, 451-482.

Nakatsu, F., Perera, R.M., Lucast, L., Zoncu, R., Domin, J., Gertler, F.B., Toomre, D., and De Camilli, P. (2010). The inositol 5-phosphatase SHIP2 regulates endocytic clathrin-coated pit dynamics. J Cell Biol 190, 307-315.

N'Diaye, E.N., Hanyaloglu, A.C., Kajihara, K.K., Puthenveedu, M.A., Wu, P., von Zastrow, M., and Brown, E.J. (2008). The ubiquitin-like protein PLIC-2 is a negative regulator of G protein-coupled receptor endocytosis. Mol Biol Cell 19, 1252-260.

Pierce, K.L., Premont, R.T., and Lefkowitz, R.J. (2002). Seven-transmembrane receptors. Nat Rev Mol Cell Biol *3*, 639-50-.

Puthenveedu, M.A., and von Zastrow, M. (2006). Cargo regulates clathrin-coated pit dynamics. Cell *127*, 113-124.

Puthenveedu, M.A., Lauffer, B., Temkin, P., Vistein, R., Carlton, P., Thorn, K., Taunton, J., Weiner, O.D., Parton, R.G., and von Zastrow, M. (2010). Sequence-dependent sorting of recycling proteins by actin-stabilized endosomal microdomains. Cell *143*, 761- 773.

Rao, Y., Rückert, C., Saenger, W., and Haucke, V. (2012). The early steps of endocytosis: from cargo selection to membrane deformation. Eur J Cell Biol *91*, 226- 233.

Reiter, E., Ahn, S., Shukla, A.K., and Lefkowitz, R.J. (2012). Molecular mechanism of β- arrestin-biased agonism at seven-transmembrane receptors. Annu Rev Pharmacol Toxicol *52*, 179-197.

Ritter, B., Denisov, A.Y., Philie, J., Allaire, P.D., Legendre-Guillemin, V., Zylbergold, P., Gehring, K., and McPherson, P.S. (2007). The NECAP PHear domain increases clathrin accessory protein binding potential. EMBO J *26*, 4066-077.

Saffarian, S., and Kirchhausen, T. (2009). Distinct Dynamics Of Endocytic Clathrin Coated Pits And Coated Plaques. Biophys J 96, 569-570.

Shenoy, S.K., Barak, L.S., Xiao, K., Ahn, S., Berthouze, M., Shukla, A.K., Luttrell, L.M., and Lefkowitz, R.J. (2007). Ubiquitination of beta-arrestin links seven-transmembrane receptor endocytosis and ERK activation. J Biol Chem 282, 29549-562.

Schmid, S.L., and Frolov, V.A. (2011). Dynamin: Functional Design of a Membrane Fission Catalyst. Annu Rev Cell Dev Biol *27*, 1-27.

Segredo, V., Burford, N.T., Lameh, J., and Sadee, W. (1997). A constitutively internalizing and recycling mutant of the mu-opioid receptor. J Neurochem *68*, 2395- 404-.

Shin, N., Ahn, N., Chang-Ileto, B., Park, J., Takei, K., Ahn, S.G., Kim, S.A., Di Paolo, G., and Chang, S. (2008). SNX9 regulates tubular invagination of the plasma membrane through interaction with actin cytoskeleton and dynamin 2. J Cell Sci *121*, 1252-263.

Sorkin, A., and von Zastrow, M. (2009). Endocytosis and signalling: intertwining molecular networks. Nat Rev Mol Cell Biol *10*, 609-622.

Tanowitz, M., and von Zastrow, M. (2003). A novel endocytic recycling signal that distinguishes the membrane trafficking of naturally occurring opioid receptors. J Biol Chem *278*, 45978-986.

Taylor, M.J., Lampe, M., and Merrifield, C.J. (2012). A feedback loop between

dynamin and actin recruitment during clathrin-mediated endocytosis. PLoS Biol *10*, e1001302.

Taylor, M.J., Perrais, D., and Merrifield, C.J. (2011). A high precision survey of the molecular dynamics of mammalian clathrin-mediated endocytosis. PLoS Biol *9*, e1000604.

Terrillon, S., Barberis, C., and Bouvier, M. (2004). Heterodimerization of V1a and V2 vasopressin receptors determines the interaction with beta-arrestin and their trafficking patterns. Proc Natl Acad Sci U S A 101, 1548-53.

Tosoni, D., Puri, C., Confalonieri, S., Salcini, A.E., De Camilli, P., Tacchetti, C., and Di Fiore, P.P. (2005). TTP specifically regulates the internalization of the transferrin receptor. Cell *123*, 875-88.

von Kleist et al. (2011) Role of the clathrin terminal domain in regulating coated pit dynamics revealed by small molecule inhibition. Cell *146,* 471-84.

Wolfe, B.L., and Trejo, J. (2007). Clathrin-dependent mechanisms of G protein-coupled receptor endocytosis. Traffic *8*, 462-470.

Yu, Y.J., Dhavan, R., Chevalier, M.W., Yudowski, G.A., and von Zastrow, M. (2010). Rapid delivery of internalized signaling receptors to the somatodendritic surface by sequence-specific local insertion. J Neurosci *30*, 11703-714.

Yudowski, G.A., Puthenveedu, M.A., Henry, A.G., and von Zastrow, M. (2009). Cargo- mediated regulation of a rapid Rab4-dependent recycling pathway. Mol Biol Cell *20*, 2774-784.

Zhang, B., Koh, Y.H., Beckstead, R.B., Budnik, V., Ganetzky, B., and Bellen, H.J. (1998). Synaptic vesicle size and number are regulated by a clathrin adaptor protein required for endocytosis. Neuron *21*, 1465-475.

Chapter 2: Extension of Clathrin-Coated Pits Exhibit Signaling Changes.

Introduction

The chemical messages that cells receive from both other cells and from the external world define our experiences, and keep us alive. These messages often depend on one cell transmitting a molecular signal, or ligand that must be received by the protein receptors of another cell. Often times, these protein receptors must be present on the cell surface in order to detect the incoming signal. The largest group of these protein receptors are the G-Protein Coupled Receptors or GPCRs. GPCRs convey a large number of signals including taste, sight, smell, pain, adrenaline, serotonin, and opiates. However, this diverse array of receptors converges on the same signaling and trafficking machinery. For example, there are 1265 known GPCRs in the human genome that are coupled to only six G-proteins (Insel et al., 2012). How do GPCRs maintain such diversity of signals when they utilize the same downstream machinery?

One answer is that only certain receptors are present in a cell type. This is certainly true in the olfactory system where each cell only expresses one type of olfactory receptor (Rodriguez, 2013). However, other systems are not so simplistic and the same cell can easily express multiple GPCRs (Insel et al., 2012). In some cases the cell can differentiate between GPCR subtypes because of their different associated G-proteins. The trigeminal-ganglia neurons, for example, co-express the $G_{\alpha/i}$ coupled mu-opioid receptor along with the $G_{\alpha/q}$

coupled neurkinin-1 receptor. Alternatively, both the mu-opioid receptor and the delta opioid receptor, both $G_{\alpha/i}$ coupled receptors can be co-expressed in a subset dorsal root ganglia neurons (Beaudry, Dubois, & Gendron, 2011). It is thought that the two opioid receptors, which have similar functions, can dimerize and work in concert those cells where they are co-expressed (Gomes et al., 2000). However, certain locus coeruleus neurons co-express the mu opioid receptor along with the more distally related canabanoid-1 receptor, another $G_{\alpha/i}$ receptor (Scavone, Mackie, & Van Bockstaele, 2010). Cells must use a different mechanism to discern the signals between these receptors.

A potential mechanism for differentiating GPCR signals is if the cell can take into account not only to what the propagated signals are, but additionally to where the signals are coming from and how long they may last. This positioning of GPCRs is largely dependent on GPCR intracellular trafficking to determine where the receptors are in the cell (Marchese, Paing, Temple, & Trejo, 2008). However this dependency on trafficking also creates a redundancy problem, as most receptors require β-arrestin to mediate their internalization (DeWire, Ahn, Lefkowitz, & Shenoy, 2007). To have a trafficking derived spatial-temporal impact on its signaling, a receptor must be able to impact its own trafficking.

To examine the role that intracellular trafficking may impact on signaling we focused on the clinically relevant mu-opioid receptor (MOR), a receptor that can mediate its own trafficking (Soohoo & Puthenveedu, 2013). The MOR mediates analgesia when activated. Its activity transmits the most potent and

effective analgesics in clinical and research settings (Brownstein, 1993) (Fields, 2011). However, these analgesics are largely addictive (Brownstein, 1993) (Jordan & Devi, 1998) (Fields, 2011). There are diverse arrays of endogenous and exogenous opiate agonists, which activate the receptor. The clear differences in physiological response to these opiates implicates that they must propagate different signals to the cell while using the same receptor (Jordan & Devi, 1998). We sought to determine if changes in trafficking could cause the subsequent changes in downstream signaling between these different agonists.

The trafficking phenomenon we chose to focus on was the clathrin-mediated endocytosis of the MOR. We chose this pathway because we have recently discovered that the MOR has the capacity to impact and change this pathway by extending endocytic dwell times of the individual endocytic events it is present in (Soohoo & Puthenveedu, 2013). In other words, its own individual clathrin-mediated endocytic events take a longer time to fully mature into an internalized vesicle. Furthermore, we learned that the ability for the receptor to impact these events is dependent on a sequence in the C-terminal tail of the receptor. The clathrin-mediated endocytosis (CME) of the MOR begins with the activation of the receptor (Keith et al., 1996) (Segredo, Burford, Lameh, & Sadée, 2002). This activation causes separation of the coupled $G_{\alpha/i}$ protein subsequent signaling (Ueda et al., 1988). The departure of the $G_{\alpha/i}$ opens the cytoplasmic face the MOR for phosphorylation by GRK (Arden, Segredo, Wang, Lameh, & Sadée, 1995). The phosphorylated receptor recruits β-arrestin (Kovoor, Celver,

Wu, & Chavkin, 1998). The function of β-arrestin is two-fold first to act as the endocytosis adaptor for the activated GPCR, and second to act as a signaling scaffold primarily acting through epidermal receptor kinase (ERK1/2). (DeWire et al., 2007) (Lefkowitz, 2004). β-arrestin recruits adaptor protein-2 (AP2) and clathrin to mediate the internalization of the activated MOR (Goodman et al., 1996). CME is a process that involves the timely recruitment over 30 accessory proteins across four basic modules: initiation, coat-formation, vesicle scission and uncoating (Doherty & McMahon, 2009) (McMahon & Boucrot, 2011) (Kaksonen, Toret, & Drubin, 2005) (Taylor, Perrais, & Merrifield, 2011). We have shown the MOR delays the vesicle scission step of CME by prolonging the recruitment of dynamin during endocytosis events. This prolonged dynamin association is very uncharacteristic in the CME process and suggests a deficiency in vesicle scission (Soohoo & Puthenveedu, 2013). It has been shown that β-arrestin disassociates with the receptor at the time of vesicle scission (Oakley, Laporte, Holt, Caron, & Barak, 2000). We inquired to whether the characteristic extension of MOR endocytic dwell times could cause changes in downstream signaling through the β-arrestin scaffold.

Herein, we describe a novel trafficking-dependent-signaling phenomenon for different opiate agonists. We use live-cell total internal reflection fluorescent microscopy (TIR-FM) to show that different agonists lead to differences in endocytic dwell times (EDT) of the receptor. These changes in EDT are propagated to the endocytic adaptor and signaling scaffold, β-arrestin. We also

show that altering EDT through pharmacological and mutational manipulations that downstream ERK1/2 signaling is effected as seen through conventional western blot and live-cell microscopy of a fluorescent resonance energy transfer (FRET)-based sensor. Our FRET analysis has allowed us to further uncover that the increase in ERK1/2 signaling is nuclear based.

Results and Discussion

β-Arrestin exhibits changes in EDT as previously determined for clathrin

To measure the EDT of individual CME events we utilized live-cell TIRF microscopy. This technique allows for visualization of individual CME events as resolution limited spots, as previously described (Puthenveedu & Zastrow, 2006) (Soohoo & Puthenveedu, 2013). The quantifications of EDTs were performed as previous described (Puthenveedu & Zastrow, 2006) (Soohoo & Puthenveedu, 2013). We had previously established that the MOR redistributes into puncta and that these puncta are individual clathrin-coated pits, Fig 2-1A, middle. Beta-arrestin also co-localizes to these endocytic puncta, Figure 2-1A, top and merge. β-arrestin is present in the individual CME events for the same duration as the receptor and clathrin itself. Quantification of β-arrestin EDT are not significantly different from clathrin EDT with the wild type MOR receptor after stimulation with the synthetic enkephalin DAMGO (D-Ala^2, N-MePhe^4, Gly-ol]-enkephalin). Figure 2-1B displays the average EDT for clathrin and β-arrestin as box plots, with

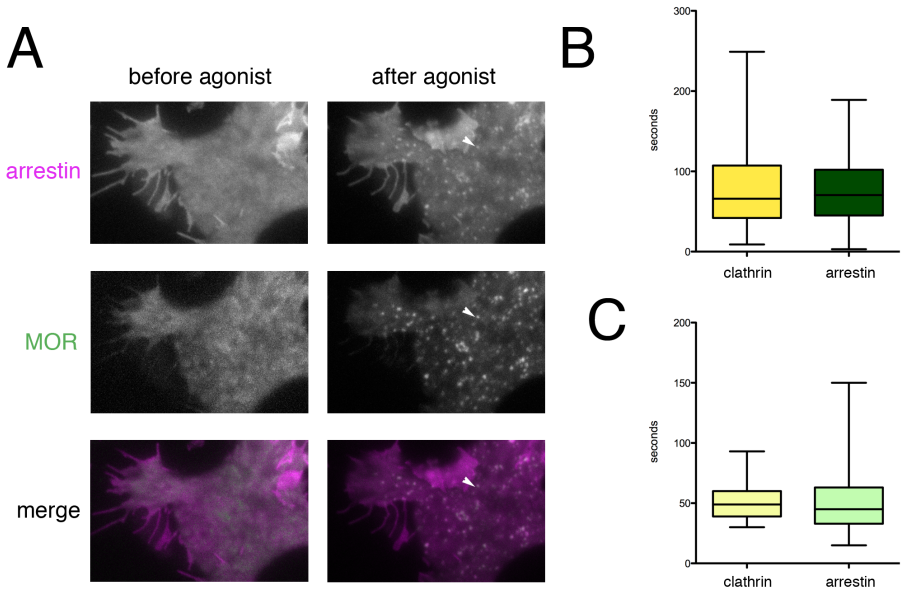

Figure 2-1: Beta-arrestin localizes to extended clathrin-coated pits. A) Images showing the redistribution of β-arrestin and the MOR into endocytic puncta after agonist stimulation. These puncta are highly colocalized. B) The EDT of clathrin and beta-arrestin are not significantly different for the wildtype MOR after agonist stimulation. n = 100, 90 p = 0.71. Box showcases 25-75% percentile, line denotes the median. Whiskers denote 90% and 10% percentiles. B) The EDT of clathrin and beta-arrestin are not significantly different for the LLAA mutant MOR after agonist stimulation. n = 150, 100 p = 0.61. Box showcases 25-75% percentile, line denotes the median. Whiskers denote 90% and 10% percentiles.

the center line designating the median. Additionally, we had previous identified a critical sequence in the C-terminal tail, LENLEAE, that is required for the extension of EDT. Mutation of the LENLEAE sequence to AENAEAE renders (abbreviated as the LLAA mutant) the receptor unable to extend EDT. The β-arrestin EDT for the mutated receptor are comparable to the clathrin EDT for the mutated receptor, displayed as box plots in Figure 2-1B. More importantly, as a whole, the EDT for the LLAA mutant MOR are significantly shorter than the wild type MOR, Figure 2-1C.

Differential β-arrestin EDT with different opiate stimulation

We next tested if the β-arrestin EDT changed with activation of the receptor with different opiate agonists. Activation of the MOR with the enkephalin DAMGO yields a mean dwell time of around 80 seconds as shown in a bar graph in Figure 2-2A, left. We tested the EDT for the endogenous MOR agonist, endomorphin-2. Endomorphin-2 has previously been described as an arrestin-biased ligand, based on its downstream readouts (Rivero et al., 2012). Since the only association of the MOR with β-arrestin is during CME, we hypothesized that endomorphin-2 would exhibit an extended EDT, beyond the enkephalin DAMGO. Our data supported this hypothesis, with the average EDT for endomorphin-2 activated receptors at around 100 seconds, shown in Figure 2-2A, left. We also tested the LLAA mutant with endomorphin-2. Conversely, the LLAA mutant does

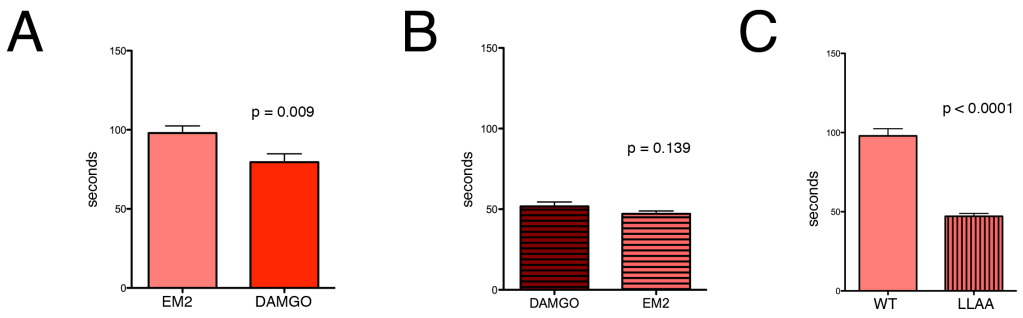

Figure 2-2: Different agonist differently effect EDT of the MOR. A) Activation of the MOR with endomorphin-2 (EM2) extends EDT of beta-arrest beyond MORs stimulated by DAMGO. n = 150, 100. B) EDTs are not significantly different for the LLAA mutant between EM2 and DAMGO activated receptors. n = 100, 150. C) Extension of EDT is very significant between the wild type and LLAA mutants that have been activated by EM2. n = 150, 150. All error bars are s.e,m.

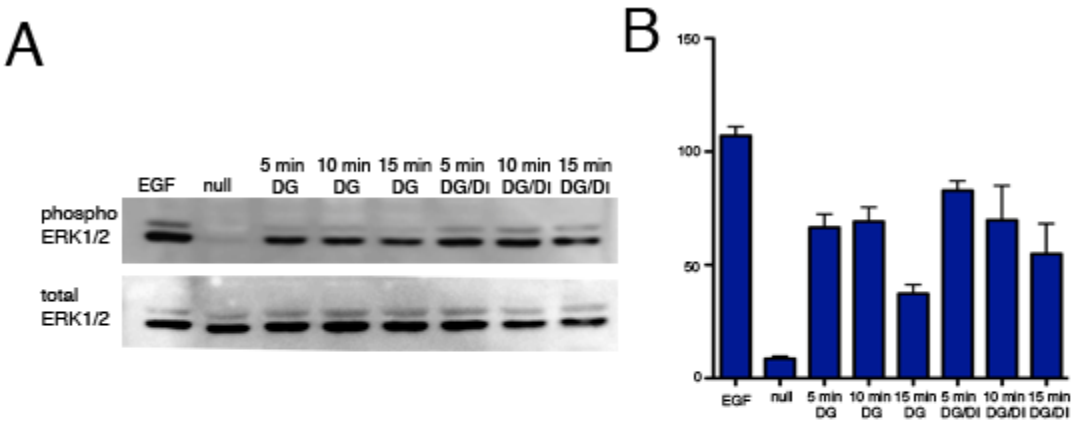

Figure 2-3 Extension of EDT increases EKR1/2 signaling. A) Western blot for phosphorylated ERK1/2 (top) and the re-probed control blot of total ERK1/2 (bottom). HEK293 cells were stimulated with 10μM DAMGO (DG) with or without 30μM dynole, the dynamin inhibitor for 5, 10 or 15 minutes. Cells incubated with dynole showed increased ERK1/2 signaling. All signaling was well above the negative control of null treatment and the positive control of EGF addition. B) Quantification of 3 separate experimental trials for procedure outlined in A. All error bars are s.e.m

not exhibit significantly different beta-arrestin EDT in endomorphin-2 activated cells versus DAMGO activated cells, Figure 2-2B. Likewise, the LLAA mutant exhibits extremely shorter EDT when compared to the wild type receptor, Figure 2-2C.

Differential EDT give different signaling readouts

The canonical readout for β-arrestin signaling is phosphorylated ERK1/2. Previous reports have shown an increase in phosphorlyated-ERK1/2 levels via western blot with extended EDT (Flores-Otero et al., 2014). When we artificially extended MOR EDT with 30μM of the dynamin inhibitor, dynole, we observed a marked increase in phospho-ERK1/2 levels, particularly in ERK1, blot Fig2-3A, quantification across three blots in Fig2-3B.

To further delve into the signaling process we used a FRET-based ERK1/2 sensor, EKAR (Harvey et al., 2008) (Fritz et al., 2013). When ERK is activated it phosphorylates EKAR causes a conformational change that brings the FRET pairs closer together, increasing their FRET signal (Harvey et al., 2008) (Fritz et al., 2013). This sensor allowed for simultaneous read-out of ERK signaling in a live-cell. In these experiments we first serum starved the cells for 4 hours in Leibovitz's L-15 media. Then we activated the receptors with the opiate endomorphin-2, to see an increase in ERK1/2 signaling. As a final binary control for the working sensor we either increase ERK1/2 signaling via EGF. Figure 2-4A shows the FRET/CFP ratios of an example cell before an after stimulation by

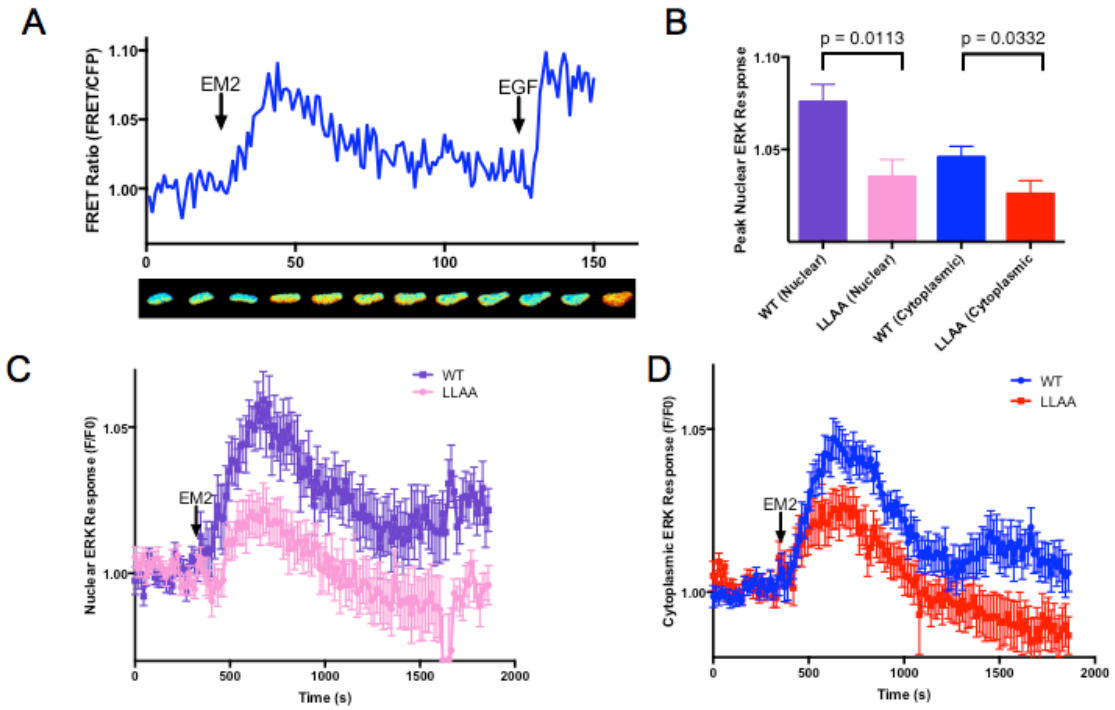

Figure 2-4: Differential EDT result in different EK1/2 signaling. A) EKAR FRET-sensor to visual ERK activity. An example trace (top) of FRET/CFP ratios, normalized to baseline measurements. Increases in ERK signaling can be seen with addition of EM2 and EGF. EGF was used as a binary control for sensor activity. Bottom, montage of nuclear ERK sensor being activated. B) Peak ERK responses for MOR activation with 10μM endomorphin 2 (EM2), measured in both the nucleus and cytoplasm. EM2 causes an increase in ERK activation for both the WT and LLAA variants of MOR, with WT MOR producing stronger ERK activation in both cases, n = 7, 6, 24, 23, respectively. Error is s.e.m. C) Average trace for nuclear ERK activation after EM2 treatment (10μM) in cells stably expressing either WT MOR (purple) or the LLAA mutant of the receptor (pink). Error is s.e.m., EM2 added at 300s. D) Average traces for cytoplasmic ERK activation under same conditions as C for either WT MOR (blue) or LLAA MOR (red). Note that although B only focuses on the peak response, there is a distinct difference in activation across the entire measured timeline in both C and D

endomorphin-2 and EGF. The bottom panels show a montage of the increase in ERK signal with the drug additions, warmer colors indicate an increase in signal.

We compared the peak EKAR sensor readouts between the wild type receptor that exhibits extended EDT and the LLAA mutant, which does not. Both the nuclear localized (Figure 2-4B, left and Figure 2-4C) and the cytoplasmic localized (Figure 2-4B, right and Figure 2-4D) EKAR sensors showed that ERK signaling was clearly correlated with the EDT of the two different receptors. However the difference in signal appears to be much more pronounced through the nuclear localized EKAR sensor. This suggests that the ERK activated through extended EDT is quickly transported to the nucleus. Previous data has shown that β-arrestin signaling through certain MOR agonists results increase in nuclear ERK signaling (Zheng, Loh, & Law, 2008). Our data provides a mechanism for this signaling response. Looking at the average ERK signaling over time shows a clear increase in not only peak ERK signaling of wild type receptor over the LLAA mutant but an increase the duration of ERK signaling, Figure 2-4C-D.

The clinically relevant MOR is capable of mediating a unique trafficking phenomenon through its extension of EDT. This extension of EDT is tightly regulated and is dependent on a sequence on the receptor and the agonist used to activate the receptor. This work implies a physiological consequence for this tight regulation of a trafficking phenomenon, as we have shown that these changes in EDT can differentiate downstream signaling through both Western blot and a FRET-based sensor. We have pinpointed this change in signaling to

an increase in the nuclear pool of ERK. Overall, our work suggests that subtle changes in confirmations brought on by different agonists can affect both the trafficking and signaling of the receptor and create a distinct signal for the cell to interpret.

Methods

Cell culture

HEK293 cells were grown in High Glucose DMEM with 10% fetal bovine serum in a 37°C incubator with 5% CO_2. Before any signaling experiments the cells were serum starved for 4 hours in Leibovitz's L-15 medium. Cells were selected to stably express the MOR and the LLAA mutant. All other constructs were transiently transfected using Effectene and imaged 48-72 hours later.

Live-cell total internal fluorescent microscopy

Images were acquired using a iXon+ 897 electron-multiplying charge-coupled device camera using solid state 405, 488, 515, 561 and 647 nm lasers on a Nikon Eclipse Ti inverted microscope. The cells were imaged through a Nikon 60x/1.45 NA TIRF objective. EDT were captured at 0.3 Hz using through-the-objective TIR-FM. EKAR images were collected every 15 seconds using the same objective outside of the critical angle for whole-field epi-fluoresence. The cells were imaged in Leibovitz's L-15 medium, supplemented with 5% fetal bovine serum during the EDT experiments. Serum was absent during the EKAR

experiments. All analysis was done on raw 16-bit images. The microscope was outfitted with a temperature, humidity and CO_2 controlled chamber.

Western blot

Cells were seeded 48 hours before the experimental procedure in separate 35mm flat-bottom tissue culture dishes. Cells were serum starved for 4 hours in Leibovitz's L-15 medium to bring the baseline of ERK signaling down. One subset of cells were treated with 10μM DAMGO alone for 5, 10 and 15 minutes. Another subset was exposed to DAMGO and 30μM dynole for 5, 10, and 15 minutes. A null treatment and EGF treated cells served as the negative and positive controls. The cells were lysed in 10 mM Hepes, 150 mM NaCl, 1 mM EGTA, 0.1 mM MgCl2, 0.5% Triton-X at pH 7.4. The lysate concentrations were assayed via Bradford and an equal amount was loaded to each well. The samples were run on an 8% SDS-Page gel at 120V. The gel was transferred to a 0.4μm nitrocellulose membrane overnight at 35V at 4°C in a wet transfer apparatus. The membrane was blocked for 1hr at 4°C with mild agitation in 5% BSA in TBST with phosphatase inhibitors. The primary anti-phosphorylated ERK1/2 was incubated for 1hr at 4°C with mild agitation in 5% BSA in TBST with phosphatase inhibitors. After three washes in TBST the secondary horseradish peroxidase (HRP) conjugated goat-anti-rabbit was incubated for 1hr at 4°C with mild agitiation in 5% BSA in TBST with phosphatase inhibitors. After three washes in TBST and one wash in PBS, the membrane was incubated with HRP

substrate for 5 minutes before imaging. After imaging the membrane was washed with PBS, stripped and re-probed for total ERK1/2 levels using the same procedure.

References

Arden, J. R., Segredo, V., Wang, Z., Lameh, J., & Sadée, W. (1995). Phosphorylation and agonist-specific intracellular trafficking of an epitope-tagged mu-opioid receptor expressed in HEK 293 cells. *Journal of Neurochemistry*, *65*(4), 1636–1645.

Beaudry, H., Dubois, D., & Gendron, L. (2011). Activation of spinal mu- and delta-opioid receptors potently inhibits substance P release induced by peripheral noxious stimuli. *Journal of Neuroscience*, *31*(37), 13068–13077. doi:10.1523/JNEUROSCI.1817-11.2011

Brownstein, M. J. (1993). A brief history of opiates, opioid peptides, and opioid receptors. *Proceedings of the National Academy of Sciences of the United States of America*, *90*(12), 5391.

DeWire, S. M., Ahn, S., Lefkowitz, R. J., & Shenoy, S. K. (2007). Beta-arrestins and cell signaling. *Annual Review of Physiology*, *69*, 483–510. doi:10.1146/annurev.ph.69.013107.100021

Doherty, G. J., & McMahon, H. T. (2009). Mechanisms of Endocytosis. *Annual Review of Biochemistry*, *78*(1), 857–902. doi:10.1146/annurev.biochem.78.081307.110540

Fields, H. L. (2011). The Doctor's Dilemma: Opiate Analgesics and Chronic Pain. *Neuron*, *69*(4), 591–594. doi:10.1016/j.neuron.2011.02.001

Flores-Otero, J., Ahn, K. H., Delgado-Peraza, F., Mackie, K., Kendall, D. A., & Yudowski, G. A. (2014). Ligand-specific endocytic dwell times control functional selectivity of the cannabinoid receptor 1. *Nature Communications*, *5*, –. doi:10.1038/ncomms5589

Fritz, R. D., Letzelter, M., Reimann, A., Martin, K., Fusco, L., Ritsma, L., et al. (2013). A Versatile Toolkit to Produce Sensitive FRET Biosensors to Visualize Signaling in Time and Space. *Science Signaling*, *6*(285), rs12–rs12. doi:10.1126/scisignal.2004135

Gomes, I., Jordan, B. A., Gupta, A., Trapaidze, N., Nagy, V., & Devi, L. A. (2000). Heterodimerization of mu and delta opioid receptors: A role in opiate synergy. *Journal of Neuroscience*, *20*(22), RC110.

Goodman, O. B., Jr, Krupnick, J. G., Santini, F., Gurevich, V. V., Penn, R. B., Gagnon,

A. W., et al. (1996). β-Arrestin acts as a clathrin adaptor in endocytosis of the β2-adrenergic receptor. *Nature*, *383*(6599), 447–450. doi:10.1038/383447a0

Harvey, C. D., Ehrhardt, A. G., Cellurale, C., Zhong, H., Yasuda, R., Davis, R. J., & Svoboda, K. (2008). A genetically encoded fluorescent sensor of ERK activity. *Proceedings of the National Academy of Sciences*, *105*(49), 19264–19269. doi:10.1073/pnas.0804598105

Insel, P. A., Snead, A., Murray, F., Zhang, L., Yokouchi, H., Katakia, T., et al. (2012). GPCR expression in tissues and cells: are the optimal receptors being used as drug targets? *British Journal of Pharmacology*, *165*(6), 1613–1616. doi:10.1111/j.1476-5381.2011.01434.x

Jordan, B., & Devi, L. A. (1998). Molecular mechanisms of opioid receptor signal transduction. *British Journal of Anaesthesia*, *81*(1), 12–19.

Kaksonen, M., Toret, C. P., & Drubin, D. G. (2005). A Modular Design for the Clathrin- and Actin-Mediated Endocytosis Machinery. *Cell*, *123*(2), 305–320. doi:10.1016/j.cell.2005.09.024

Keith, D. E., Murray, S. R., Zaki, P. A., Chu, P. C., Lissin, D. V., Kang, L., et al. (1996). Morphine activates opioid receptors without causing their rapid internalization. *The Journal of Biological Chemistry*, *271*(32), 19021–19024.

Kovoor, A., Celver, J. P., Wu, A., & Chavkin, C. (1998). Agonist induced homologous desensitization of mu-opioid receptors mediated by G protein-coupled receptor kinases is dependent on agonist efficacy. *Molecular Pharmacology*, *54*(4), 704–711.

Lefkowitz, R. J. (2004). Historical review: a brief history and personal retrospective of seven-transmembrane receptors. *Trends in Pharmacological Sciences*, *25*(8), 413–422. doi:10.1016/j.tips.2004.06.006

Marchese, A., Paing, M. M., Temple, B. R. S., & Trejo, J. (2008). G protein-coupled receptor sorting to endosomes and lysosomes. *Annual Review of Pharmacology and Toxicology*, *48*, 601–629. doi:10.1146/annurev.pharmtox.48.113006.094646

McMahon, H. T., & Boucrot, E. (2011). Molecular mechanism and physiological functions of clathrin-mediated endocytosis. *Nature Reviews Molecular Cell Biology*, *12*(8), 517–533. doi:10.1038/nrm3151

Oakley, R. H., Laporte, S. A., Holt, J. A., Caron, M. G., & Barak, L. S. (2000). Differential affinities of visual arrestin, beta arrestin1, and beta arrestin2 for G protein-coupled receptors delineate two major classes of receptors. *The Journal of Biological Chemistry*, *275*(22), 17201–17210. doi:10.1074/jbc.M910348199

Puthenveedu, M. A., & Zastrow, von, M. (2006). Cargo Regulates Clathrin-Coated Pit Dynamics. *Cell*, *127*(1), 113–124. doi:10.1016/j.cell.2006.08.035

Rivero, G., Llorente, J., McPherson, J., Cooke, A., Mundell, S. J., McArdle, C. A., et al.

(2012). Endomorphin-2: a biased agonist at the μ-opioid receptor. *Molecular Pharmacology*, *82*(2), 178–188. doi:10.1124/mol.112.078659

Rodriguez, I. (2013). Singular Expression of Olfactory Receptor Genes. *Cell*, *155*(2), 274–277. doi:10.1016/j.cell.2013.09.032

Scavone, J. L., Mackie, K., & Van Bockstaele, E. J. (2010). Characterization of cannabinoid-1 receptors in the locus coeruleus: relationship with mu-opioid receptors. *Brain Research*, *1312*, 18–31. doi:10.1016/j.brainres.2009.11.023

Segredo, V., Burford, N. T., Lameh, J., & Sadée, W. (2002). A Constitutively Internalizing and Recycling Mutant of the μ-Opioid Receptor. *Journal of Neurochemistry*, *68*(6), 2395–2404. doi:10.1046/j.1471-4159.1997.68062395.x

Soohoo, A. L., & Puthenveedu, M. A. (2013). Divergent modes for cargo-mediated control of clathrin-coated pit dynamics. *Molecular Biology of the Cell*, *24*(11), 1725–1734. doi:10.1091/mbc.E12-07-0550

Taylor, M. J., Perrais, D., & Merrifield, C. J. (2011). A High Precision Survey of the Molecular Dynamics of Mammalian Clathrin-Mediated Endocytosis. *PLoS Biology*, *9*(3), e1000604. doi:10.1371/journal.pbio.1000604.g008

Ueda, H., HARADA, H., NOZAKI, M., KATADA, T., Ui, M., Satoh, M., & Takagi, H. (1988). Reconstitution of rat brain mu opioid receptors with purified guanine nucleotide-binding regulatory proteins, Gi and Go. *Proceedings of the National Academy of Sciences of the United States of America*, *85*(18), 7013–7017.

Zheng, H., Loh, H. H., & Law, P.-Y. (2008). β-Arrestin-dependent μ-opioid receptor-activated extracellular signal-regulated kinases (ERKs) translocate to nucleus in contrast to G protein-dependent ERK activation. *Molecular Pharmacology*, *73*(1), 178–190.

Chapter 3: Regulation of Mu-opioid Receptor Recycling via Protein Kinase C

Summary

Trafficking of signaling receptors is critical to the overall sensitivity of the cell to the signals those receptors detect. Endocytosis removes receptors from the cell surface, desensitizing the cell to further signals. The post-endocytic recycling of receptors reintroduces receptors to the cell surface, re-sensitizing the cell to further signals. Because of this critical downstream consequence, post-endocytic recycling must be kept under careful regulation to maintain the balance of signaling to the cells. We sought to explore the signaling regulation that controls mu-opioid receptor (MOR) recycling. We found that Protein Kinase C (PKC) signaling can increase MOR recycling by phosphorylation at two specific amino acids S363 and T370 on the C-terminal tail of MOR. PKC is both required and sufficient to increase MOR recycling. There are two possible mechanisms for PKC activation through different GPCR controlled mechanisms. PKC is activated downstream of GPCRs coupled to the $G_{\alpha/q}$ receptors. PKC can be also be activated downstream of the MOR itself, through $G_{\beta y}$ activation. Part I explores the role of heterologous control, where the $G_{\alpha q}$ coupled pain receptor, neurokinin-1 receptor (NK1-R) is able to increase MOR recycling. Part II of this chapter details the PKC driven positive feedback loop wherein the MOR receptor increases its own recycling.

Part I: Cell-autonomous regulation of mu-opioid receptor recycling by substance P

This manuscript was published as an article in *Cell Reports.*
Bowman*, S. L., Soohoo*, A. L., Shiwarski, D. J., Schulz, S., Pradhan, A. A. & Puthenveedu, M. A. Cell-Autonomous Regulation of Mu-Opioid Receptor Recycling by Substance P. *Cell Reports*, doi:10.1016/j.celrep.2015.02.045 (2015).

This is a co-first author manuscript with S. Bowman. A. Soohoo generated the PKC mutants by site-directed mutagenesis, and performed and analyzed all live-cell single-event recycling assay experiments with the exception of the SP inhibition by chelerythrine experiment. The SP experiments were performed and analyzed by both A. Soohoo and S. Bowman.

Introduction

Most neurotransmitter signals are transduced by G protein-coupled receptors (GPCR), the largest family of signaling receptors (Pierce et al., 2002; Rosenbaum et al., 2009; Premont and Gainetdinov, 2007; Shepherd and Huganir, 2007; von Zastrow and Williams, 2012). The strength of a neuronal response directly depends on surface receptor numbers. Therefore, regulation of this number via membrane trafficking is critical for modulating neuronal responsiveness to a given signal (Anggono and Huganir, 2012; Gainetdinov et al., 2004; Marchese et al., 2008; Yudowski et al., 2009). It is accepted that membrane trafficking can control the number of surface receptors and therefore signaling, and many mechanisms have been identified. Emerging evidence suggests that signaling can also control membrane trafficking, but the mechanisms that underlie such crosstalk are still largely unresolved (Jean-Alphonse and Hanyaloglu, 2011).

Post-endocytic receptor sorting, a trafficking step critical for receptor physiology (Sorkin and von Zastrow, 2009; Anggono and Huganir, 2012; Marchese et al., 2008; Scita and Di Fiore, 2010; Williams et al., 2012), provides a potential point for such crosstalk. Activated surface receptors are rapidly internalized by clathrin-mediated endocytosis and transported to the endosome, causing receptor removal from the cell surface, which is associated with loss of cellular sensitivity (Alvarez et al., 2002; Claing et al., 2002; Hanyaloglu and Zastrow, 2007; Keith et al., 1996; Martini and Whistler, 2007). Cellular sensitivity to further extracellular signals is then determined by post-endocytic receptor sorting between the degradative and recycling pathways, as small changes in recycling rates can cause relatively large changes in surface receptor numbers over physiological timescales (Sorkin and von Zastrow, 2009; Arttamangkul et al., 2012; Jean-Alphonse and Hanyaloglu, 2011; von Zastrow and Williams, 2012). How receptor recycling is controlled by heterologous signaling pathways in a physiological context is a fundamental question that is still not very well understood (Marchese et al., 2008; Williams et al., 2012).

Here, we focused on two signaling pathways that functionally interact - pain and analgesia - as physiologically relevant examples for potential signaling crosstalk. Pain in nociceptive neurons is associated with activation of the neurokinin-1 receptor (NK1R) by substance P (Perl, 2007; de Felipe, 1998), while analgesia is primarily mediated by opioids via the mu opioid receptor (MOR) (Chen and Marvizón, 2009; Kieffer, 1995; Lao et al., 2008). Here we show that

NK1R activation by substance P increases MOR post-endocytic recycling in sensory neurons, via a novel cross-regulatory mechanism based on direct modification of MOR. NK1R signaling also increases the resensitization of MOR-mediated antinociception in mice. Our results provide a physiologically relevant example for crosstalk between signaling pathways at the level of receptor trafficking.

Results

Substance P signaling through NK1R increases post-endocytic recycling of MOR

To test if NK1R signaling cross-regulates MOR recycling, we chose trigeminal ganglia (TG) neurons as model cells. TG neurons are highly relevant for neuralgia, a common and severe pain disorder, and they endogenously express MOR and NK1R (Aicher et al., 2000). To measure MOR recycling, we used an assay to quantitate recycled FLAG-tagged MORs (Fig 3-1A). These tagged receptors were fully competent for signaling and trafficking, as reported previously (Arttamangkul et al., 2008; Just et al., 2013; Keith et al., 1996; Soohoo and Puthenveedu, 2013). TG neurons expressing FLAG-MOR were labeled with fluorescent Alexa 488-conjugated anti-FLAG antibodies to detect the existing pool of MOR on the cell surface (Fig 3-1B, surf ctrl). MOR activation by the specific agonist [D-Ala2, N-MePhe4, Gly-ol]-enkephalin (DAMGO, noted as DG) induced robust MOR internalization, detected by the appearance of intracellular MOR fluorescence (Fig 3-1B, intern). DG was then washed out to allow MOR recycling. The cells were then labeled by Alexa 568-conjugated secondary

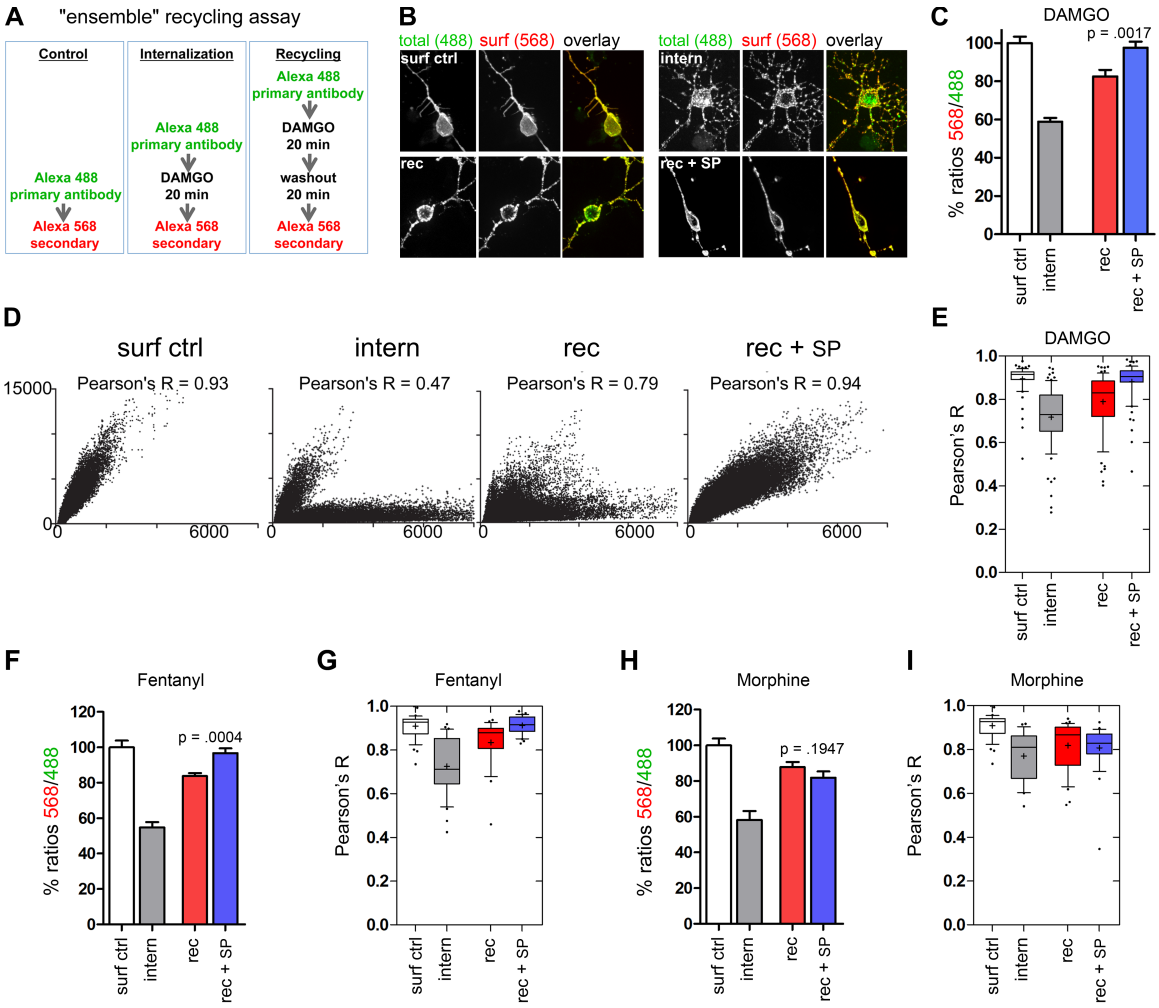

Figure 3-1. Substance P increases post-endocytic recycling of MOR. A) Schematic of the quantitative ratiometric recycling assay in TG neurons. **B)** Example images of FLAG-MOR in primary TG neurons: surface control (surf ctrl), internalization control (intern), DG washout (rec), and washout with SP (rec + SP). Primary anti-FLAG (total 488) is green in the overlay. Secondary antibody (surf 568) is red in the overlay. **C)** Percent recycling calculated from the ratios of surface (568) to total (488) in each condition (mean ± s.e.m; n = 77 surf ctrl, 78 intern, 69 rec, and 68 rec + SP). **D)** Cytofluorograms showing pixel-level fluorescence correlation between total and surface-only pools. The surf ctrl shows strong correlation between the two channels; the intensity values trend to a single diagonal line. DG (intern) caused separation of the points into two populations and DG washout increased the correlation, which was further enhanced by SP. Pearson's correlation coefficients are shown for each example. **E)** Tukey box plots showing the 1st and 3rd quartiles of the distribution of Pearson's coefficients across multiple cells (n as above). Middle bar shows the median, outside bars show 10th and 90th percentiles, and "+" shows the mean. Scale bars are 5μm. **F)** Percent recycling increased during washout, following activation of TGs with fentanyl. DG (n = 37 surf ctrl, 33 intern, 29 rec, and 38 rec + SP). **G)** Tukey box plots showing Pearson's coefficients across multiple cells treated with fentanyl (n as in F). **H)** Percent recycling increased during washout, following activation of TGs with morphine. (n = 37 surf ctrl, 34 intern, 37 rec, and 30 rec + SP). **I)** Tukey box plots showing Pearson's coefficients across multiple cells treated with morphine (n as in H).

antibodies, which only label surface anti-FLAG-labeled MOR. MOR recycling was quantitated as the ratio of the secondary (surface) to primary (total) antibody fluorescence values. This ratiometric assay allowed us to differentiate recycling from the insertion of newly synthesized MOR. Activation of endogenous NK1Rs by by substance P (SP) during the agonist washout increased the ratio of surface to total fluorescence, indicating increased MOR recycling (Fig 3-1B and C, rec vs. rec + SP) (Hunt and Mantyh, 2001; Nichols et al., 2014; de Felipe et al., 1998). We measured the pixel-based colocalization of the surface to total MOR by calculating the Pearson's correlation between the two fluorophores. Before DG, a strong correlation was observed as seen in the cytofluorogram (e.g. cell in Fig 3-1D-E. After DG, colocalization decreased and two separate populations emerged, consistent with MOR endocytosis and decreased labeling with the secondary antibody on the surface (Fig 3-1D and E). Colocalization increased when SP was added to the washout (Fig 3-1E), suggesting an increase in surface MOR. We next asked if SP was capable of regulating MOR recycling when MORs were stimulated with two clinically relevant opioids, fentanyl and morphine. SP increased MOR recycling after endocytosis induced by fentanyl (Fig 3-1 F-G, but not morphine (Fig 3-1 H-I).

To directly visualize and quantify MOR recycling at the level of individual recycling events (Yudowski et al., 2006), we imaged MOR N-terminally tagged with a pH-sensitive green fluorescent protein (SpH-MOR) (Miesenböck et al., 1998). When expressed in HEK293 cells, MOR fluorescence was quenched in

acidic endosomal compartments and dequenched upon recycling (Yudowski et al., 2009). Rapid imaging (10 Hz) using total internal reflection fluorescence microscopy (TIR-FM) (Puthenveedu et al., 2010; Yu et al., 2010) after MOR endocytosis revealed individual exocytic events as transient bursts of fluorescence at the cell surface (Fig 3-2A). The fluorescence burst showed a localized peak of maximum intensity that diffuses across a larger area as vesicles fuse and receptors diffuse across the cell surface (Fig 3-2B, heat map of intensity shown below, Fig 3-2C), consistent with our previous data that these are individual recycling events (Puthenveedu et al., 2010; Yudowski et al., 2009).

We calculated the percentage change in the number of recycling events after SP by normalizing to the initial rate before SP (Fig 3-2D). In cells expressing HA-NK1R, the percentage of MOR recycling events per minute increased after SP (Fig 3-2E,F), consistent with the increase we saw with endogenous NK1R (Fig 3-1C, E). In adjacent cells not expressing HA-NK1R, SP did not increase SpH-MOR recycling (Fig 3-2F). As HEK293 cells do not express noticeable levels of endogenous NK1R, this indicates that NK1R signaling is sufficient to increase MOR recycling. MOR recycling was not reduced by cycloheximide treatment, confirming that these were post-endocytic recycling events, and not insertion of newly synthesized protein (Fig 3-S1A). Additionally, very few MOR recycling events were seen without DG stimulation, and SP did not change this (Fig 3-S1B). Together, our results show that SP signaling increases MOR recycling through activation of the NK1R.

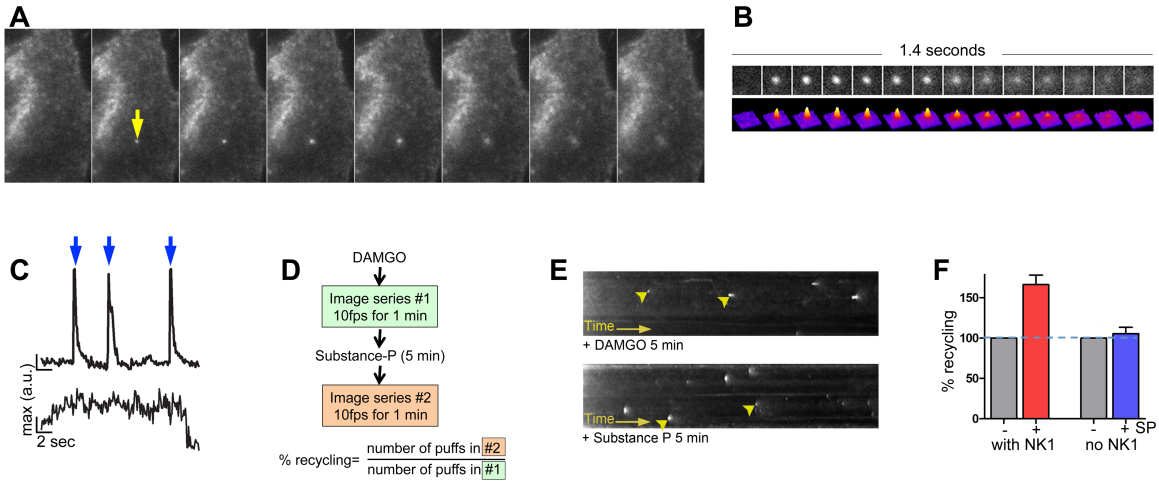

Fig 3-2. Substance P signaling through NK1-R regulates individual MOR recycling events. **A)** Cells expressing SpH-MOR imaged with TIR-FM 5 min after DG addition. Frames are 100ms apart. An individual exocytic event is indicated by yellow arrow. Scale bar is 5μm. **B)** Lifetime of an SpH-MOR exocytic event. Insertion events begin as a localized, intense burst of fluorescence that diffuses within a second. Heat map of intensity is shown below as a surface plot. **C)** Maximum intensity traces of an SpH-MOR vesicle exocytic event (top, arrows), showing characteristic rapid spikes, and an endocytic cluster (bottom), which persists for much longer with a characteristic exponential decrease at the end. **D)** Experimental workflow to quantify acute regulation of recycling. **E)** Kymographs of SpH-MOR fusion events from the same region in the same cell, expressing both SpH-MOR and an HA-tagged NK1-R, following sequential DG and SP addition. Arrowheads show exocytic events which increase after SP. Scale bar is 2 seconds **F)** Number of SpH-MOR exocytic events per min after SP addition normalized to before (i.e., with just DG) in cells expressing NK1-R and in adjacent cells not expressing NK1-R. Error bars are s.e.m. (n = 20).

Protein Kinase C signaling is required and sufficient for SP-induced increase in MOR recycling and resensitization.

We next addressed the intracellular NK1R signaling cascade that mediated the regulation of MOR recycling. NK1R couples to Gq/11, which activates Protein Kinase C (PKC) (Macdonald et al., 1996). The PKC inhibitor chelerythrine (chel) abolished the SP-induced increase in MOR recycling in NK1R-expressing cells (Fig 3-3A), indicating that PKC was required for SP- and NK1R-mediated regulation of MOR recycling. Additionally, PKC activation by Phorbol 12-myristate 13-acetate (PMA) increased SpH-MOR recycling in the absence of NK1R and SP (Fig 3-3B), indicating that PKC was sufficient for increasing MOR recycling. Addition of chel or PMA alone had no effect on SpH-MOR exocytic events (Fig 3-S2A-B).

To investigate the functional consequences of PKC-mediated regulation of MOR recycling, we first measured DG-mediated inhibition of cAMP levels as a readout of the number of functional surface MOR (Talbot et al., 2005). HEK293 cells expressing MOR were stimulated with DG for 15 min to induce MOR endocytosis and cellular desensitization. DG was washed out to allow MOR recycling, and cAMP inhibition in response to a rechallenge with DG measured as an index of cellular resensitization. Addition of chel during the washout decreased cAMP inhibition after the rechallenge (green line) compared to the control (red line). In contrast, PMA increased cAMP inhibition in response to the DG rechallenge (blue line) (Fig 3-3C). Chel and PMA alone, with no prior DG

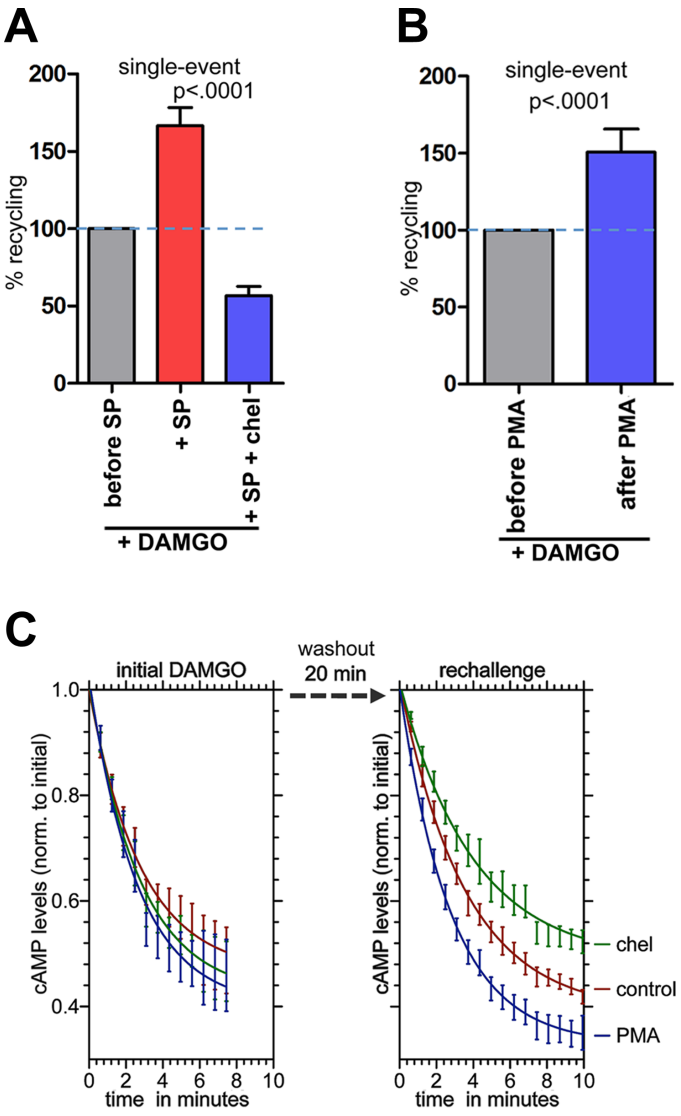

Fig 3-3. PKC activation is required and sufficient for SP-induced increase in MOR recycling. A) Percent change in number of MOR recycling events, comparing SP to SP + chel. Chel blocked the SP-mediated increase. DG and either SP or SP + chel were added sequentially, and a paired comparison was made in the same cell (n = 12). **B)** PMA was sufficient to increase MOR recycling (n = 47 cells). **C)** Assay to detect resensitization of cells to MOR signaling using luminescence-based real-time detection of cAMP levels. DG, *Left panel*, cAMP levels after initial DG challenge.. *Right panel*, DG cells were rechallenged with DG. Chel (green) reduced recycling of functional MOR, while PMA (blue) enhanced it compared to control cells (red). The initial DG challenge was identical across all experiments. Error bars are s.e.m. across 9 experiments.

stimulation, had no effect on DG induced inhibition of cAMP production (Fig S3-2C).

We next tested if PKC inhibition abolishes the SP-induced increase in MOR recycling in TG neurons, using the ratiometric recycling assay (Fig 3-1). Addition of chel during the washout abolished the SP-mediated increase in MOR recycling (Fig 3-4A, B). Pixel-based colocalization was lower when PKC was inhibited in the washout, even in the presence of SP (Fig 3-4C). Adding PMA, without SP, during the washout increased MOR recycling (Fig 3-4D-F). Together, this suggests that PKC is both required and sufficient for regulation of MOR recycling and cellular sensitivity to opioid signaling.

Substance P and PKC-mediated regulation of MOR recycling requires MOR phosphorylation at Ser 363 and Thr 370

Considering that PKC was required and sufficient for heterologous regulation of MOR recycling through SP, we sought to identify the target of PKC. The MOR itself presented an interesting candidate. PKC can phosphorylate three sites on the C-terminal tail of MOR - serine 363, threonine 370, and serine 375 (Fig 3-5A) (Doll et al., 2011; Feng et al., 2011). To test whether MOR phosphorylation was required, we mutated each of these sites to alanine to block phosphorylation (Feng et al., 2011) and quantified SP-mediated regulation of MOR recycling. SP did not increase the percentage of recycling events per unit

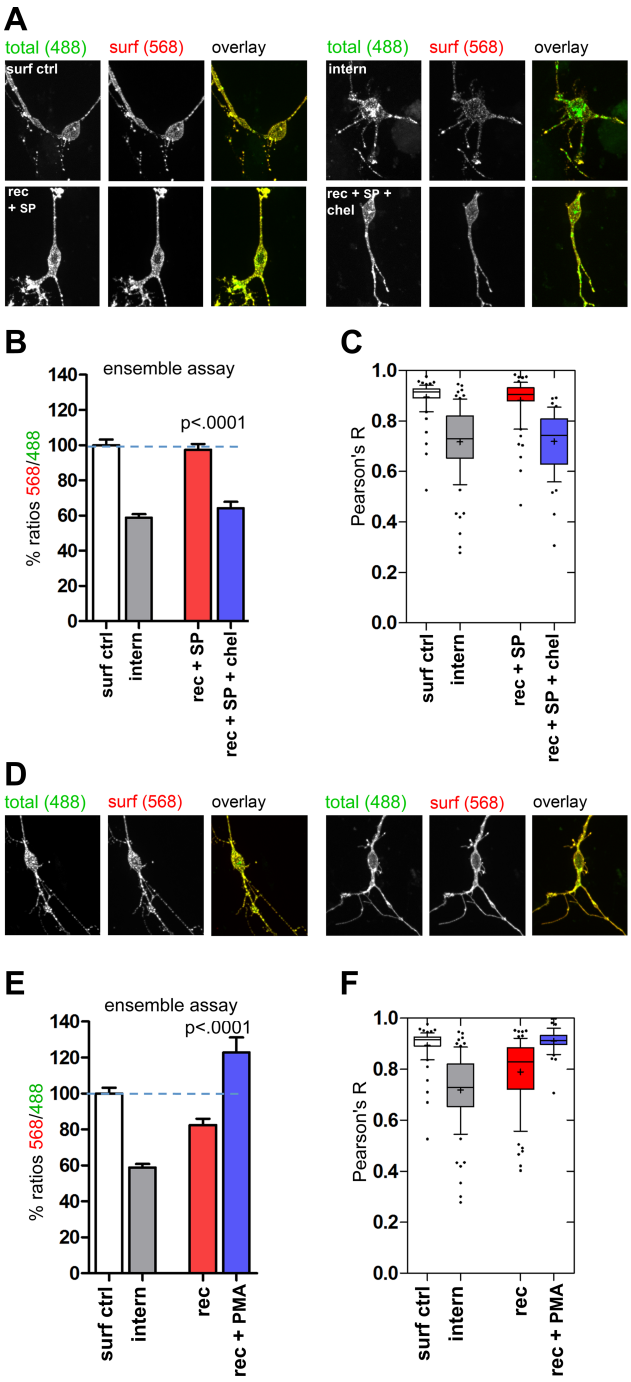

Fig 3-4. PKC activation is required and sufficient for SP-induced increase in MOR recycling in TG neurons. A) Ratiometric recycling assay in TG neurons comparing MOR recycling in the presence of SP alone vs. SP with chel. **B)** Quantitation across multiple cells, as in Fig 1C (n = 77 surf ctrl, 78 intern, 72 rec + SP, 47 rec + SP + chel). **C)** Tukey box plots of Pearson's coefficients denoting pixel-level correlation between receptors (n as in B). **D-E)** Ratiometric recycling assay in TG neurons testing the effect of PKC activation by PMA in the absence of SP. (n = 77 surf ctrl, 78 intern, 69 rec, 47 rec + PMA. **F)** Tukey box plots of Pearson's coefficients denoting pixel-level correlation between receptors. (n as in E).

time when either S363 or T370 was mutated (Fig 3-5B, C). In contrast, the recycling of S375A increased to a level comparable to wild type in response to SP (Fig 3-5B, C). This indicates that S363 and T370 are required for SP-mediated regulation, but S375 is not (Fig 3-5B, C). Additionally, PMA increased SpH-MOR exocytic events for S375A, but not S363A or T370A, comparable to wild type MOR (Fig 3-5D). In TG neurons, SP failed to increase S363A or T370A recycling (Fig 3-5E-G for S363A, and Fig 3-5H-J for T370A), indicating that both S363 and T370 are required for PKC to regulate MOR recycling.

PKC enhances recycling and resensitization of endogenous MORs in TG neurons.

We next asked if endogenous MOR trafficking was regulated by PKC. To test this, we utilized a rabbit monoclonal anti-MOR antibody (UMB-3), to detect the subcellular localization of endogenous MORs (Lupp et al., 2011). UMB-3 staining showed strong staining at the periphery of TG neurons (Fig 3-6A), further indicated by the surface plot of intensity (Fig 3-6A insets). To quantitate intracellular vs. membrane MOR levels, UMB-3 fluorescence was measured across concentric circles increasing in size from the center to the periphery of the cell (Fig 3-6B). At steady state, the majority of UMB-3 maximum fluorescence intensity was detected in larger circles, consistent with more MOR localized to the surface (Fig 3-6B). After DG addition, UMB-3 staining was visible in punctate

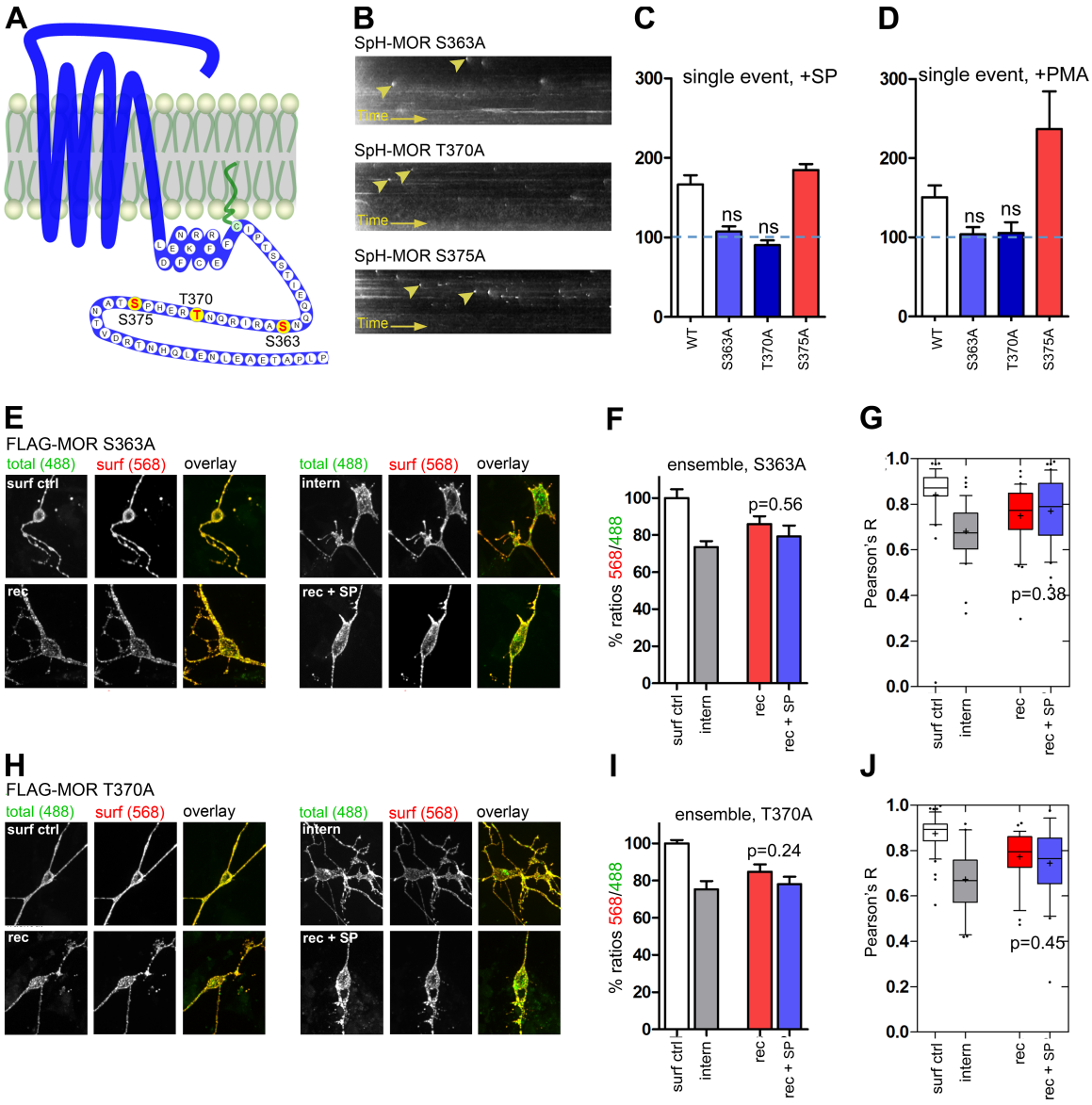

Fig 3-5. PKC requires S363 and T370 to regulate MOR recycling. A) Schematic of PKC phosphorylation sites on C-terminal tail of MOR (S363, T370, and S375). **B)** Kymographs of SpH-MOR single exocytic events for MOR S363A, T370A, and S375A after SP. **C)** Quantitation of percent recycling across cells (n = 20, 14, 18, and 22) in HA-NK1R expressing cells with MOR mutants S363A and T370A, and S375, compared to wildtype. Dashed line shows number of events in same cells prior to SP normalized to 100%. **D)** Percent recycling with PMA-treated cells expressing MOR mutants S363A, T370A, and S375A (n = 52, 29, 18, and 17). **E)** Ratiometric recycling assay in TG neurons for S363A with and without SP. **F)** Ratio quantitation across multiple cells (n = 35 surf ctrl, 38 intern, 33 rec, 41 rec + SP) between the washout without and with SP for S363A. **G)** Box plots of Pearson's coefficients for S363A showing no increase in correlation with SP. **H)** Ratiometric recycling assay in TG neurons for T370A with and without SP. **I)** Ratio quantitation (n = 47, 27, 29, and 27) without and with SP for T370A. **J)** Box plots of Pearson's coefficients for T370A showing no increase in correlation with SP. Scale bars are 5μm.

structures, and fluorescence intensity was uniform across the cell (Fig 3-6A-B), suggesting redistribution of MOR to endosomes. DG washout restored UMB-3 staining at the periphery of TG neurons (Fig 3-6A-B), consistent with MOR recycling. PKC inhibition during the washout inhibited MOR recycling, as evidenced by retention of UMB-3 fluorescence in punctate structures and uniform fluorescence in smaller circles (Fig 3-6A-B). Conversely, PKC activation during the washout caused strong UMB-3 staining at the cell periphery (Fig 3-6A-B), suggesting that PKC increases endogenous MOR recycling.

To further test PKC's regulation of endogenous MOR recycling in TG neurons, we used a fluorescent ligand, Alexa 594-conjugated dermorphin (derm594), previously described to bind MORs (Arttamangkul et al., 2000). To induce recycling, we treated TG neurons with DG, followed by a washout as in the resensitization experiment in Fig 3-3C. At the end, the cells were labeled with ice-cold derm594 to detect surface MOR. When compared to the control, DG significantly decreased derm594 fluorescence, consistent with MOR endocytosis. After washout, derm594 fluorescence was higher than the DG control, as expected after MOR recycling. PKC inhibition decreased derm594 fluorescence, and PKC activation increased it, suggesting that PKC increases recycling of endogenous MOR (Fig 3-6C). HEK 293 cells not expressing MOR did not show fluorescence, confirming specificity of derm594 binding (Fig 3-6C). Together, these results suggest that PKC is required and sufficient to regulate recycling of endogenous MORs.

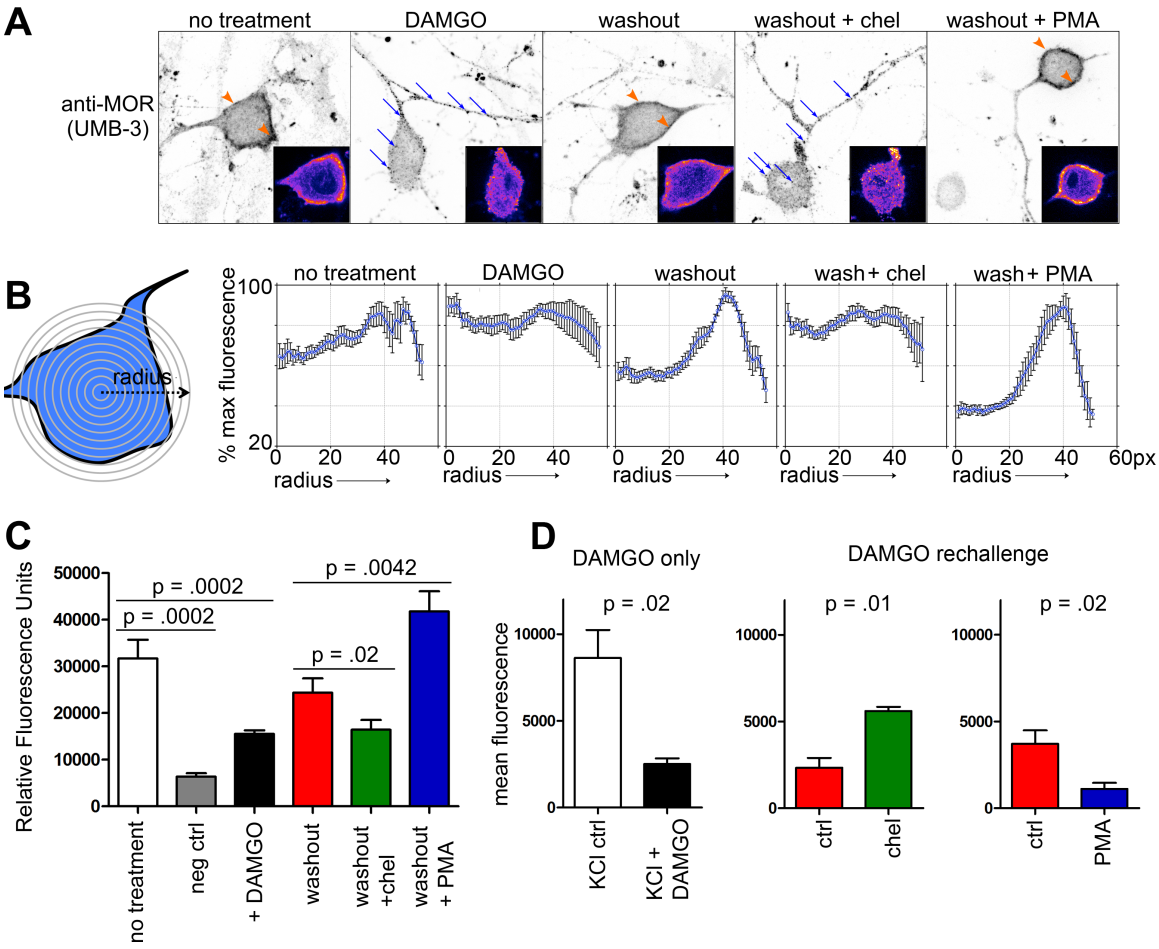

Fig 3-6. PKC increases recycling of endogenous MOR and opioid resensitization in TG neurons. A) Example images of anti-MOR (UMB-3) in TG neurons. UMB-3 staining was primarily localized to the periphery of cells with no treatment (orange arrowheads). Addition of DG for 20 min induced a redistribution of UMB-3 staining to intracellular punctate structures (blue arrows). Surface plot of intensity shows greater fluorescence intensity concentrated at the cell periphery in the no treatment control, and recycling conditions than with DG treatment (insets). Addition of chel during the washout inhibited periphery staining, while PMA addition enhanced staining at the cell periphery **B)** Schematic of radial profile method used to analyze fluorescence intensity of UMB-3 staining from the center to the periphery of cells. Intensity traces from multiple cells (n>8 in each condition) show increased UMB-3 fluorescence in circles of larger radii, consistent with increased MOR on the surface. **C)** Graph of average mean intensity of derm-A594 signal labeling endogenous MOR in TG neurons across 3 trials. Derm-A594 fluorescence was significantly greater in non-treated TGs (no treatment) than HEK cells (neg ctrl),.Black, plus DG is the internalization control. Red, recycling condition alone. Green, recycling with chel. Blue, recycling with PMA. *, **, and *** denote p values less than .01, .001, and .0001 respectively. **D)** Graphs of mean fluorescence values of $DiBAC_4(5)$ in TG neurons, at 15 min after DG addition and DG rechallenge after the washout alone (left), with chel (center) and with PMA (right). Corresponding p values (n>5 in each condition) are shown for each.

SP and PKC regulate the opioid resensitization in neurons and opioid analgesia in mice.

We next asked if PKC regulated the resensitization of opioid activity in physiologically relevant sensory neurons. TG neurons were incubated with the sulfonyl voltage-sensitive anionic dye $DiBAC_4(5)$ (George et al., 1998), which increases fluorescence on depolarization and decreases on hyperpolarization. DG decreased the fluorescence of KCl-activated TG neurons, consistent with opioid-induced hyperpolarization (Fig 3-6D). To measure MOR recycling and resensitization, we used the agonist-washout paradigm above (Fig 3-6A-C). After the initial DG challenge, DG was washed out for 20 min to allow recycling and resensitization. A rechallenge with DG decreased the KCl-induced voltage change similarly to the initial challenge, indicating that neurons were resensitized to opioid signaling (Fig 3-6D, left graph). However, when PKC was inhibited during the DG washout, the DG rechallenge did not decrease fluorescence, consistent with fewer receptors recycling back to the surface (Fig 3-6D, middle graph). Further, PKC activation during the DG washout enhanced the effect of the DG rechallenge (Fig 3-6D, right graph). This suggests that PKC regulates opioid resensitization in sensory neurons, consistent with our model that SP-mediated PKC activation positively regulates MOR recycling and resensitization.

To test if SP regulated the resensitization of MOR-mediated analgesia in

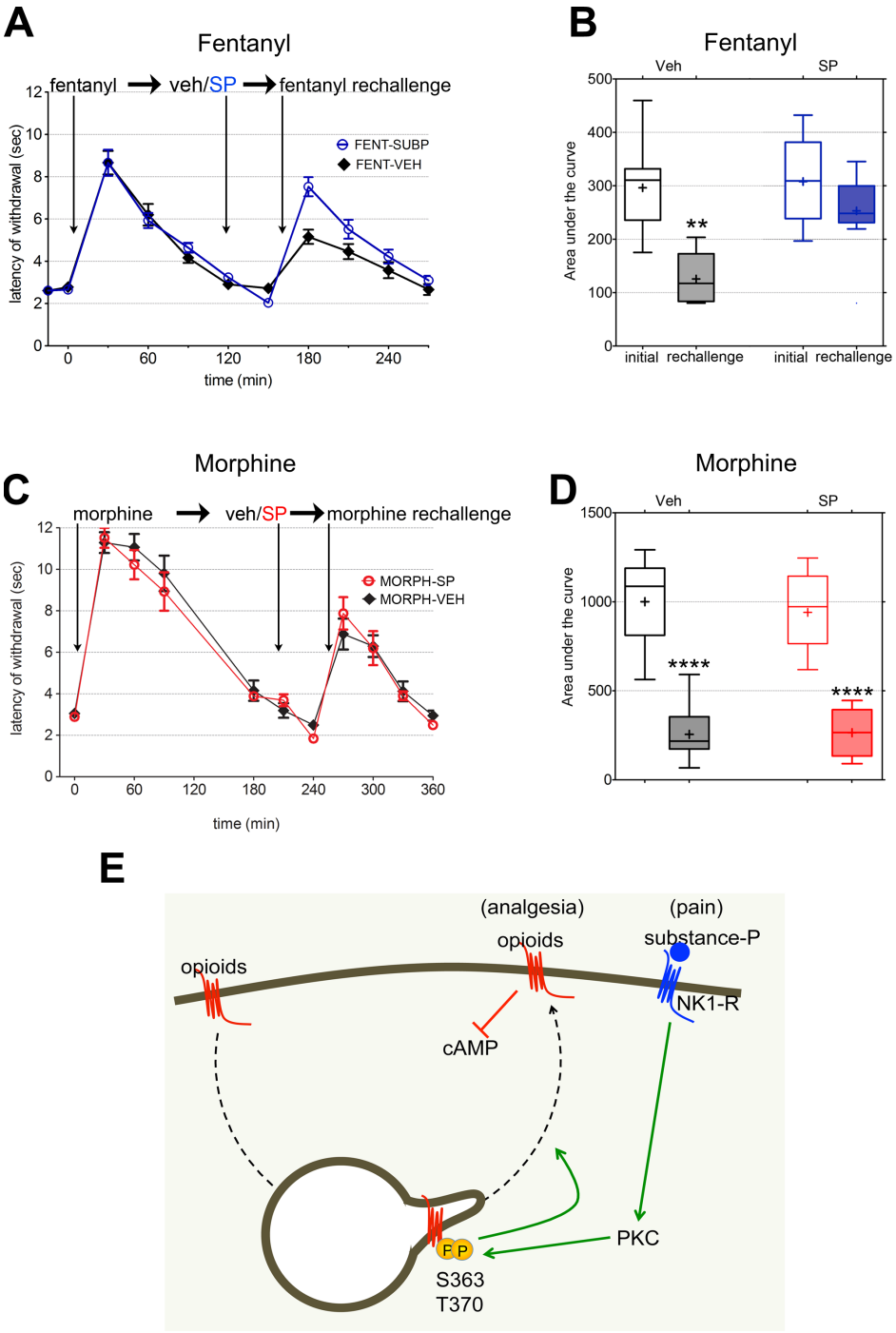

Fig 3-7. Substance P reduces acute tolerance to fentanyl but not morphine. A) Time course of fentanyl-induced antinociceptive responses. An increase in tail withdrawal latencies denotes antinoception. Results are mean across multiple animals, error are s.e.m., n = 9 animals for both experimental conditions. **B)** Graph of areas under the curve for initial response and rechallenge for each condition. **C)** Time course of morphine-induced antinociceptive responses. Results are mean across multiple animals, error are s.e.m., n = 10 animals for morphine vehicle control and 11 animals for SP. **D)** Graph of areas under the curve as in B.

mice, we measured the development of acute tolerance to the antinociceptive effects of fentanyl, a short-acting MOR agonist, using a warm water tail-withdrawal assay (Melief et al., 2010; Pradhan et al., 2010) (Fig S3-3A). After baseline measurements, animals were injected with fentanyl, and tail-withdrawal latencies were measured every 30 min. A significant but sub-maximal increase in tail-withdrawal latencies, persisting for approximately 120 min, was observed with fentanyl (Fig 3-7A). Either saline (vehicle control) or SP was injected intrathecally 120 min after the first fentanyl challenge. In control mice, a fentanyl rechallenge, given 30 min later, attenuated (~40% of initial) the antinociceptive response, indicating acute tolerance to fentanyl (Fig 3-7A). In contrast, SP-injected mice showed an antinociceptive response to the rechallenge that was comparable to the initial response (Fig 3-7A, Fig 3-S3B). Calculation of the areas under the curve showed that saline-injected mice showed a significantly reduced response to the fentanyl rechallenge compared to the initial response, while SP-injected mice showed comparable responses to both fentanyl injections (Fig 3-7B). Because morphine-activated MORs were not subject to SP-regulated recycling, we next tested if SP could sensitize morphine-induced analgesia in mice. Consistent with our cellular data, a morphine rechallenge following SP injection did not increase tail withdrawal latency in contrast to fentanyl (Fig 3-7C-D, Fig 3-S3C). Taken together, our results indicate that SP signaling through PKC inhibits acute tolerance to fentanyl, but not morphine, by increasing MOR recycling in peripheral neurons.

Discussion

We show that SP signaling, through endogenous NK1R, enhances MOR recycling following DG- and fentanyl-, but not morphine-induced endocytosis (Fig 1, 2). PKC activity downstream of NK1R is required and sufficient for this crosstalk (Fig 3-3, 3-4). We identify two PKC sites on the C-terminal tail of MOR as the targets for this NK1R-mediated regulation (Fig 3-5), and show a functional effect of PKC regulation in recycling of exogenous and endogenous MOR in sensory neurons (Fig 3-6). Further, we show that SP increases opioid antinociception in mice by attenuating acute tolerance to fentanyl, but not morphine.

Studies over the last decades have suggested a complex and paradoxical interaction between the neurokinin and opioid pathways. SP, a pain-associated neurotransmitter, can induce antinociceptive effects (Mohrland and Gebhart, 1979). Further, NK1R antagonists can modify opioid reward, withdrawal, and reinforcement, and NK1R is required for morphine reward but not morphine analgesia (Gadd et al., 2003; Murtra et al., 2000). Our data, that SP regulates MOR recycling and acute tolerance to fentanyl but not morphine (Fig 3-7), are consistent with this, but suggest a complex agonist-selective cross-talk between these pathways. At a cellular level, co-activation of NK1R and MOR in CNS neurons has been reported to inhibit MOR endocytosis, partly because NK1R non-specifically sequesters beta-arrestin, the common adapter required for GPCR endocytosis (Pierce et al., 2002; Yu et al., 2009), and partly because the

receptors might heterodimerize (Pfeiffer et al., 2003). We directly measure individual recycling events which allows us to test acute regulation of MOR recycling induced by NK1R signaling in the same cell (Fig 3-2), free of the potential confounding effect of NK1R on MOR endocytosis. Further, in our ratiometric assay, NK1Rs are activated after MOR is endocytosed, and the presence of a MOR antagonist prevents subsequent endocytosis. Therefore, we believe endocytosis has a negligible effect on the crosstalk we observe here. Further, blocking new MOR synthesis (Fig 3-S1) had no effect on the surface delivery of MOR in our assays, and inhibition or activation of PKC without DG did not cause any change in MOR surface levels or induce surface insertion (Fig S3-2). Therefore, the increase in surface MOR we observe is primarily a result of increased recycling (Fig 3-1-2).

The precise role of PKC in modulating opioid physiology and MOR trafficking is unresolved (Raehal et al., 2011; Williams et al., 2012), but it provides a potential control point for physiological regulation of opioid signaling. PKC has been implicated in controlling opiate resensitization, tolerance, and dependence, and PKC activation during prolonged MOR agonist exposure increases desensitization, possibly by endocytosis (Dang, 2004; Inoue and Ueda, 2000; Bailey et al., 2004; Kramer and Simon, 1999). As MOR itself can activate PKC, such homologous PKC activation during chronic MOR activation might regulate desensitization and endocytosis, while injury and inflammatory pain might alter the balance of MOR trafficking and resensitization through

heterologous SP regulation, consistent with data that peripheral MORs are less active prior to injury or pain (Berg et al., 2007; Chen and Marvizón, 2009).

Such distinct cell-type or environment-dependent consequences could be brought about by differential MOR phosphorylation. Because we add SP after the major fraction of MOR is already internalized, we believe that the endosomal pool of MOR can be phosphorylated by PKC. Of the two MOR PKC targets required for SP-mediated increase in MOR recycling, S363 is constitutively phosphorylated, while T370 phosphorylation is regulated. Interestingly, T370 is phosphorylated by DG, but not morphine (Doll et al., 2011). However, it is robustly phosphorylated by heterologous SP and PKC activity (Illing et al., 2014; Mann et al., 2014), so it is unlikely to be the primary explanation for the differences we see between DG and morphine. S375 might primarily be phosphorylated by GPCR Kinases (GRK) rather than PKC (Doll et al., 2012), consistent with our result that S375 is not required for NK1R's regulation of MOR recycling via PKC. Additionally, T370 might also be phosphorylated by GRK 2/3 following MOR activation with a hierarchical dependence on S375 phosphorylation (Just et al., 2013), and inhibition of GRK2 alleviates opiate tolerance (Dang et al., 2011). Further, substance P induces PKC-dependent phosphorylation of MOR at T370 without dependence on S375 phosphorylation (Illing et al, 2014). It is possible that T370 is differentially phosphorylated by PKCs and GRKs by homologous vs. heterologous regulation to control physiological consequences in different cell types. Homologous GRK-mediated

phosphorylation of MOR following addition of opioid agonists might promote opioid tolerance in the CNS, while PKC phosphorylation at T370 following NK1R activation induces resensitization of MORs in the context of inflammatory pain in the PNS.

T370 and S363 are adjacent to a bi-leucine sequence that is required and sufficient for MOR recycling (Tanowitz and Zastrow, 2003). This raises the possibility that combinatorial MOR phosphorylation by homologous and heterologous signaling pathways might rapidly reprogram receptor recycling and cellular resensitization by changing the biochemical interactions of MOR. Reprogramming in response to homologous regulation has been suggested for B2AR recycling, which switches between a sequence-dependent and bulk recycling pathway based on PKA phosphorylation (Puthenveedu et al., 2010; Vistein and Puthenveedu, 2013). MOR recycling in striatal neurons has been reported to be inhibited by forskolin, though PKA was not directly tested (Roman-Vendrell et al., 2012). Striatal neurons do not co-express NK1R and MOR, and it is possible that different neuronal subtypes exhibit distinct mechanisms of regulation, depending on the expression profiles of signaling receptors and kinases. Rapid reprogramming by receptor phosphorylation could therefore be a general mechanism to switch receptors between different recycling pathways depending on the physiological circumstance. For MOR, such reprogramming, causing sensitization of nociceptors to opioid signaling, could in part explain the paradoxical analgesic effects of capsaicin and substance P. (Komatsu et al.,

2009; Mohrland and Gebhart, 1979). We show that peripheral administration of substance P is capable of increasing MOR-mediated analgesia in mice. This is consistent with data that peripheral endogenous opioids are released following tissue damage and painful stimuli, and that this is accompanied by an increase in opioid receptors to nerve terminals (Stein and Lang, 2009). As the opioid system serves as a physiological check for the maladaptive consequences of pain, our results provide a proof of principle for how signaling crosstalk between these systems at the level of receptor trafficking could represent a general homeostatic mechanism of signaling crosstalk.

Experimental Procedures

Plasmid DNA and Constructs

FLAG-MOR and SpH-MOR have been described previously (Keith et al., 1996; Soohoo and Puthenveedu, 2013). HA-tagged rat NK1R was provided by Dr. Mark Von Zastrow. Point mutants were generated using site directed mutagenesis with QuikChange (Agilent). All constructs were confirmed by DNA sequencing.

Cell Cultures and Transfections

TG neurons were obtained as previously described (Malin, et al, 2007), and transfected using Lipofectamine 2000 (Invitrogen) 2d after plating. Cells were maintained 2d in culture before imaging. HEK-293 cells were obtained from

ATCC and maintained in DMEM (Fisher Scientific) +10% FBS. Cells were transfected with Effectene (Qiagen). Stable cell lines were generated with Geneticin (Invitrogen) selection. Cells were passed to 25mm coverglass 1d after transfection and imaged the following day.

Immunofluorescence Ratiometric Recycling Assay and Quantification

TGs expressing FLAG-MOR were labeled with Alexa 488 conjugated M1 anti-FLAG to label surface receptors for 10m, followed by incubation with 10μM DG (Sigma) for 20 m to promote receptor internalization. Agonist media was washed out and replaced with media containing 10 μM naltrexone (Sigma), a MOR antagonist, to prevent additional activation and internalization of MOR for 20 m. Recycled surface M1-anti-FLAG labeled receptors were then labeled with secondary goat anti-mouse conjugated to Alexa 568 for 10 m at 4˚C. All other incubations were performed at 37˚C. Cells were then fixed with 4 % PFA for 20 m, and blocked with 0.1M glycine in complete PBS for 10 m. A surface control, where cells were labeled for 10 m with Alexa 488-M1 anti-FLAG, immediately followed by Alexa 568-secondary goat anti mouse to quantify steady state amount of surface receptors. An endocytosis control was performed, where cells were labeled with the secondary antibody and fixed, to quantify the amount of receptors internalized in the presence of DG. Percent recycling was calculated from the ratio of intensities of the secondary antibody to the primary anti-FLAG and dividing experimental conditions by the surface control minus the endocytosis control (expt condition-endo ctrl.)/ (surf ctrl-endo ctrl.)%. Just

Another Colocalization Plugin (JACoP) for ImageJ was used to generate a cytofluorogram and Pearson's Correlation Coefficient of intensities between primary and secondary antibody fluorescence. Statistical analyses and graphing were done using Microsoft Excel and Graphpad Prism. P values are from Mann-Whitney tests.

Individual Exocytic Event Recycling Assay

HEK-293 cells stably expressing SpH-MOR were incubated in DG for 5 min, and a 1 min movie acquired at 10 Hz using TIRF-M, followed by subsequent incubation with the second drug and a 1 m movie, at 37˚C. For SP experiments, cells were transiently transfected with HA-NK1R. Cells were incubated in anti-HA (Sigma), followed by Alexa-568 goat-anti mouse, both for 10 m. Cells were incubated for 5 min with DG, and a 1 min movie was acquired. SP was added for 5m, followed by a 1 min movie. Individual insertion events were manually counted using a double blind process. A paired comparison was made within the same cell, normalizing to the agonist only treatment. Significance was determined through Student's paired t-test.

Live Cell and Fluorescence Imaging

Cells were imaged using a Nikon TE-2000E inverted microscope with a 60X 1.49 NA TIRF objective, Andor Revolution XD spinning disk confocal system, and 488 and 568 nm solid-state lasers. Cells were imaged in Opti-MEM or Leibowitz's L15 medium (Gibco), 5% FBS, at 37˚C. Time lapses were acquired

using an Andor iXon+ EM-CCD camera using Andor IQ. Original 16-bit tiff files acquired directly from camera were used for image analysis.

Fluorescent Ligand Binding

TG neurons were plated on a clear-bottom black 96-well plate, for 2d. Cells were stimulated with DG for 15 m to induce internalization, followed by a 15 m DG washout with naltrexone to induce MOR recycling, at 37˚C. Two parallel controls, no DG or naltrexone treatment and a DG only treatment, were performed. Cells were washed and labeled with 100 nM Derm594 (in cold PBS, Ca/Mg) at RT, then washed out two times. Fluorescence was recorded on a Tecan Safire II Plate Reader at (at 25˚C). Derm594 was generously donated by Dr. John Williams, Vollum Institute.

UMB-3 Immunofluorescence staining

TG neurons, plated on coverglass, were treated either with DG (endocytosis ctrl), no drug (surf ctrl), or incubated with DG for 20 m, followed by agonist washout with antagonist and vehicle, chel, or PMA for 20 m (recycling). Cells were then fixed in 4% PFA for 25 m, blocked and permeabilized in PBS + Ca/Mg, FBS, and .01% Triton for 45 m. Cells were incubated with UMB-3 in PBS + Ca/Mg at 4 ˚C overnight, and labeled with Alexa-488 goat anti-rabbit secondary antibody, mounted and imaged.

cAMP Measurement

Assays were performed on HEK293 cells stably expressing MOR and cAMPGlo Sensor 20F (Promega), at 35˚C with IBMX. Luminescence was continuously recorded using a Tecan Infinite M1000 Plate Reader. After 5 m of baseline, DG was added for 10 m to record the initial response and allow endocytosis, media was washed out and replaced with media with naltrexone and either PMA, chel, or vehicle for 20 m for recycling. A rechallenge with DG was used to measure resensitization of recycled MORs.

Voltage Sensitive Dye Measurement

For control KCl and DG experiments, TG neurons were labeled with $DiBAC_4(5)$ and imaged every 30 s. 80 mM KCl was added to depolarize TGs, and DG was added 5 m after KCl to activate endogenous MORs. Cells were incubated with 10 μM DG for 15 m. Agonist was washed out and replaced with media and 10 μM naltrexone and PMA or chel , and compared to naltrexone only washout. Antagonist was washed out, for 20 m (chel) or 10 m (PMA), and cells were labeled with $DiBAC_4(5)$. 5 m after KCl, cells were rechallenged with 10 μM DG and imaged. Mean fluorescence was analyzed using imageJ, and statistical analyses and graphing were performed in Graphpad Prism.

Tail Immersion Assay

Subjects were male C57BL6/J mice, between 9-12 weeks old. Animals were group housed in a 14h-10h light–dark cycle, and food and water was available *ad libitum*. All experiments were in accordance with AALAC guidelines, and were approved by the Animal Care Committee at the University Of Illinois at

Chicago. Thermal nociception was determined using the warm water tail withdrawal assay. Animals were initially habituated to the test apparatus for 2 days before testing. On the test day, mice were lightly restrained in a conical restraint bag, and their tails were immersed (5 cm from the tip) into a 52.5°C water bath. Tail withdrawal latencies were determined, and a cut-off of 12 s was established. After 3 basal measurements, mice were injected with fentanyl (0.1 mg/kg, SC) or morphine (5 mg/kg, SC) and tested every 30 m for 4.5-6 h (Melief et al., 2010). At 120 m (fentanyl) or 210 m (morphine) mice were injected intrathecally with 5 μl of substance P (10 ng) or 0.9% saline. Intrathecal injections were performed with a 30 gauge, 1/2-inch needle at the L4-5 lumbar interspace on lightly anesthetized mice. Tail twitch was used to confirm needle placement, and any mice that exhibited motor impairment following IT injection were excluded. Mice were injected 30 m later with a second injection of fentanyl (0.1 mg/kg, SC) or morphine (5 mg/kg, SC), and tested every 30 m until tail withdrawal latencies returned back to baseline responses.

References

Aicher, SA., Punnoose, A., and Goldberg, A. (2000). μ-Opioid receptors often colocalize with the substance P receptor (NK1) in the trigeminal dorsal horn. J Neurosci 20, 4345-4354.

Alvarez, V.A., Arttamangkul, S., Dang, V., Salem, A., Whistler, J.L., von Zastrow, M., Grandy, D.K., and Williams, J.T. (2002). mu-Opioid receptors: Ligand-dependent activation of potassium conductance, desensitization, and internalization. J Neurosci 22, 5769-5776.

Anggono, V., and Huganir, R.L. (2012). Regulation of AMPA receptor trafficking and synaptic plasticity. Curr Opin In Neurobiol 22, 461-469.

Arttamangkul, S., Alvarez-Maubecin, V., Thomas G., Williams, J.T., Grandy, D.K. (2000) Binding and internalization of fluorescent opioid peptides conjugates in living cells. Mol Pharmacol 58, 1570-1580.

Arttamangkul, S., Lau, E.K., Lu, H.W., and Williams, J.T. (2012). Desensitization and trafficking of μ-opioid receptors in locus ceruleus neurons: modulation by kinases. Mol Pharmacol 81, 348-355.

Arttamangkul, S., Quillinan, N., Low, M.J., von Zastrow, M., Pintar, J., and Williams, J.T. (2008). Differential activation and trafficking of mu-opioid receptors in brain slices. Mol Pharmacol 74, 972-979.

Bailey, C., Kelly, E., and Henderson, G. (2004). Protein kinase C activation enhances morphine-induced rapid desensitization of μ-opioid receptors in mature rat locus ceruleus neurons. Mol Pharmacol 66, 1592-1598.

Berg, K.A., Patwardhan, A.M., Sanchez, T.A., Silva, Y.M., Hargreaves, K.M., and Clarke, W.P. (2007). Rapid modulation of mu-opioid receptor signaling in primary sensory neurons. J Pharmacol Exp Ther 321, 839-847.

Chen, W., and Marvizón, J.C.G. (2009). Acute inflammation induces segmental, bilateral, supraspinally mediated opioid release in the rat spinal cord, as measured by mu-opioid receptor internalization. Neuroscience 161, 157-172.
Claing, A., Laporte, S.A., Caron, M.G., and Lefkowitz, R.J. (2002). Endocytosis of G protein-coupled receptors: roles of G protein-coupled receptor kinases and beta-arrestin proteins. Prog Neurobiol 66, 61-79.

Dang, C.V., Williams, J.T. (2004). Chronic Morphine Treatment Reduces Recovery from Opioid Desensitization. J Neurosci 24, 7699-7706.

Dang, V.C., Chieng, B., Azriel, Y., and Christie, M.J. (2011). Cellular morphine tolerance produced by beta-arrestin-2-dependent impairment of mu-opioid receptor resensitization. J Neurosci 31, 7122-7130.

de Felipe, C., Herrero, J.F., O'Brien, J.A., Palmer, J.A., Doyle, C.A., Smith, A.J., Laird, J.M., Belmonte, C., Cervero, F., Hunt, S.P. (1998). Altered nociception, analgesia and aggression in mice lacking the receptor for substance P. Nature 392, 394-397.

Doll, C., Konietzko, J., Pöll, F., and Koch, T., Hollt, V, Schulz, S. (2011). Agonist-selective patterns of μ-opioid receptor phosphorylation revealed by phosphosite-specific antibodies. Br J Pharmacol 164, 298-307.

Doll, C., Pöll, F., Peuker, K., Loktev, A., Gluck, L., Schulz, S. (2012). Deciphering μ-opioid receptor phosphorylation and dephosphorylation in HEK293 cells. Br J Pharmacol 167, 1259-1270.

Feng, B., Li, Z., and Wang, J.B. (2011). Protein kinase C-mediated phosphorylation of the mu-opioid receptor and its effects on receptor signaling. Mol Pharmacol 79, 768-775.

Gadd, C., Murtra, P., and Felipe, C., Hunt, S.P. (2003). Neurokinin-1 receptor-expressing neurons in the amygdala modulate morphine reward and anxiety behaviors in the mouse. J Neurosci 23, 8271-8280.

Gainetdinov, R.R., Premont, R.T., Bohn, L.M., Lefkowitz, R.J., and Caron, M.G. (2004). Desensitization of G protein-coupled receptors and neuronal functions. Ann Rev Neurosci 27, 107-144.

George, E., Nyirjesy, P., Pratap, P., Freedman, J., Waggoner, A. (1988). Impermeant potential-sensitive oxonal dyes: III. The dependence of the absorption signal on membrane potential. J Membr Biol 105, 55-64.

Hanyaloglu, A.C., and von Zastrow, M. (2007). A novel sorting sequence in the beta2-adrenergic receptor switches recycling from default to the Hrs-dependent mechanism. J Biol Chem 282, 3095-3104.
Hunt, S., and Mantyh, P. (2001). The molecular dynamics of pain control. Nat Rev Neurosci 2, 83-91.

Illing, S, Mann, A., Schulz, S. (2014). Heterologous regulation of agonist-dependent mu-opioid receptor phosphorylation by protein kinase C. Br J Pharmacol 171, 1330-1340.

Inoue, M., and Ueda, H. (2000). Protein kinase C-mediated acute tolerance to peripheral mu-opioid analgesia in the bradykinin-nociception test in mice. J Pharmacol Exp Ther 293, 662-669.

Jean-Alphonse, F., and Hanyaloglu, A.C. (2011). Regulation of GPCR signal networks via membrane trafficking. Mol Cell Endocrinol 331, 205-214.

Just, S., Illing, S., Trester-Zedlitz, M., Lau, E.K., Kotowski, S.J., Miess, E., Mann, A., Doll, C., Trinidad, J.C., Burlingame, A.L., von Zastrow, M., Schulz, S. (2013). Differentiation of opioid drug effects by hierarchical multi-site phosphorylation. Mol Pharmacol 83, 633-639.

Keith D.E., Murray, S.R., Zaki, P.A., Chu, P.C., Lissin, D.V., Kang, L., Evans, C.J., von Zastrow, M. (1996). Morphine activates opioid receptors without causing their rapid internalization. J Biol Chem 271, 19021-19024.

Kieffer, B.L. (1995). Recent advances in molecular recognition and signal transduction of active peptides: receptors for opioid peptides. Cell Mol Neurobiol 15, 615-635.

Komatsu, T., Sasaki, M., Sanai, K., Kuwahata, H., Sakurada, C., Tsuzuki, M., Iwata, Y., Sakurada, S., and Sakurada, T. (2009). Intrathecal substance P augments morphine-induced antinociception: possible relevance in the production of substance P N-terminal fragments. Peptides 30, 1689-1696.

Kramer, H.K., and Simon, E.J. (1999). Role of protein kinase C (PKC) in agonist-induced mu-opioid receptor down-regulation : II . Activation and Involvement of the alpha, epsilon, and zeta isoforms of PKC. J Neurochem 72, 594-604.

Lao, L., Song, B., Chen, W., and Marvizón, J. (2008). Noxious mechanical stimulation evokes the segmental release of opioid peptides that induce μ-opioid receptor internalization in the presence of peptidase inhibitors. Brain Res 1197, 85-93.

Lupp, A., Richter, N., Doll, C., Nagel, F., Schulz, S. (2011) UMB-3, a novel rabbit monoclonal antibody, for assessing μ-opioid receptor expression in mouse, rat, and human formalin-fixed and paraffin-embedded tissues. Peptides 167, 9-13.
Macdonald, S., Dumas, J., and Boyd, N. (1996). Chemical cross-linking of the substance P (NK-1) receptor to the α subunits of the G proteins Gq and G11. Biochemistry 35, 2909-2916.

Malin, S., Davis, B., Molliver, D. (2007). Production of dissociated sensory neuron cultures and considering their use in studying neuronal function and plasticity. Nat Protoc 2, 152-160.

Mann, A., Illing, S., Miess, E., Schulz, S. (2014). Different Mechanisms of homologous and heterologous μ-opioid receptor phosphorylation. Br J Pharmacol Epub ahead of print, Feb 12, 2014.

Marchese, A., Paing, M.M., Temple, B.R.S., and Trejo, J. (2008). G Protein–Coupled Receptor Sorting to Endosomes and Lysosomes. Ann Rev Pharmacol Toxicol 48, 601-629.

Martini, L., and Whistler, J.L. (2007). The role of mu opioid receptor desensitization and endocytosis in morphine tolerance and dependence. Curr Opin Neurobiol 17, 556-564.

Melief, E., Miyatake, M., Bruchas, M., and Chavkin, C. (2010). Ligand-directed c-Jun N-terminal kinase activation disrupts opioid receptor signaling. Proc Natl Acad Sci USA 107, 11608-11613.

Miesenböck, G., de Angelis,D.A., and Rothman, J.E. (1998). Visualizing secretion and synaptic transmission with pH-sensitive green fluorescent proteins. Nature 394, 192-195.

Mohrland, J.S., and Gebhart, G.F. (1979). Substance P-induced analgesia in the rat. Brain Research 171, 556-559.

Murtra, P., Sheasby, A.M., Hunt, S.P., and de Felipe, C. (2000). Rewarding effects of opiates are absent in mice lacking the receptor for substance P. Nature *405*, 180-183.

Nichols, M.L., Allen, B.J., Rogers, S.D., Ghilardi, J.R., Honore, P., Luger, N.M., Finke, M.P., Li, J., Lappi, D.A., Simone, D.A., Mantyh, P.W. (2014). Transmission of chronic nociception by spinal neurons expressing the substance P receptor. Science *286*, 1558-1561.

Patwardhan, A.M., Berg, K.A., Akopain, A.N., Jeske, N.A., Gamper, N., Clarke, W.P., Hargreaves, K.M. (2005). Bradykinin-induced functional competence and trafficking of the mu-opioid receptor in trigeminal nociceptors. J Neurosci 25, 8825-8832.
Perl, E.R. (2007). Ideas about pain, a historical view. Nat Rev Neurosci 8, 71-80.
Pettinger, L., Gigout, S., Linley, J.E., and Gamper, N. (2013). Bradykinin controls pool size of sensory neurons expressing functional mu-opioid receptors. J Neurosci 33, 10762-10771.

Pfeiffer, M., Kirscht, S., Stumm, R., Koch, T., and Wu, D., Laugsch, M, Schroder, H, Hollt, V., Schulz, S. (2003). Heterodimerization of substance P and μ-opioid

receptors regulates receptor trafficking and resensitization. J Biol Chem 278, 51630-51637.

Pierce, K.L., Premont, R.T., and Lefkowitz, R.J. (2002). Seven-transmembrane receptors. Nat Rev Mol Cell Biol 3, 639-650.

Pradhan, A.A.A., Walwyn, W., Nozaki, C., Filliol, D., Erbs, E., Matifas, A., Evans, C., and Kieffer, B.L. (2010). Ligand-directed trafficking of the mu-opioid receptor in vivo: two paths toward analgesic tolerance. J Neurosci 30, 16459-16468.

Premont, R.T., and Gainetdinov, R.R. (2007). Physiological Roles of G Protein–Coupled Receptor Kinases and Arrestins. Ann Rev Physiol 69, 511-534.

Puthenveedu, M., Lauffer, B., Temkin, P., and Vistein, R., Carlton, P., Thorn, K., Taunton, J., Weiner, O.D., Parton, R.G., von Zastrow, M. (2010). Sequence-dependent sorting of recycling proteins by actin-stabilized endosomal microdomains. Cell 143, 761-763.

Raehal, K.M., Schmid, C.L., Groer, C.E., and Bohn, L.M. (2011). Functional selectivity at the mu -opioid receptor: implications for understanding opioid analgesia and tolerance. Pharmacol Rev 63, 1001-1019.

Roman-Vendrell, C., Yu, Y.J., and Yudowski, G.A. (2012). Fast modulation of μ-opioid receptor (MOR) recycling is mediated by receptor agonists. J Biol Chem 287, 14782-14791.

Rosenbaum, D.M., Rasmussen, S.G.F., and Kobilka, B.K. (2009). The structure and function of G-protein-coupled receptors. Nature 459, 356-363.

Scita, G., and Di Fiore, P.P. (2010). The endocytic matrix. Nature 463, 464-473.
Shepherd, J.D., and Huganir, R.L. (2007). The cell biology of synaptic plasticity: AMPA receptor trafficking. Ann Rev Cell Dev Biol 23, 613-643.

Soohoo, A.L., and Puthenveedu, M.A. (2013). Divergent modes for cargo-mediated control of clathrin-coated pit dynamics. Mol Biol Cell 24, 1725-1734.

Sorkin, A. and von Zastrow, M. (2009). Endocytosis and signalling: intertwining molecular networks. Nat Rev Mol Cell Bio 10, 609-622.

Stein, C., and Lang, L.J. (2009). Peripheral mechanisms of opioid analgesia. Curr Opin Pharmacol 9, 3-8.

Talbot, J.N., Happe, H.K., Murrin, L.C. (2005). Opioid Receptor Coupling to Gi/o Proteins Increases during Postnatal Development in Rat Brain. J Pharmacol Exp Ther 314, 596-602.

Tanowitz, M., and von Zastrow, M. (2003). A novel endocytic recycling signal that distinguishes the membrane trafficking of naturally occurring opioid receptors. J Biol Chemistry 278, 45978-45986.

Vistein, R., and Puthenveedu, M.A. (2013). Reprogramming of G protein-coupled receptor recycling and signaling by a kinase switch. Proc Of Natl Acad Sci USA 110, 15289-15294.

von Zastrow, M. and Williams, J. (2012). Modulating neuromodulation by receptor membrane traffic in the endocytic pathway. Neuron 76, 22-32.

Wang, F., Chen, X., Zhang, X., and Ma, L. (2008). Phosphorylation State of μ-Opioid Receptor Determines the Alternative Recycling of Receptor via Rab4 or Rab11 Pathway. Mol Endocrinol 22, 1881-1892.

Williams, J.T., Ingram, S.L., Henderson, G., Chavkin, C., von Zastrow, M., Schulz, S., Koch, T., Evans, C.J., and Christie, M.J. (2012). Regulation of mu-opioid receptors: desensitization, phosphorylation, internalization, and tolerance. Pharmacol Rev 65, 223-254.

Yu, Y.J., Dhavan, R., Chevalier, M.W., Yudowski, G.A., and von Zastrow, M. (2010). Rapid delivery of internalized signaling receptors to the somatodendritic surface by sequence-specific local insertion. J Neurosci 30, 11703-11714.

Yu, Y.J., Arttamangkul, S., and Evans, C.J., Williams, J.T., von Zastrow, M. (2009). Neurokinin 1 receptors regulate morphine-induced endocytosis and desensitization of μ-opioid receptors in CNS neurons. J Neurosci 29, 222-223.

Yudowski, G.A., Puthenveedu, M.A., Henry, A.G., and von Zastrow, M. (2009). Cargo-Mediated Regulation of a Rapid Rab4-Dependent Recycling Pathway. Mol Biol Cell 20, 2774-2784.

Yudowski, G.A., Puthenveedu, M.A., and von Zastrow, M. (2006). Distinct modes of regulated receptor insertion to the somatodendritic plasma membrane. Nat Neurosci 9, 622-627.

Part II: Protein Kinase C Mediated Positive Feedback of Mu-Opioid Receptor Recycling

Abstract

Protein kinase C (PKC) has been shown to be required and sufficient to increase recycling of the mu-opioid receptor (MOR). Since activation of the MOR causes separation of the $G_{\beta\gamma}$ from the $G_{\alpha/i}$ and subsequent activation of PKC through phospholipase C (PLC), we sought to determine if the MOR could reinforce its own recycling through this mechanism. We utilized a pH-sensitive GFP in combination with Total Internal Reflection Fluorescence Microscopy (TIR-FM) to visualize single-event recycling of the MOR, as described previously (Yudowski, Puthenveedu, Henry, & Zastrow, 2009) (Bowman et al., 2015). First we observed that removal of agonist results in a rapid loss of MOR recycling. Since, $G_{\beta\gamma}$ activates PKC through PLC (McCudden, Hains, Kimple, Siderovski, & Willard, 2005) we sought if inhibition of PLC by the inhibitor U73122 results in decreased MOR recycling. Downstream of PLC is PKC, whose inhibition and activation decreases and increases MOR recycling, respectively (Bowman et al., 2015). Single mutations of two known PKC phosphorylation sites: T370A, S363A resulted in loss of PKC driven increase in recycling (Bowman et al., 2015). This suggests direct phosphorylation of PKC on the MOR mediates a positive feedback in MOR recycling.

Introduction

GPCRs are widely considered to be important signaling molecules as they carry on many of important and diverse signals that are necessary for life. However the molecular signals that govern the intracellular trafficking of the GPCRs are of equal importance, as they determine when, if, and where the receptor can signal in the first place. Some receptors, such as the delta opioid receptor, are retained in intracellular pools and cannot signal until they have been released to the cell surface (Kim, 2002). The β2-adrenergic receptor (β2AR) has been well studied in this regard. Its internalization prevents signaling from the surface, however once the receptor reaches endosomal compartments the receptor has been shown to coordinate a second wave signaling (Tsvetanova & Zastrow, 2014) (Irannejad & Zastrow, 2014). It is thought that these geographically separate signaling receptors result in differential consequences.

The post-endocytic recycling of GPCRs has been of interest since it determines the re-sensitization of receptors at the cell surface. This re-sensitization primes the cell to respond to agonist stimulation. Recycling is not an attribute shared by all receptors, suggesting that recycling may exist to give control over the re-sensitization rate. In the case of the clinically relevant MOR, a muted desentization to opiates requires more and more agonists to achieve the same activation of signal leading to a build up of opiate tolerance and addiction. GPCR post-endocytic recycling has been best defined for the β2-adrenergic

receptor. The β2AR has a known sequence shown to be required for the recycling of the receptor; this sequence is the C-terminal PDZ-ligand (Yudowski et al., 2009). The function of this PDZ-ligand is thought to connect the receptor to the actin cytoskeleton, as replacing the PDZ-ligand with an actin binding domain restores this function. In fact, all three known binding partners of this PDZ-ligand (MAGI3, NHERF, SNX27) all associate with the actin cytoskeleton (Yang et al., 2010) (Cao, Deacon, Reczek, Bretscher, & Zastrow, 1999) (Lauffer et al., 2010). Furthermore, live-cell confocal microscopy at the endosomes from which the receptor recycles from show that β2AR has been localizes to actin-stabilized tubules on endosomes. Signaling regulation of the β2AR recycling has been shown to be a self-regulatory process through Protein Kinase A (PKA) which is activated downstream of the receptors' activation of $G_{\alpha/s}$ protein (Yudowski et al., 2009). Removal of agonist results in a decrease in recycling suggesting a negative feedback loop with PKA. This may be due to downstream effect of PKA activated Src kinase phosphorylating cortactin, as inhibition of Src kinase decreases β2AR recycling (Vistein & Puthenveedu, 2014). Additionally, PKA acts directly on the receptor and controls the tubules the receptor traverses through.

Some insights have been made towards the mechanics of MOR recycling. The MOR lacks a C-terminal PDZ-ligand, however the required sequence for MOR recycling has been attributed to leucine 387 and 390 (Tanowitz & Zastrow, 2003). Mutation of these leucines to alanines significantly reduces the ability of the MOR to recycle (Tanowitz & Zastrow, 2003). Regulation of MOR recycling

can occur through the pain receptor, neurokinin-1 (NK1R) through G_q activation of Protein Kinase C (PKC) (Bowman et al., 2015). However, the MOR itself can activate PKC through Gβγ activation (Jordan & Devi, 1998). We sought to determine if PKC regulation of MOR recycling could be a mechanism used by MOR to regulate its own recycling or if receptor self-regulation occurs through a different mechanism, perhaps through protein kinase A (PKA). Removal of agonist results in a decrease in MOR recycling. Downstream of $G_{\beta\gamma}$, we showed that inhibition of phospholipase C (PLC) resulted in decreased levels of MOR recycling. The inhibition and activation of the downstream protein kinase C (PKC) resulted increase and activation of MOR recycling, respectively. We also tested if PKA also had regulatory MOR recycling in HEK293 cells. Furthermore, we found that known PKC-phosphorylation sites, T370 and S363 were required for PKC mediated increase.

Methods

Cell Culture and Microscopy

HEK293 cells were kept in DMEM with 10% Fetal Bovine Serum by volume at 37ºC in 5% CO_2. Cells were plated onto 25mm number 1 glass coverslips 48 hours before plating to allow the cells to settle on the glass before imaging. Cells were transferred to Phenol-Red free Opti-MEM media with 10% serum before imaging. Cells were imaged on a Nikon Ti-Eclipse 2000 microscope with an Andor XD spinning disk confocal system through a 100x or 60x 1.49 NA TIRF

objective with 488 solid-state lasers. Images were acquired with an Andor iXon+ EM-CCD camera through Andor IQ software. Raw 16-bit image files were quantified.

Measuring individual rapid recycling events by TIR-FM microscopy

To visualize individual recycling events, HEK293 cells stably expressing Super ecliptic pHulorin-tagged MOR (SpH-MOR) were incubated for 5-minutes with the MOR specific agonist, DAMGO (D-Ala , N-Me-Phe, Gly-ol) at 10μM to induce internalization MOR. SpH-MOR is quenched inside the cell. When the SpH-MOR cells return to the cell surface into the TIR-FM field the receptors are visible as distinct puncta. The cells were then imaged for 1 minute at 10 frames per second to record the number of recycling events. Pharmacological test drugs were incubated with the cells for one minute. Once again, the cells are imaged for 1 minute at 10 frames per second to record the number of recycling events for this condition. An experimental timeline schematic accompanies the figures. For analysis, the number of observed exocytic events is normalized to the number of exocytic events, which occur in that cell with DAMGO alone to give a paired comparison. Each cell was quantified manually in a double blind manner. The number of events were quantified manually significance was determined by paired Student's t-test.

Results

Agonist removal decreases MOR recycling

To visualize individual recycling events, we utilized a HEK293 cell line stably expressing an N-terminal superecliptic pHluorin-tagged MOR (Sph-MOR) with total internal reflection fluorescent microscopy (TIR-FM), as described previously (Yudowski et al., 2009). Figure 3-8A shows time-lapse images of a single cell as it transitions from endocytic clustering events to exocytic events. Before the addition of DAMGO, the SpH-MOR is expressed smoothly on the plasma membrane. After the addition of DAMGO, the MOR condenses into distinct puncta representative of clathrin-mediated endocytosis events. These endocytic puncta are readily apparent by the 180-second time point, denoted by the white arrowhead. After about 330 seconds endocytic clusters are diminished and are easily distinguishable from the recycling event shown in the upper left corner marked by the arrow. Note the difference in size of the endocytic and exocytic structures. Figure 3-8B shows a time lapse of a single SpH-MOR recycling event at the cell surface (top) with a corresponding heat map diagram (bottom). An exocytic event is characterized as an initial bright, concentrated peak of intensity when it reaches the cell surface. As fusion with the cell membrane occurs, SpH-MOR spreads across the cell surface causing a rapid loss of fluorescence. In the heat map diagram, both height and lighter colors represent a brighter fluorescent signal, therefore we observe a tall bright spike initially and end with a flat purple structure. We can also define a recycling event

by plotting the mean fluorescence values (right y-axis, green) of the area with the maximum fluorescence (left y-axis, red), Fig 3-8C. Due to the sharp rise and spread features of the exocytosis events, we expect to see the maximum fluorescence decrease over time, while the average fluorescence increases.

We used this single-event recycling assay to demonstrate that when agonist was removed the recycling rate of MOR decreased significantly. The experimental design is schematized in the top panel of Fig 3-8D. First, the cells are pre-incubated with DAMGO for 5 minutes. This causes internalization of the MOR and creates a pool whose post-endocytic recycling can be measured. Then we capture a 1-minute movie at 10 frames per second (10 hertz), to gain a baseline measurement for recycling level of that particular cell. We then assayed for recycling rates at both 1-minute and 5 minutes after agonist removal. The recycling rates for each cell are normalized to the initial baseline measurement. This analysis allows for a paired comparison of recycling rates within a cell, and helps to eliminate cell-to-cell variability. We did not observe any discernable change in recycling 1-minute after agonist removal, but observed a sharp decrease in recycling rates at 5 minutes after washout. This supports previous reports (Roman-Vendrell, Yu, & Yudowski, 2012) and suggests a possible feedback loop for the MOR to impact its own recycling through its own downstream signaling.

The MOR Recycles Independently from the PKA- Regulated Mechanism

Previously Determined for the β2-Adrenergic Receptor

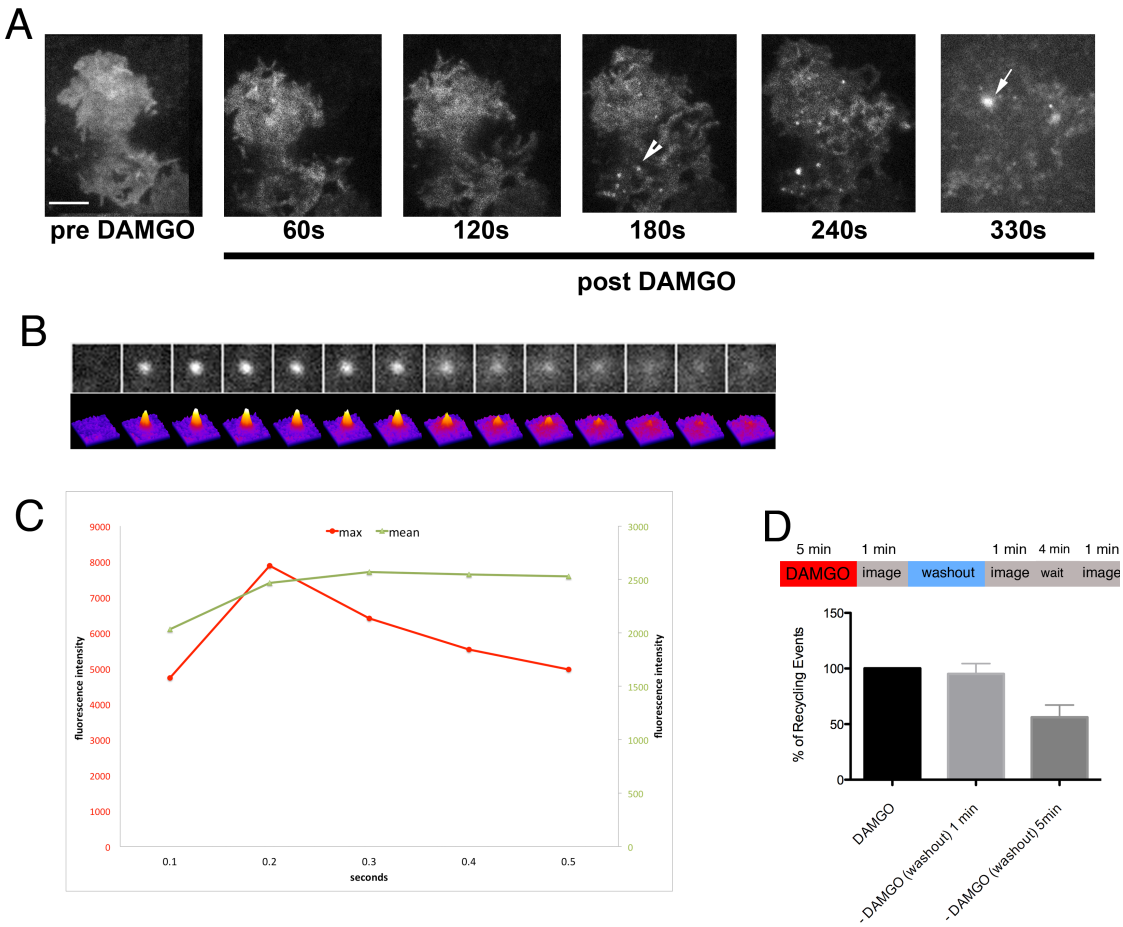

Figure 3-8. Visualizing the decrease in MOR recycling events after agonist removal.
A) Different morphologies of endocytic and exocytic events in the same cell. Images of the same cell through time before and after DAMGO treatment as the MOR transitions from and endocytic to an exocytic state. Endocytic puncta (arrowhead, in 180s panel) are significantly smaller than exocytic recycling events (arrow, in 330s panel). The scale bar is 4μm. B) A close-up of a single exocytic event, top panel. Exocytic events are characterized by an initial bright fluorescent spot followed by a distinct spreading of that signal. A heat map, bottom panel, forms a visual representation of the fluorescent signal of that image. The taller and lighter in color the protrusion is, the brighter the signal. C) Exocytic events are characterized by sharp increase in local maximum fluorescence (red, left y-axis), which decreases over time while the mean fluorescence increases over time. (green, right y-axis) This occurs because of the fusion of the exocytic vesicle. D) Removal of agonists in decreases the recycling rate of MOR. The recycling rate was measured after DAMGO for a baseline measurement and then one 1 min and 5 min after washout of DAMGO, as diagramed in the top panel. After normalization to the baseline measurement, MOR recycling rate drops to 50% by 5 min after washout. n = 7. $p < 0.01$ by Student's paired t-test. Error bars are s.e.m.

One possibility is that PKA could be regulating the recycling of the MOR. PKA has been previously implied in a mechanism for the β2AR to control its recycling rate through its signaling. The MOR is G_i coupled, and thus inhibits adenylyl cyclase and therefore PKA (Jordan & Devi, 1998). Conversely to the MOR, the recycling of the β2AR has been shown to increase with washout of its agonist isoproternanol (Yudowski et al., 2009). The β2AR is coupled to different G-protein subtypes $G_{\alpha/s}$ which stimulates the activity of adenylate cyclase. This leads to increased levels of cyclic adenosine monophosphate (cAMP) that activate PKA. The differential effects on PKA by the inhibitory MOR or activating β2AR signaling could explain how removal of agonist results in differential control of GPCR recycling.

Previously, it has been shown that inhibition of PKA by the inhibitor KT5720 (KT) leads to increased levels of recycling of the β2AR that mimic the effect seen with the washout of agonist. This suggests that the activation of the receptor creates a negative-feedback loop through PKA that inhibits the recycling of the receptor. We first tested to see if further inhibition of PKA by its pharmacological inhibitor KT5720 (KT) would affect recycling rates of the MOR. We first activated HEK293 cells with saturating 10μM of DAMGO for five minutes to cause the internalization of the receptors. We then imaged the cell for one minute at 10 frames per second to record a baseline number of recycling events for the cell. We then added 10μM KT to inhibit PKA, and waited 1 minute for the inhibitor to take affect. We then imaged the cell for 1 minute at 10 frames per

second to record the number of recycling events after (further) PKA inhibition. This procedure is schematized in the upper panel of Figure 3-9A. We observed that were was no significant change in the number of recycling events after inhibition of PKA. Figure 3-9B shows a kymograph a cell before and after PKA addition. The kymograph image is a way to observe the image across time, and the recycling events are observed as bright spots with comet tails, as denoted by the white arrowhead. The white box in the left panel denotes the subset of the image represented in the kymograph. There does not appear to be a discernable difference in the number of puncta between the DAMGO alone versus the DAMGO and KT conditions. However, condensing the recycling movies into single frames results in a loss in resolution of the distinct rise and fluorescence of recycling events, and so, the recycling events were quantified through observation of the movie and not a still frame. We quantified the number of recycling events across 14 cells, normalized to the number of recycling events with DAMGO alone, and observed no discernable difference. However, since the downstream signaling from the $G_{\alpha/i}$ from the MOR already results in inhibition of PKA, we then tested the effect of activation of PKA on the recycling of the MOR and then retested the inhibition of PKA after the activation. We recorded a baseline of exocytosis events after internalization of the MOR with 10μM DAMGO. Next we tested the number of recycling events after a one-minute incubation with 10μM forskolin,

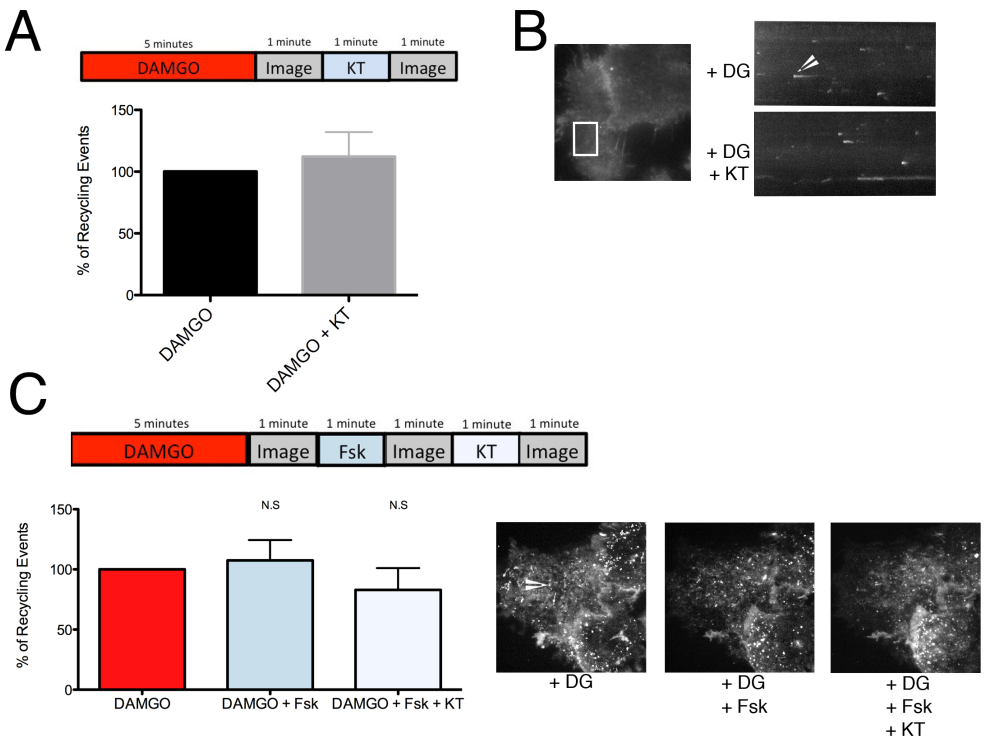

Figure 3-9: Recycling of the MOR is not affected by PKA.
A) Inhibition of PKA by KT5720 does not change MOR recycling. A baseline recycling measurement was taken before addition of KT5720, diagramed in top panel. KT treated cells showed no difference in recycling rate from the baseline measurement normalized to 100%. n = 14 p = 0.4 via Student's paired t-test. Error is s.e.m. B) Kymographs show number of excyotic events in a region of an example cell before and after KT addition. The cell subset is outlined by a white rectangle in the left panel. The excyotic events appear as spots with comet tails. An example is highlighted with the white arrowhead. C) PKA activation nor inhibition changes MOR recycling. MOR recycling levels were measured after DAMGO treatment alone, after forskolin treatment (Fsk) and KT treatment, as diagramed in the top panel. After normalization to the baseline recycling rate, neither PKA activation by Fsk nor subsequent inhibition by KT caused a significant change in MOR recycling rates. n = 14. p = 0.66 for DAMGO vs. DAMGO + FSK, p = 0.38 for DAMGO vs. DAMGO + Fsk + KT via Student's paired t-test. Error is s.e.m. Right panel, representative maximum projection images of the same cell after all three treatments. In a maximum projection the exocytic events are visible as puncta, exemplified by the arrowhead. The number of puncta are relatively the same across all three treatments.

(fsk), the PKA activator. Then, we inhibited PKA with 10μM KT to test the full range of PKA activity on the recycling of the MOR. The procedure is diagramed in Figure 3-9C, top panel. Quantification across 16 cells revealed no significant difference in levels of MOR recycling due to the increase or decrease in PKA, Figure 3-9C. An example cell is displayed through maximum projection images under each condition: the DAMGO alone, DAMGO and forskolin, and the DAMGO, forskolin and KT conditions, Figure 3-9C, right. The maximum projection displays all of the brightest pixels across a time series, thus exocytic events appear as puncta. The number of puncta shown appears to be about the same. This suggests that PKA activity has no effect on MOR recycling, and that the recycling of GPCRs is not controlled by a universal mechanism.

Recycling of the MOR is Controlled by PLC

We then sought to determine what controls the recycling of the MOR. Since PKA inhibition is the main signaling pathway downstream of $G_{\alpha/i}$, we sought after proteins down stream of $G_{\beta\gamma}$. Activation of the $G_{\beta\gamma}$ of the G protein leads to activation of phospholipase C (PLC). We tested to see of inhibition of PLC by the compound U73122 would affect MOR recycling rates. We observed a significant decrease to half of the MOR recycling compared to baseline levels, Figure 3-10A. This implies that PLC plays a role in regulation MOR recycling. PLC cleaves PIP_2 to activate two important signaling pathways: diacyl glycerol (DAG), which

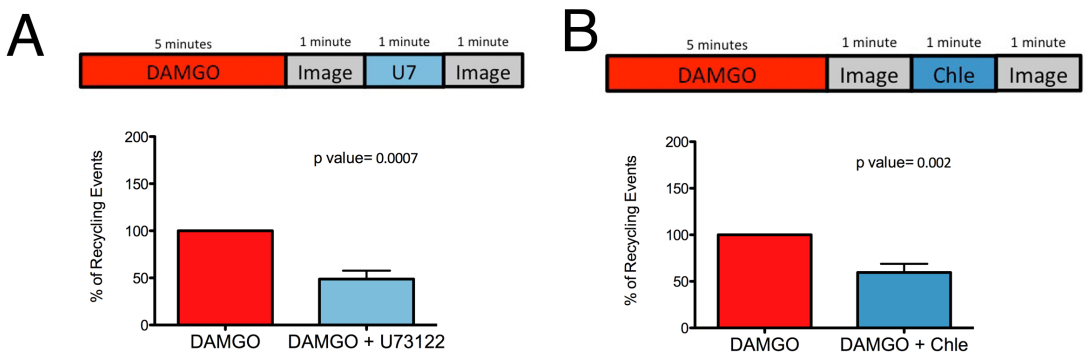

Figure 3-10: Inhibition of $G_{\beta\gamma}$ signals decrease MOR recycling
A) Inhibition of PLC by U73122 causes a decrease in MOR recycling. A baseline recycling rate was measured in addition to recycling rate after U7 treatment, as diagramed in the top panel. n = 23. Error is s.e.m. B) Inhibition of PKC by chelerythrine (Chle) causes a decrease in MOR recycling. Baseline recycling rate was measured before addition of Chle. The MOR recycling rate dropped significantly to 50% after Chle addition. n = 23. Error is s.e.m.

activates PKC and inositol-3-phosphate (IP3), which leads to intracellular calcium release. We showed that inhibition of PKC by chelerythrine (Chle) inhibited MOR recycling to the same 50% degree as the PLC inhibition, Figure 3-10B. This suggests that the PKC inhibition was responsible for the PLC inhibition affect. Additionally, the converse treatment of PKC activation via phorbol 12-mystrate 13-acetate (PMA) resulted in an increase in MOR recycling over baseline, Figure 3-3B.

Discussion

This work shows the protein kinase C is critical for regulating the recycling of the MOR. It serves as a nexus point where feedback signaling from other receptors, like the G_q coupled, neurokinin-1 receptor, and the MOR itself can interact with and control MOR signaling. Since all GPCRs utilize the same machinery for trafficking and signaling it is difficult to see how the many signals of a cell do not get lost and blended together. This conversion of receptor recycling control acts at a point where the many different signals could rely upon another.

We first examined the possibility that PKA could act as a global control mechanism for GPCRs to impact their own recycling. Regulation of recycling through both PKC and PKA are not mutually exclusive. PKA has already been shown to govern the recycling of the β2AR, through the receptors own downstream signaling. Our data does not support a role for PKA in MOR recycling. However, there are previous results that show that activation of PKA

with forskolin decreases MOR recycling in cultured striatal neurons with morphine activated receptors (Roman-Vendrell et al., 2012). This may suggest different mechanisms of recycling with different cell types. Additionally, it has been shown that the morphine-activated receptor is differentially phosphorylated from the DAMGO activated receptor; the morphine activated receptor lacks phosphorylation at T370. Data from our lab (data not shown) has visualized that the T370A phosphorylation null mutant is exclusively localized to actin stabilized endosome tubules. These are the same endosomal tubules that the β2AR localizes to. Thus the differential phosphorylation of the morphine-activated receptor could be shuttling the MOR into a fully PKA regulated pathway.

Our remaining experiments tested to see if PKC could be a mechanism in which the MOR could control its own recycling. Washout of MOR agonist caused a rapid decrease in receptor recycling. This data was confirmed by published studies. It also suggests that signaling through the receptor mediates a type of positive feedback that acts on recycling. Inhibition of PLC negates this affect. Inhibition of PKC mimicked the effect of PLC inhibition, suggesting it is what is activated by PLC to control MOR recycling. Activation of PKC worked to increase MOR recycling suggesting that is it is the signal that controls MOR recycling. This control is not limited to signals coming from the receptor itself nor from other receptors. Further work will need to explore the exact mechanism in which PKC works to increase MOR recycling rates.

References

Bowman, S. L., Soohoo, A. L., Shiwarski, D. J., Schulz, S., Pradhan, A. A., & Puthenveedu, M. A. (2015). Cell-Autonomous Regulation of Mu-Opioid Receptor Recycling by Substance P. *Cell Reports*. doi:10.1016/j.celrep.2015.02.045

Cao, T. T., Deacon, H. W., Reczek, D., Bretscher, A., & Zastrow, von, M. (1999). A kinase-regulated PDZ-domain interaction controls endocytic sorting of the beta2-adrenergic receptor. *Nature*, *401*(6750), 286–290. doi:10.1038/45816

Irannejad, R., & Zastrow, von, M. (2014). GPCR signaling along the endocytic pathway. *Current Opinion in Cell Biology*, *27*, 109–116.

Jordan, B., & Devi, L. A. (1998). Molecular mechanisms of opioid receptor signal transduction. *British Journal of Anaesthesia*, *81*(1), 12–19.

Kim, Y. M. (2002). Differential Roles of Arrestin-2 Interaction with Clathrin and Adaptor Protein 2 in G Protein-coupled Receptor Trafficking. *The Journal of Biological Chemistry*, *277*(34), 30760–30768. doi:10.1074/jbc.M204528200

Lauffer, B. E. L., Melero, C., Temkin, P., Lei, C., Hong, W., Kortemme, T., & Zastrow, von, M. (2010). SNX27 mediates PDZ-directed sorting from endosomes to the plasma membrane. *The Journal of Cell Biology*, *190*(4), 565–574. doi:10.1083/jcb.201004060

McCudden, C. R., Hains, M. D., Kimple, R. J., Siderovski, D. P., & Willard, F. S. (2005). G-protein signaling: back to the future. *Cellular and Molecular Life Sciences*, *62*(5), 551–577. doi:10.1007/s00018-004-4462-3

Roman-Vendrell, C., Yu, Y. J., & Yudowski, G. A. (2012). Fast modulation of μ-opioid receptor (MOR) recycling is mediated by receptor agonists. *The Journal of Biological Chemistry*, *287*(18), 14782–14791. doi:10.1074/jbc.M111.319616

Tanowitz, M., & Zastrow, von, M. (2003). A Novel Endocytic Recycling Signal That Distinguishes the Membrane Trafficking of Naturally Occurring Opioid Receptors. *Journal of Biological Chemistry*, *278*(46), 45978–45986. doi:10.1074/jbc.M304504200

Tsvetanova, N. G., & Zastrow, von, M. (2014). Spatial encoding of cyclic AMP signaling specificity by GPCR endocytosis. *Nature Chemical Biology*, *10*(12), 1061–1065. doi:10.1038/nchembio.1665

Vistein, R., & Puthenveedu, M. A. (2014). Src regulates sequence-dependent beta-2 adrenergic receptor recycling via cortactin phosphorylation. *Traffic*, *15*(11), 1195–1205. doi:10.1111/tra.12202

Yang, X., Zheng, J., Xiong, Y., Shen, H., Sun, L., Huang, Y., et al. (2010). Beta-2 adrenergic receptor mediated ERK activation is regulated by interaction with MAGI-3. *FEBS Letters*, *584*(11), 2207–2212. doi:10.1016/j.febslet.2010.03.039

Yudowski, G., Puthenveedu, M., Henry, A., & Zastrow, von, M. (2009). Cargo-Mediated Regulation of a Rapid Rab4-Dependent Recycling Pathway. *Molecular Biology of the Cell*, 1–11. doi:10.1091/mbc.E08

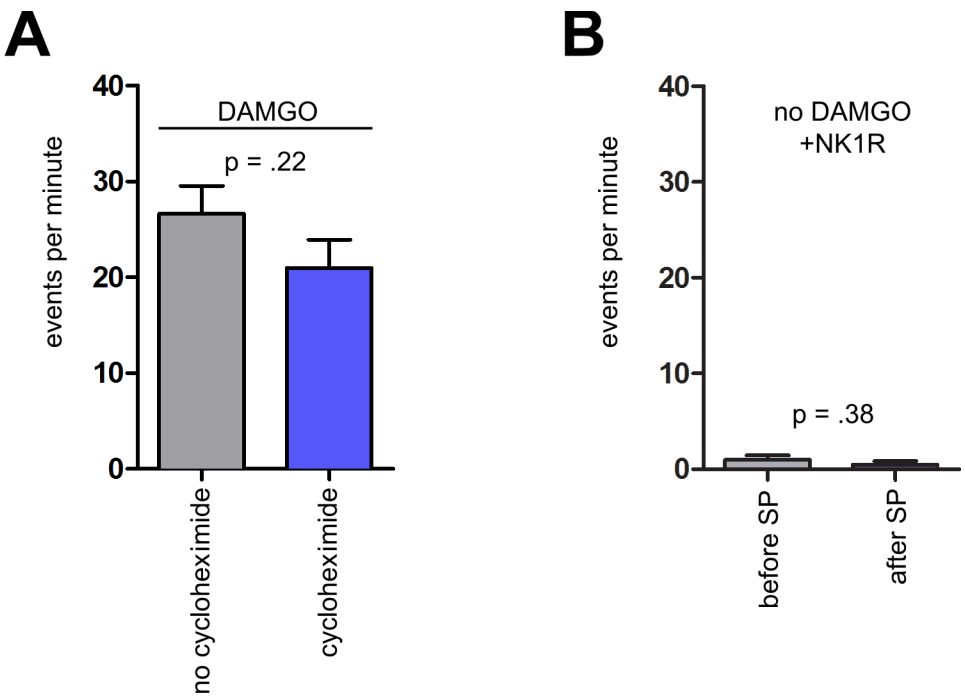

Figure S3-1. SpH-MOR Single event recycling assays are unaffected by changes in biosynthetic trafficking and NK1R trafficking, related to Fig 2. A) HEK293 cells were either pre-treated with 10μM cyclohexamaide for 4hr at 37°C or not pre-treated with cyclohexamide, and incubated with DAMG. Number of recycling events per munite after 5 min DAMGO incubation are platted (n- 52, no treatment, n = 28, + cycloheximide, error bars are S.E.M across cells). B) Number of recycling events per minute before and after 5 min SP incubation (no DAMGO pre-treatment) are plotted, from HEK293 cells co-expressing SpH-MOR and NA-NK1R (n=20, error bars are s.e.m across cells).

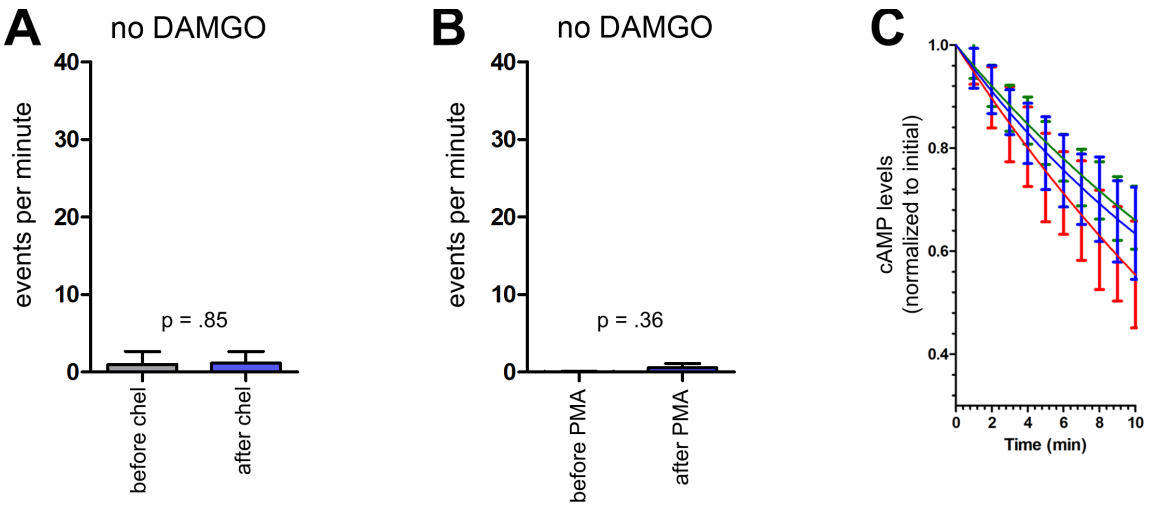

Figure S3-2. PKC inhibition or activation does not affect MOR recycling or signaling with the presence of agonist, related to Fig 3. A) Number of SpH-MOR recycling events per minute before and after 1 min chel addition in absence of DAMGO (n=17 cells, error bars are s.e.m across cells. B) Number of SpH-MOR recycling events per minute before and after 1 minute PMA addition in absence of DAMGO (n=6 cells, error bars are s.e.m across cells). C) Luminescence-based cAMP detection assay, as in Fig 3B. Chel (green), PMA (blue), or vehicle (red) were added to cells before treatment with DAMGO, Chel, and PMA pre-treatments did not affect the initial DAMGO challenge effect on cAMP levels (n = 3 separate experimental trials, error bars are s.e.m across multiple trials.

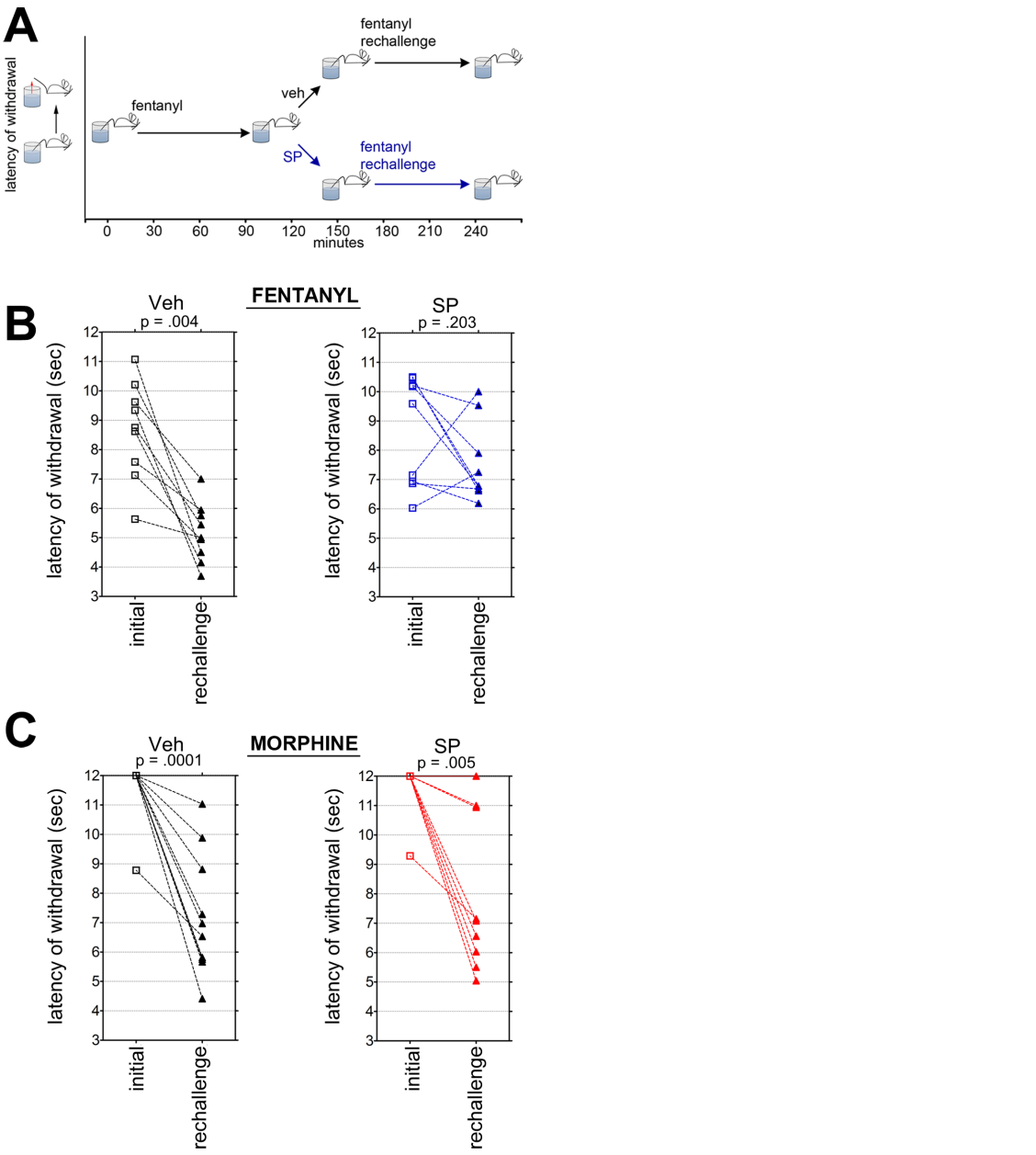

Figure S3-3. Design of thermal anti-nociception assay and paired responses from individual animals, related to Fig 7. A) Schematic of warm-water tail withdrawal assay. Baseline measurements were taken, animals were injected with agonist (fentanyl shown), and tail-withdrawal latencies were measured every 30min. Saline (vehicle ctrol) or SP was injected intrathecally after initial response reutnred to baseline (120 min for fentanyl; 210 min for morphine). B) Graph of responses for individual mice to initial fentanyl injected and rechallenge for vehicle ctrl and SP animals. C) Graph of responses of individual mice to morphine injection and rechallenge for vehicle ctrl and SP injected animals.

Chapter 4: Detection of Mu-opioid Receptor Binding Partners via Stable Isotope Labeling of Amino Acids in Cell Culture

Introduction

The trafficking of the MOR is essential to its function as it determines receptor levels on the cell surface and can affect the receptors downstream signaling. This thesis has described two pathways in MOR trafficking: endocytosis and recycling. Through microscopy and mutational analysis we have been able to pinpoint regulatory mechanisms for both of these trafficking processes. Although, these studies have led us towards unique motifs on the receptor that govern these processes, they do not detail the exact mechanisms that make these trafficking phenomena possible. These specific motifs responsible for modulating trafficking suggest that there may be unique binding partners specific for these motifs. We sought to find as many candidate binding partners as possible by using stable isotope labeling of amino acids in cell culture (SILAC). These candidates may be further leveraged in additional SILAC experiments or other proteomic studies to find binding partner candidates.

Many previous studies have sought to determine binding partners for the MOR. Proteins such as RanBPM, periplakin and filamin A have all previously been identified as MOR binding partners (Talbot et al., 2009) (Feng et al., 2003) (Wang & Burns, 2009) (Milligan, 2005). RanBPM is a scaffolding protein that binds to a variety of signaling proteins, including Ran GTPase. RanBPM was

identified in a yeast-two hybrid screen, and verified by pure protein binding assays (Talbot et al., 2009). RanBPM is thought to interact along the C-terminal tail of the MOR, although the exact binding site is undefined. The authors suggest that RanBPM overexpression inhibits beta-arrestin mediated agonist-induced internalization of the MOR, but does not affect agonist binding or cAMP inhibition. However, further studies have neither confirmed nor expanded upon these assays. Periplakin is an intermediate filament interacting protein. It has been shown to interact with both the MOR and the delta-opioid receptor. It is thought to interfere with G-protein binding (Milligan, 2005). No trafficking phenotype has been associated with periplakin modulation of MOR. The actin binding protein Filamin A has been the most studied MOR-interaction protein. Filamin A is thought to bind to the C-terminal tail of MOR. It has been suggested that filamin A is required for normal levels of internalization of the receptor (Onoprishvili et al., 2003) and the chronic morphine induced G_i to G_s switched pairing of the MOR (Wang & Burns, 2009). We had not perused our own binding experiments with these proteins because the binding sites have not been attributed to our identified trafficking sequences of interest on the receptor. The trafficking sequences of query are: the LENLEAE motif in the C-terminal tail, which required for MOR recycling (Tanowitz & Zastrow, 2003) and MOR extension of endocytic dwell times (Soohoo & Puthenveedu, 2013), and the PKC phosphorylation sites that affect recycling rates (Bowman et al., 2015). Additionally, none of these phenotypes match those of the receptor mutations.

However when perusing proteomic assays, such as SILAC, we hope to re-confirm some of these known binding proteins, and to seek them out as a marker for whether or not the assay is working.

Our own previous work to find candidate binding partners has focused on using GST-fusion proteins fused with the last 17 amino acids of the MOR C-terminal tail. These fusion proteins were favored for two main reasons, first to eliminate the refractory trans-membrane domains, and to easily compare two mutants to determine sequence specific binding. Unfortunately, these experiments were largely unsuccessful. This could stem from the fact that there are additional required elements for binding in the intracellular loop domains of the receptor, a brought us to move towards an immunoprecipitation experiment that would include the entire receptor.

Since so few, functional, and reproducible MOR binding partners have been found, we chose to broaden the scope of our studies to try to capture as many MOR binding partners as possible. We chose to use SILAC because it would give us the ability to identity a broad scope of proteins like shotgun mass spectrometry, but also the ability to seek out careful comparisons against different conditions. The basis of SILAC is to grow the two samples in either heavy or light isotope amino acid containing media, once pooled together the samples can be readily differentiated by mass spectrometry (Ong et al., 2002). A major problem in immunoprecipitation studies is the appearance of false positives. These false positives may bind to the antibody or beads non-

specifically. In order to help to eliminate these false positives we chose compare our MOR immunoprecipitation to a control immunoprecipitation. SILAC has been used successfully to determine binding proteins for other transmembrane proteins (Gokhale, Perez-Cornejo, Duran, Hartzell, & Faundez, 2012), including the β2-adrenergic receptor. We sought to adapt this protocol for the MOR, and have identified 294 candidate proteins. This data set size is comparable to previous studies. It also includes known binding proteins such as filamin A, and $G_{i,}$ as well as a few potential new binding candidates such as 14-3-3 and adseverin.

Results

Optimization of Co-immunoprecipitation of the MOR

In this SILAC test we sought to determine as many MOR receptor binding partners as possible. Previous SILAC studies on other transmembrane proteins have suggested that initial comparison of the immunoprecipitation of the target protein with a precipitation inhibited negative control would help to eliminate non-specific binding partners from the data set via the quantitative mass spectrometry analysis (Zlatic, Ryder, Salazar, & Faundez, 2010). This initial SILAC would serve as a basis to compare future sequence dependent data against. By keeping the protocol consistent with past experiments, we could draw comparison to other GPCRs as well, including our previous experiments on the β2-adrenergic receptor. The basis for the co-immunoprecipation was using the

lysate of HEK293 cell line stably expressing FLAG-tagged MOR. This N-terminal FLAG-tag on the MOR has been verified by us and others to be shown not interfere with MOR trafficking or agonist binding (Soohoo & Puthenveedu, 2013) (Bowman et al., 2015) (Puthenveedu & Zastrow, 2006). An anti-FLAG mouse monoclonal antibody was preloaded onto IgG magnetic-Dynabeads in order to precipitate MOR containing complexes. We first had to confirm that we were not only able to co-immunoprecipiate the MOR, but other candidate proteins as well.

Since we are searching for candidate partners that impact endocytosis and recycling, we chose to use a 10-minute agonist stimulation before preforming the binding experiments. At this time point we would be able to capture the MOR in both endosomes, and in clathrin-coated pits, as previously determined by our microscopy data. After this 10-minute agonist stimulation the cells are quickly moved to ice to stop trafficking. The cells are then crosslinked in the dark, in the cold room for 2 hours with 1mM DSP (dithiobis(succinimidyl propionate), see schematic in Figure 4-1A. Presence of DSP has previously been shown to inhibit the overall number of receptors captured in the immunoprecipitation, but it aids in increasing the number of binding partners that accompany the receptor (Zlatic et al., 2010).

To maximize the number of receptors that could be recovered in the pull-down experiment, we queried for the number of receptors that could be co-immunoprecipated across three different HEK293 cell lines stable, all stably

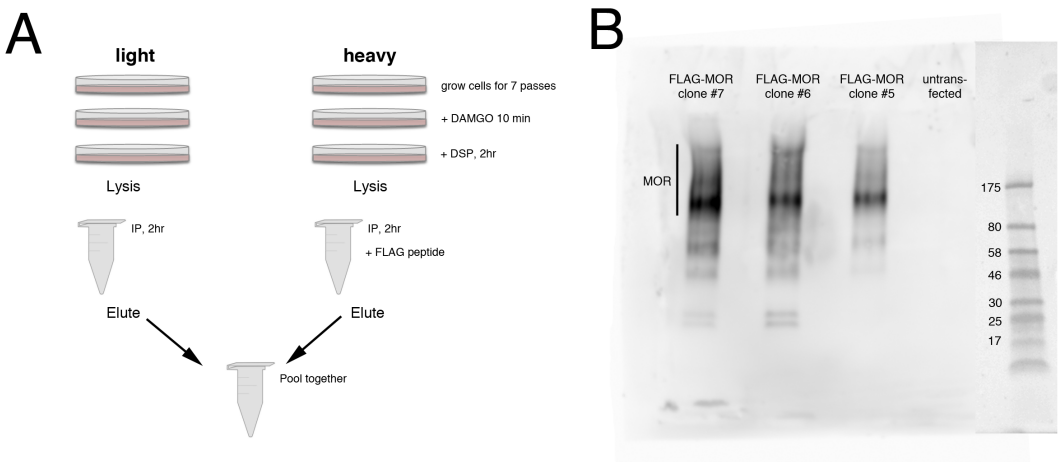

Figure 4-1: Ensuring high expression of MOR for SILAC. A) Schematic of SILAC and immunoprecipitation. B) Western blot testing for the highest MOR expression across three cell lines. Cell line #7 shows the greatest number of expressed receptors.

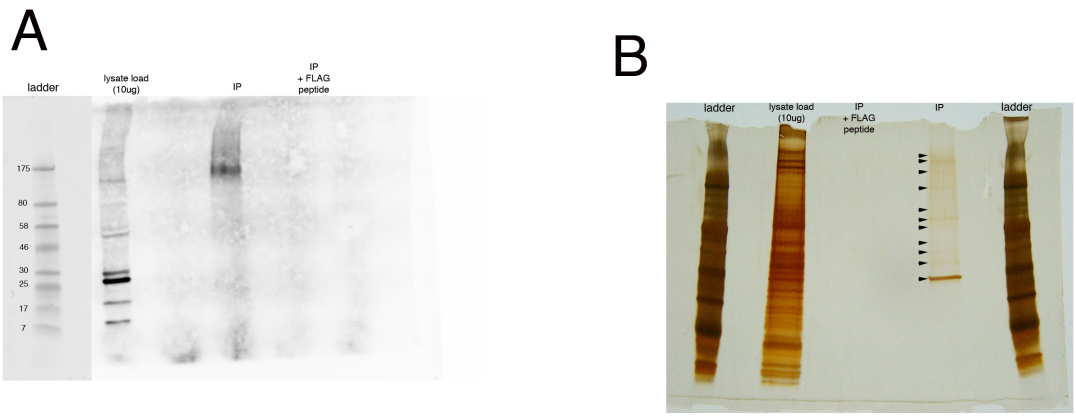

Figure 4-2: Validating MOR and candidate protein immunoprecipitation A) Silver stain showcasing immunoprecipitation of the MOR (center lane). MOR does not precipitate in the negative control, right. B) Silver stain showcasing the presence of about 11 proteins immunoprecipitation with the MOR. All bands are absent in the FLAG peptide immunoprecipitation control.

expressing the FLAG-tagged MOR, see Figure 4-1B. Receptor immunoprecipitation was confirmed by immunoblot using an anti-FLAG antibody.

The anti-FLAG antibody used in the immunoblot was a rabbit polyclonal antibody, a different antibody than the mouse monoclonal anti-FLAG antibody used for the immunoprecipitation. The FLAG-MOR signal in the immunoblots of all three cells runs as a smear from about 200-58 KDa. This smearing pattern is characteristic of GPCRs in western blots because of the high number of post-translational modifications the receptor undergoes, and has been readily seen in previous studies (Schulz et al., 2004). Receptor immunoprecipitations were done after the 2hr treatment of DSP crosslinking compound to be analogous to the future experiments. These tests were done in a small-scale version whole protocol. These tests utilized a single immunoprecipitation reaction with 500μL of cell lysate containing 500μg of protein loaded onto 30μL of beads, per each reaction condition. For perspective, the full-scale immunoprecipitation used for the SILAC experiment used 18 of these 500μg of protein lysate immunoprecipitation reactions. The cell line designated clone #7 yielded the highest number of receptors in the immunoprecipitation, leftmost lane in Figure 4-1B. This amount of receptor recovery was comparable to previous experiments.

The two critical tests needed to determine if the co-immunoprecipations of the MOR were robust enough to provide useful SILAC data were a Western blot to ensure the receptor was being pulled down, and a silver stained gel to ensure that other proteins were present. The negative control for both of these tests was

an immunoprecipitation reaction done in the presence of 100ng/mL FLAG peptide. The FLAG-peptide would competitively inhibit MOR from interacting with the anti-FLAG antibody loaded onto the IgG-dynabeads, and therefore MOR would not precipitate down with the IgG in the reaction. This control should yield no receptor signal in the immunoblot and little to no other protein signals in the silver stained gel. The inclusion of this negative control in these preliminary tests was critical, as it verified the FLAG-peptide co-incubation as a true negative control. These tests were done in small scale, with a single 500μg protein lysate load immunoprecipitation reaction per condition. Of additional note, this co-immunoprecipiation protocol can readily be adapted for general immunoprecipitation experiments. The preliminary western blot showed a clear immuno-staining of FLAG-MOR in the characteristic high-molecular weight smearing pattern, Figure 4-2A, center lane. This is similar to the patterning seen in the previous immunoblot in Figure 4-1B. No such GPCR staining was detected in the negative control, the immunoprecipitation done in the presence of FLAG peptide binding, Figure 4-2A, right most lane. The 30μg of lysate loading control shows several non-specific bands due to the cross reactivity of the antibody, left most lane, after the ladder in Figure 4-2A. None of these cross-reactive bands are enriched for in the receptor immunoprecipitation. The silver stain experiment also yielded about 11 clearly detectable bands in the MOR immunoprecipitation, Figure 4-2B. Additionally, there were no visible bands present in the control lane, with the FLAG peptide inhibition of MOR immunoprecipitation, Figure 4-2B

compare center two lanes. These tests indicate that both the MOR and other candidate binding proteins were immunoprecipiated with the MOR.

Quantitative Mass Spectromentry results from MOR SILAC

The SILAC experiment consisted of 18 individual 500μg immunoprecipitation reactions for both the experimental and control conditions. Before the immunoprecipitation, the stably expressing cell line, FLAG-MOR clone #7 was grown for seven passages in light or heavy isotope containing media. The light media lysate was used for the experimental immunoprecipitation and the heavy isotope media was used for the control immunoprecipitation in the presence of FLAG peptide, see diagram in Figure 4-1A. The elutions from the immunoprecipitation reactions were all pooled together at the end of the experiment and concentrated down from about 1mL of total elute to about 30μL of solution. Before sending the sample for mass spectrometry analysis we verified the presence of both receptor via western blot and the presence of other proteins via silver stain, Figure 4-3A and B, respectively. We used 2.5μL of the total sample, (about 8% of the total) for the western blot and silver stained gel. The western blot shows a clear enriched MOR signal, Figure 4-3A, middle lane, that is not readily apparent in the lysate control. The numerous non-specific bands in the lysate lane are not enriched in the SILAC sample. This gel looks very similar to the preliminary test Western blot from Figure 4-2A. The silver stained gel shows at least 10 distinct visible bands, Figure 4-2B. Both of these

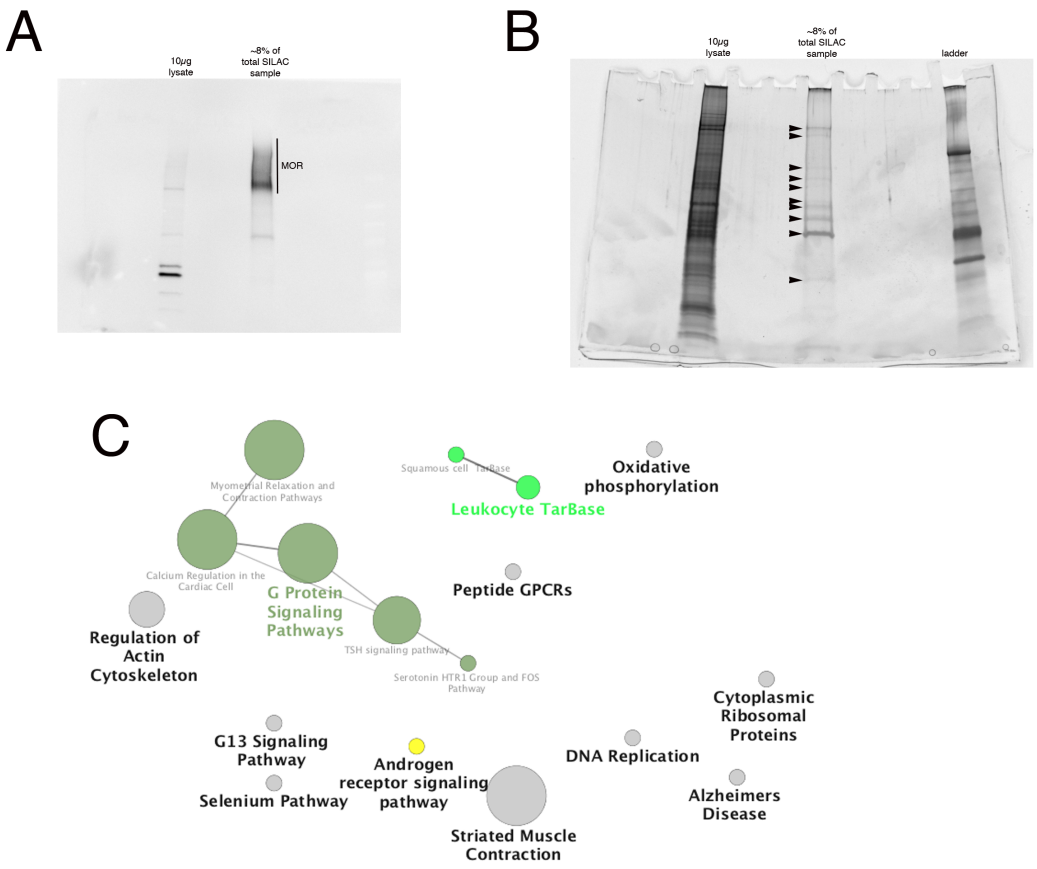

Figure 4-3: Validation of SILAC immunoprecipitation. A) Western blot showing that the MOR was immunoprecipitated in the SILAC sample. This is 8% of the total sample on the gel. B) A) Silver stain gel showing other candidate proteins immunoprecipitated in the SILAC sample. This is 8% of the total sample on the gel. C) A GO term based map showcasing the large number of GPCR and actin related proteins in the SILAC candidate protein list. Larger circles indicate a larger number of proteins in that category.

tests were encouraging enough for further analysis. The sample was run out on a gel before the mass spectrometry analysis.

The mass spectrometry results detected 387 total proteins. Due to the presence of heavy isotope amino acids in the control immunoprecipitation sample and light isotope amino acids in the experimental MOR immunoprecipitation, the mass spectrometer is also able to measure which experimental condition a detected protein originated from. By comparing the levels of detection in the light sample to the heavy sample, we can separate which proteins from the MOR immunoprecipitation are above background. There were 294 with a clear light-to-heavy ratio. The 71 proteins had a two-fold or higher ratio of detection towards the light sample over the heavy sample, see Table 4-1 for the complete list. Near the top of this list was the MOR itself, which was present 53x higher in the experimental condition over the light sample. We were also able to detect the known MOR binding partner, filamin A. We did not detect periplakin or RanBPM. However, we were able to detect other intermediate filament interaction proteins. Additionally, the interactions between MOR and periplakin or RanBPM are not extensively studied, and it is not unreasonable that under very different conditions that these interactions could not be reproduced. There were also 61 proteins detected in only the light sample, in other words only in the experimental MOR precipitation, and not the control, see Table 4-2 for the complete list.

To further analyze the candidate binding proteins we used Cytoscape to make gene ontology (GO terms) based maps from the protein candidates with

the highest ratios. In using these maps as tools were able see a high percentage of proteins involved with in GPCR signaling and the actin cytoskeleton, see Figure 4-2C. The larger the circle is on the map, the more associated proteins there are associated with those categories. The large percentage of GPCR related proteins are a good confirmation that we were able to precipitate related proteins. The large percentage of actin-related proteins present in the GO term map is also a reassuring conformation. Unpublished work in our lab has shown that the MOR recycles through actin-stabilized tubules. Additionally previous work has suggested that actin inhibition also decreases MOR recycling (Roman-Vendrell, Yu, & Yudowski, 2012). It has also been suggested that control of actin can work as a mechanism to control clathrin-coated pits dynamics (Grassart et al., 2014). A MOR interaction partner that interacts with actin could be a potential mechanism for inhibition vesicle scission. One actin-associated protein candidate of note is the relatively uncharacterized actin severing protein, adserverin. A potential mechanism here could be that MOR binding to adserverin would cleave actin and nullify its role in aiding vesicle scission, thus extending the duration of the vesicle step. Finally, mapping the protein candidates based on known protein-protein-interactions using another biological mapping software, Genemania pointed out 14-3-3 as the protein with the most known interaction partners that were also precipitated.

Discussion

This technique and the subsequent data set in yielded is a significant milestone in determining MOR binding partners. We were able to detect a total of 387 proteins. By using the SILAC method, instead of shotgun mass spectrometry we were able to further differentiate this large data set. By looking at the light-to-heavy detection ratios of each protein, we could determine which proteins were present in the MOR immunoprecipitation over the negative control. The light-to-heavy ratios narrowed the candidate pool down to 71 candidate-binding proteins that were detected to be two-fold or more abundant in the MOR immunoprecipitation sample over the negative control. Furthermore, we were also able to detect 61 proteins only present in the MOR immunoprecipitation. Both of these lists of proteins should be references in testing potential MOR binding partners.

Our initial analysis of the data set from building GO term and protein-protein-interaction based maps highlighted two proteins adseverin and 14-3-3. Preliminary tests focused on 14-3-3, particularly the zeta isoform, which was the most abundantly detected isoform. Unfortunately, preliminary binding tests did not re-confirm binding of 14-3-3 to the MOR. However, 14-3-3 was only one of over 71 candidate-binding proteins. Additional binding trials, perhaps beginning with adseverin, need to be performed to verify MOR binding partners.

The advances of this assay expand beyond this data set. This immunoprecipitation protocol can be readily adapted to test other binding

partners that capture our attention from the literature or future studies. The data set may also be improved by conducting additional SILAC tests. Based on the low or lack of detection of plasma membrane localized associated proteins such as beta-arrestin, we are inclined to believe that most of the receptors were in endosomes at the time of cell lysis. A repeat SILAC immunoprecipitation experiment with a shorter 2-5 minute agonist stimulation should yield more plasma membrane associated proteins that may be more likely to play a role in allowing the MOR to alter its clathrin-mediated endocytosis. Additionally, further SILAC experiments comparing the wild type receptor with the mutants for the important trafficking related sequences: the C-terminal LENLEAE sequence and PKC phosphorylation will help to elucidate sequence specific binding partners. An alternative approach is to adapt this this protocol for use with differential gel electrophoresis (DIGE). Preliminary tests to outline this procedure have begun. By using the principles of DIGE, where the elution for the wild type receptor will be differentially labeled from its mutant will allow for the visual showcase of sequence dependent binding partners before mass spectrometry analysis (Minden, Dowd, Meyer, & Stühler, 2009).

An additional suggestion from the data set is the appearance of $G_{\alpha/s}$, which does not canonically associate with the MOR except for under chronic morphine (Chakrabarti, Regec, & Gintzler, 2005). The light-to-heavy ratio of detection is even greater than those for $G_{\alpha/i}$, the typical coupled G-protein for the MOR. Additionally, there is lower presence of plasma membrane associated proteins

that are involved in the trafficking of MOR such as beta-arrestin and clathrin. This loosely suggests that at this time the bulk of receptors may to localized to endosomes. While these two observations may seem contradictory, in fact there has been much recent work on uncovering secondary signaling pathways at the endosomal populations (Tsvetanova & Zastrow, 2014) (Irannejad & Zastrow, 2014). And so perhaps the G-proteins are associated with MOR at the endosome.

Overall, this procedure marks a major step forward in finding function MOR receptor binding partners. Many of the candidate proteins showcase related functions, and therefore exhibit great promise. There is a high potential for false positives, as unfortunately showcased by the preliminary 14-3-3 trials. However, there still remains great potential in this data set itself and its ability to build upon it.

Methods

Cell culture

N terminal FLAG-tagged MOR was transfected into HEK293 cells. The cells were maintained in High Glucose DMEM with 10% fetal bovine serum at 5% CO_2. The cells were kept under 200μg/mL G418 for 14 days to select for FLAG-MOR expressing cells. After the 14 days, clonal populations of cells were picked and their expression was verified by fluorescent microscopy. Clones with ample receptor expression were expanded and cryogenically frozen. Cells were grown

on 10 cm (for small scale single immunoprecipitation reactions) or 15 cm (for the large scale immunoprecipitation in the SILAC experiment) flat-bottomed tissues culture dishes. Cells were lysed when they reached 80-100% confluency. The cells intended for the SILAC experiment were thawed into unmodified High Glucose DMEM with 10% fetal bovine serum, before being moved to the heavy isotope or light isotope containing High Glucose DMEM with 10% fetal bovine serum. The cells were maintained in either the heavy or light isotope containing media for seven passages for full isotope incorporation, and the cells were slowly expanded into ten 15 cm flat-bottom tissue cultures dishes. The cells were lysed once they reached 80-100% confluency.

Co-immunoprecipation of FLAG-MOR

Cells were treated with 10μM DAMGO for 10 minutes to internalize the FLAG-MOR. Cells were quickly placed on ice, transferred to the cold room, washed twice with ice old Dulbecco's phosphate buffered saline with 1mM CaCl and 1 mM MgCl (complete DBPS), and treated with 1mM DSP dissolved into complete DPBS. The DSP incubation lasted for 2 hours in a dark cold room. After the crosslinking step, the DSP was quenched with 20mM Tris pH 7.4 for 15 minutes. After two washes of complete PBS the cells were scraped into a minimal amount (250μL for a 10cm plate, 500μL for a 15cm plate) of Lysis Buffer. The Lysis buffer was composed of: 10 mM Hepes, 150 mM NaCl, 1 mM EGTA, 0.1 mM MgCl2, 0.5% Triton-X at pH 7.4. The cells sat on ice for 15 minutes, before being

vortexed 5 times in 5 second internals alternating with 5 second incubations on ice. The lysate was spun at 13.2K x g for 15 minutes in a cold centrifuge. The supernatant was assayed for protein concentration via a Bradford assay and diluted to a final protein concentration of 1mg/mL. Meanwhile, 30μL of IgG-dynabeads were incubated with 10μg of M2 mouse monoclonal anti-FLAG antibody both suspended in 500μL of IP buffer for 2 hours at room temperature. The IP buffer was comprised of: 10 mM HEPES, 150 mM NaCl, 1 mM EGTA, 0.1 mM MgCl2, and 0.1% Triton-X at pH 7.4. After two washes of IP buffer, 500μL of cell lysate contain 500μg of total protein were loaded onto the IgG-Dynabeads. If it was required, 0.1mg/mL of FLAG peptide was also added at to the immunoprecipitation reaction at this step. The lysate and beads were incubated for 2 hours at 4°C to allow for FLAG-MOR complexes to bind the IgG-Dynabeads. After removal of the excess lysate, the IgG-Dynabeads were washed six times with 1mL of IP buffer. The FLAG-MOR containing complexes were the eluted with 1mg/mL FLAG-peptide dissolved into Lysis buffer. The complexes were eluted slowly incubating on ice for 2 hours with manual agitation every 15 minutes. The elution was removed from the IgG-dynabeads with a gel loading tip and kept on ice until its next application.

Western blot and silver staining

SDS-PAGE gels were run on pre-cast 4-20% gradient mini-gels. Proteins were transferred onto 0.4μm pore nitrocellulose at 4°C overnight at 35V. The

membrane was blocked with 5% BSA in Tris-buffered saline with Tween (TBST) for 1 hour at 4°C. The rabbit polyclonal anti-FLAG antibody was incubated at 1:1000 concentration for 1 hour at 4°C with mild agitation. After three washes in TBST, horseradish peroxidase (HRP) conjugated goat anti-rabbit secondary antibody was incubated with the membrane at 1:10,000 concentration for 1 hour at 4°C with mild agitation. After three washes in TBST and one wash in TBS, the membrane was incubated with HRP substrate for 5 minutes. Excess substrate was removed before the blot was imaged. Silver staining was done using the Pierce mass spectrometry compatible silver staining kit.

References

Bowman, S. L., Soohoo, A. L., Shiwarski, D. J., Schulz, S., Pradhan, A. A., & Puthenveedu, M. A. (2015). Cell-Autonomous Regulation of Mu-Opioid Receptor Recycling by Substance P. *Cell Reports*. doi:10.1016/j.celrep.2015.02.045

Chakrabarti, S., Regec, A., & Gintzler, A. R. (2005). Biochemical demonstration of mu-opioid receptor association with Gsα: enhancement following morphine exposure. *Molecular Brain Research*, *135*(1-2), 217–224. doi:10.1016/j.molbrainres.2004.12.016

Feng, G.-J., Kellett, E., Scorer, C. A., Wilde, J., White, J. H., & Milligan, G. (2003). Selective Interactions between Helix VIII of the Human -Opioid Receptors and the C Terminus of Periplakin Disrupt G Protein Activation. *The Journal of Biological Chemistry*, *278*(35), 33400–33407. doi:10.1074/jbc.M305866200

Gokhale, A., Perez-Cornejo, P., Duran, C., Hartzell, H. C., & Faundez, V. (2012). A comprehensive strategy to identify stoichiometric membrane protein interactomes. *Cellular Logistics*, *2*(4), 189–196. doi:10.4161/cl.22717

Grassart, A., Cheng, A. T., Hong, S. H., Zhang, F., Zenzer, N., Feng, Y., et al. (2014). Actin and dynamin2 dynamics and interplay during clathrin-mediated endocytosis. *The Journal of Cell Biology*, *205*(5), 721–735. doi:10.1083/jcb.201403041

Irannejad, R., & Zastrow, von, M. (2014). GPCR signaling along the endocytic pathway. *Current Opinion in Cell Biology*, *27*, 109–116.

Milligan, G. (2005). Opioid receptors and their interacting proteins. *Neuromolecular Medicine*, *7*(1-2), 51–59. doi:10.1385/NMM:7:1-2:051

Minden, J. S., Dowd, S. R., Meyer, H. E., & Stühler, K. (2009). Difference gel electrophoresis. *Electrophoresis*, *30*(S1), S156–S161. doi:10.1002/elps.200900098

Ong, S.-E., Blagoev, B., Kratchmarova, I., Kristensen, D. B., Steen, H., Pandey, A., & Mann, M. (2002). Stable isotope labeling by amino acids in cell culture, SILAC, as a simple and accurate approach to expression proteomics. *Molecular & Cellular Proteomics*, *1*(5), 376–386. doi:10.1074/mcp.M200025-MCP200

Onoprishvili, I., Andria, M. L., Kramer, H. K., Ancevska-Taneva, N., Hiller, J. M., & Simon, E. J. (2003). Interaction between the mu opioid receptor and filamin A is involved in receptor regulation and trafficking. *Molecular Pharmacology*, *64*(5), 1092–1100. doi:10.1124/mol.64.5.1092

Puthenveedu, M. A., & Zastrow, von, M. (2006). Cargo Regulates Clathrin-Coated Pit Dynamics. *Cell*, *127*(1), 113–124. doi:10.1016/j.cell.2006.08.035

Roman-Vendrell, C., Yu, Y. J., & Yudowski, G. A. (2012). Fast modulation of -Opioid receptor (MOR) recycling is mediated by receptor agonists. *Journal of Biological Chemistry*, *287*(18), 14782–14791. doi:10.1074/jbc.M111.319616

Schulz, S., Mayer, D., Pfeiffer, M., Stumm, R., Koch, T., & Ilt, V. H. (2004). Morphine induces terminal l-opioid receptor desensitization by sustained phosphorylation of serine-375. *The EMBO …*.

Soohoo, A. L., & Puthenveedu, M. A. (2013). Divergent modes for cargo-mediated control of clathrin-coated pit dynamics. *Molecular Biology of the Cell*, *24*(11), 1725–1734. doi:10.1091/mbc.E12-07-0550

Talbot, J. N., Skifter, D. A., Bianchi, E., Monaghan, D. T., Toews, M. L., & Murrin, L. C. (2009). Regulation of mu opioid receptor internalization by the scaffold protein RanBPM. *Neuroscience Letters*, *466*(3), 154–158.

doi:10.1016/j.neulet.2009.09.048

Tanowitz, M., & Zastrow, von, M. (2003). A Novel Endocytic Recycling Signal That Distinguishes the Membrane Trafficking of Naturally Occurring Opioid Receptors. *Journal of Biological Chemistry*, *278*(46), 45978–45986. doi:10.1074/jbc.M304504200

Tsvetanova, N. G., & Zastrow, von, M. (2014). Spatial encoding of cyclic AMP signaling specificity by GPCR endocytosis. *Nature Chemical Biology*, *10*(12), 1061–1065. doi:10.1038/nchembio.1665

Wang, H.-Y., & Burns, L. H. (2009). Naloxone's Pentapeptide Binding Site on Filamin A Blocks Mu Opioid Receptor–Gs Coupling and CREB Activation of Acute Morphine. *PLoS ONE*, *4*(1), e4282. doi:10.1371/journal.pone.0004282.g007

Zlatic, S. A., Ryder, P. V., Salazar, G., & Faundez, V. (2010). Isolation of Labile Multi-protein Complexes by in vivo Controlled Cellular Cross-Linking and Immuno-magnetic Affinity Chromatography. *Journal of Visualized Experiments*, (37). doi:10.3791/1855

Table 4-1: SILAC candidate proteins with two-fold or greater abundance

Protein IDs	Protein names	L/H ratio
Q6TDP4	Kelch-like protein 17	355.5176337
P35372	Mu-type opioid receptor	53.84449709
Q15058	Kinesin-like protein KIF14	48.93564962
P18206	Vinculin	37.72873043
P16401	Histone H1.5	35.32695093
Q99714	3-hydroxyacyl-CoA dehydrogenase type-2	20.37572843
P01617	Ig kappa chain V-II region TEW	18.74308849
P81605	Dermcidin;Survival-promoting peptide;DCD-1	17.17357331
Q86YZ3	Hornerin	14.26513174
Q562R1	Beta-actin-like protein 2	14.00070004
Q5T749	Keratinocyte proline-rich protein	13.58289642
P05109	Protein S100-A8;Protein S100-A8, N-terminally processed	13.43002955
Q12955	Ankyrin-3	11.72044397
P31944	Caspase-14;Caspase-14 subunit p19;Caspase-14 subunit p10	10.25178381
P22531	Small proline-rich protein 2E	10.08034031
P02810	Salivary acidic proline-rich phosphoprotein 1/2	9.637625289
P15924	Desmoplakin	9.244707405
P31151	Protein S100-A7;Protein S100-A7A	6.707807888
P69892	Hemoglobin subunit gamma-2;Hemoglobin subunit gamma-1	6.242586928
Q9Y6U3	Adseverin	6.169792695
Q9NU53	Glycoprotein integral membrane protein 1	6.156877232
P30101	Protein disulfide-isomerase A3	5.483658697
P63261	Actin, cytoplasmic 2	5.348451623
Q13394	Protein mab-21-like 1	5.315473343
P48444	Coatomer subunit delta	4.971661529
P68133	Actin, alpha skeletal muscle	4.746535029
P35232	Prohibitin	4.621926419
P60709	Actin, cytoplasmic 1;Actin, cytoplasmic 1, N-terminally processed	4.572891897
Q16643	Drebrin	4.351610096
P68871	Hemoglobin subunit beta;LVV-hemorphin-7;Hemoglobin subunit delta	4.189183528
P08670	Vimentin	3.848225968
P12004	Proliferating cell nuclear antigen	3.826286589
Q12907	Vesicular integral-membrane protein VIP36	3.726476616
Q9UBF2	Coatomer subunit gamma-2	3.669186175
P63092	Guanine nucleotide-binding protein G(s) subunit alpha isoforms short	3.631477648
O00479	High mobility group nucleosome-binding domain-containing protein 4	3.354241438
P48047	ATP synthase subunit O, mitochondrial	3.352779454
P80723	Brain acid soluble protein 1	3.341910905
P56385	ATP synthase subunit e, mitochondrial	3.297935492
P06576	ATP synthase subunit beta, mitochondrial	3.234048058
O15145	Actin-related protein 2/3 complex subunit 3	3.223518793

P49755	Transmembrane emp24 domain-containing protein 10	3.204203916
P50552	Vasodilator-stimulated phosphoprotein	3.054554341
P52907	F-actin-capping protein subunit alpha-1	3.027367401
P60468	Protein transport protein Sec61 subunit beta	2.969826562
Q9NYL9	Tropomodulin-3	2.949243519
P61923	Coatomer subunit zeta-1	2.869769844
P60660	Myosin light polypeptide 6	2.771772271
P37802	Transgelin-2	2.739050645
P62987	Ubiquitin-60S ribosomal protein L40	2.631301968
P06753	Tropomyosin alpha-3 chain	2.625360987
P59998	Actin-related protein 2/3 complex subunit 4	2.553952241
Q9HCH0	Nck-associated protein 5-like	2.452483139
P19105	Myosin regulatory light chain 12A	2.405060247
O75083	WD repeat-containing protein 1	2.359826317
P27449	V-type proton ATPase 16 kDa proteolipid subunit	2.291213197
P47756	F-actin-capping protein subunit beta	2.282531784
P11021	78 kDa glucose-regulated protein	2.231893762
Q06830	Peroxiredoxin-1	2.223309173
P32119	Peroxiredoxin-2	2.184550856
Q7Z5G4	Golgin subfamily A member 7	2.152574479
Q9Y281	Cofilin-2	2.146429415
P04406	Glyceraldehyde-3-phosphate dehydrogenase	2.112155455
Q9ULV4	Coronin-1C	2.075248511
P63104	14-3-3 protein zeta/delta	2.041733023
P07437	Tubulin beta chain	2.023554171
P29992	Guanine nucleotide-binding protein subunit alpha-11	2.020773552
Q12792	Twinfilin-1	2.016250983
P08754	Guanine nucleotide-binding protein G(k) subunit alpha	2.009525149
Q00839	Heterogeneous nuclear ribonucleoprotein U	2.001841694

Table 4-2: Proteins only detected the experimental immunoprecipitation

Protein IDs	Protein names	Gene names
O75223	Gamma-glutamylcyclotransferase	GGCT
O95373	Importin-7	IPO7
O96002	Transmembrane protein 257	TMEM257
P00450	Ceruloplasmin	CP
P00505	Aspartate aminotransferase, mitochondrial	GOT2
P01011	Alpha-1-antichymotrypsin;Alpha-1-antichymotrypsin His-Pro-less	SERPINA3
P01023	Alpha-2-macroglobulin	A2M
P01040	Cystatin-A;Cystatin-A, N-terminally processed	CSTA
P01833	Polymeric immunoglobulin receptor;Secretory component	PIGR
P01859	Ig gamma-2 chain C region	IGHG2
P02647	Apolipoprotein A-I;Truncated apolipoprotein A-I	APOA1
P02760	Protein AMBP	AMBP
P02765	Alpha-2-HS-glycoprotein;	AHSG
P02786	Transferrin receptor protein 1	TFRC
P04083	Annexin A1	ANXA1
P19961	Alpha-amylase 2B;Pancreatic alpha-amylase;Alpha-amylase 1	AMY2B;AMY2A;AMY1A
P04899	Guanine nucleotide-binding protein G(i) subunit alpha-2	GNAI2
P05090	Apolipoprotein D	APOD
P0C0L5;	Complement C4-B	C4B;C4A
P10599	Thioredoxin	TXN
P11532	Dystrophin	DMD
P12273	Prolactin-inducible protein	PIP
P14316	Interferon regulatory factor 2	IRF2
P15880	40S ribosomal protein S2	RPS2
P18124	60S ribosomal protein L7	RPL7
P19823;	Inter-alpha-trypsin inhibitor heavy chain H2	ITIH2
P29508	Serpin B3;Serpin B4	SERPINB3;SERPINB4
P29966	Myristoylated alanine-rich C-kinase substrate	MARCKS
P32455	Interferon-induced guanylate-binding protein 1	GBP1
P32969	60S ribosomal protein L9	RPL9
P35030	Trypsin-3	PRSS3
P35606	Coatomer subunit beta	COPB2
P35612	Beta-adducin	ADD2
P47736	Rap1 GTPase-activating protein 1	RAP1GAP
P47929	Galectin-7	LGALS7
P49862	Kallikrein-7	KLK7
P52815	39S ribosomal protein L12, mitochondrial	MRPL12
P53007	Tricarboxylate transport protein, mitochondrial	SLC25A1
P53350	Serine/threonine-protein kinase PLK1	PLK1
P53618	Coatomer subunit beta	COPB1
P60763	Ras-related C3 botulinum toxin substrate 3	RAC3

P61626	Lysozyme C	LYZ
P62917	60S ribosomal protein L8	RPL8
Q00610	Clathrin heavy chain 1	CLTC
Q02338	D-beta-hydroxybutyrate dehydrogenase, mitochondrial	BDH1
Q02413	Desmoglein-1	DSG1
Q02447	Transcription factor Sp3	SP3
Q03001	Dystonin	DST
Q03989	AT-rich interactive domain-containing protein 5A	ARID5A
Q08188	Protein-glutamine gamma-glutamyltransferase E	TGM3
Q08554	Desmocollin-1	DSC1
Q13029	PR domain zinc finger protein 2	PRDM2
Q13618	Cullin-3	CUL3
Q13813	Spectrin alpha chain, non-erythrocytic 1	SPTAN1
Q13867	Bleomycin hydrolase	BLMH
Q14011	Cold-inducible RNA-binding protein	CIRBP
Q14153	Protein FAM53B	FAM53B
Q14624	Inter-alpha-trypsin inhibitor heavy chain H4	ITIH4
Q15149	Plectin	PLEC
Q16698	2,4-dienoyl-CoA reductase, mitochondrial	DECR1
Q4LE39	AT-rich interactive domain-containing protein 4B	ARID4B
Q5CZC0	Fibrous sheath-interacting protein 2	FSIP2
Q5T5P2	Sickle tail protein homolog	KIAA1217
Q6UWP8	Suprabasin	SBSN
Q6ZVX7	F-box only protein 50	NCCRP1
Q8IYT4	Katanin p60 ATPase-containing subunit A-like 2	KATNAL2
Q8N3V7	Synaptopodin	SYNPO
Q8N7X1	RNA-binding motif protein, X-linked-like-3	RBMXL3
Q8TD08	Mitogen-activated protein kinase 15	MAPK15
Q92520	Protein FAM3C	FAM3C
Q99523	Sortilin	SORT1
Q9GZS1	DNA-directed RNA polymerase I subunit RPA49	POLR1E
Q9H0V9	VIP36-like protein	LMAN2L
Q9H211	DNA replication factor Cdt1	CDT1
Q9NV96	Cell cycle control protein 50A	TMEM30A
Q9NZT1	Calmodulin-like protein 5	CALML5
Q9Y584	Mitochondrial import inner membrane translocase subunit Tim22	TIMM22
Q9Y5N5	HemK methyltransferase family member 2	N6AMT1

Conclusions and Future Directions

There still remains much to be explored of the intracellular trafficking of the MOR. We have investigated the role the MOR can play in impact its own endocytosis and post-endocytic recycling. The MOR has the ability to control the duration of its own endocytic events by extending the lifetimes of clathrin-coated pits it resides in. This ability is connected to a very specific sequence of the receptor. We have furthermore shown that the duration of endocytic events has a direct consequence on the downstream ERK signaling mediated by beta-arrestin. As the receptor returns to the cell surface from endosomes its rate of recycling is controlled by PKC, which directly phosphorylates the MOR. PKC can be activated through the $G_{\beta\gamma}$ protein propagated by the MOR itself or through $G_{\alpha q}$ signaling from the pain receptor, the neurokinin-1 receptor. Although, we have uncovered much about the regulation of trafficking of the MOR, much still needs to be discerned over the mechanisms of how these specific sequences lead to changes in trafficking.

This work has also made significant strides towards uncovering those mechanisms by providing a platform of potential interaction partners through SILAC. This list has been refined through the SILAC technique itself and by basic proteomic organization. The protein candidates must be confirmed by re-confirming binding coupled to an immunoblot, and they must be assayed for a role in MOR trafficking. Perhaps the most robust screening technique would be a knockdown coupled with the two-color-recycling assay. This assay allows

analysis of a large number of cells quickly, and allows for screening of both endocytosis and recycling defects. Repeating higher resolution microscopy studies, such as effects on clathrin-coated pit lifetimes may also prove fruitful.

The SILAC data set can also be expanded by performing additional SILAC experiments that compare the wild type receptors to any of the trafficking mutants: the LLAA or the PKC phosphorylation mutants. Alternatively, the immunoprecipitation protocol can be used with other proteomic assays, including differential gel electrophoresis (DIGE). Preliminary work has effectively translated the immunoprecipitation protocol for use with DIGE, however no clear differences between the wild type receptor and the LLAA mutant have been detected thus far.

Future studies on the mechanisms are not limited experiments rooted in protein biochemistry. We have determined that the MOR is able to impact clathrin-mediated endocytosis by extending the duration dynamin. However, we were unable to delineate a further impact on the endocytosis process even after surveying nine other endocytosis components. Recent advances in light-microscopy have allowed for the elucidation of structures below the resolution limit of light (Ji, Shroff, Zhong, & Betzig, 2008). We have begun preliminary studies using high NA TIRF linear-SIM microscopy in collaboration with Eric Betzig's lab at Janelia Farm. This microscope can resolve the clathrin-coat structure as a ring shape and will allow us to take a more detailed look at on how the receptor behaves in a clathrin-coat in a live-cell. Furthermore, through this

higher resolution microscopy we may observe distinct behaviors in dynamin or other endocytosis components, including the possible role of actin.

It is reasonable that an interconnected mechanism controls the rate of recycling of the receptor and the duration of endocytic events. The LLAA mutant is unable to recycle at all, and the PKC sites are localized near this required sequence. Furthermore, it has been suggested that PKC can associate with dynamin (Liu, Powell, Südhof, & Robinson, 1994) and that dynamin is localized to endosomal tubules (Derivery et al., 2009).

Finally, the bulk of this work was performed in cell culture lines, particularly the endocytosis work. Repeating the endocytosis and signaling experiments using primary cells expressing endogenous receptors and expanding upon the number of opiates tested will certainly broaden the impact of these studies. As we learn more of the regulation that drives MOR trafficking we will be able to fully discern that characteristics that are attributed an endogenous agonist activated receptor versus an exogenous agonist activated receptor. Perhaps when these mechanisms are fully understood, we will finally be able to uncouple the sensations of addiction and analgesia.

References

Derivery, E., Sousa, C., Gautier, J. J., Lombard, B., Loew, D., & Gautreau, A. (2009). The Arp2/3 activator WASH controls the fission of endosomes through a large multiprotein complex. *Developmental Cell*, *17*(5), 712–723. doi:10.1016/j.devcel.2009.09.010

Ji, N., Shroff, H., Zhong, H., & Betzig, E. (2008). Advances in the speed and resolution of light microscopy. *Current Opinion in Neurobiology*, *18*(6), 605–616. doi:10.1016/j.conb.2009.03.009

Liu, J. P., Powell, K. A., Südhof, T. C., & Robinson, P. J. (1994). Dynamin I is a Ca(2+)-sensitive phospholipid-binding protein with very high affinity for protein kinase C. *The Journal of Biological Chemistry*, *269*(33), 21043–21050.